Electrochemical and Gravimetric Studies towards Service-Life Prediction and Durability-based Design of RC Structures in Corrosive Environments

BY

ADAMU LAWAN

A Thesis Presented to the

DEANSHIP OF GRADUATE STUDIES

KING FAHD UNIVERSITY OF PETROLEUM & MINERALS

DHAHRAN, SAUDI ARABIA

In Partial Fulfillment of the
Requirements for the Degree of

MASTER OF SCIENCE

In

CIVIL ENGINEERING

July, 2011

KING FAHD UNIVERSITY OF PETROLEUM AND MINERALS
DHAHRAN, 31261, SAUDI ARABIA

DEANSHIP OF GRADUATE STUDIES

This thesis, written by **ADAMU LAWAN** under the direction of his Thesis advisor and approved by his Thesis Committee, has been presented to and accepted by the Dean of Graduate Studies, in partial fulfillment of the requirement for the degree of **MASTER OF SCIENCE IN CIVIL ENGINEERING**.

Thesis Committee

Dr. Saeid A. Alghamdi (Advisor)

Dr. Shamshad Ahmad (Co-advisor)

Dr. Mohammed Maslehuddin (Member)

Dr. Mazen Khaled (Member)

Dr. Ahmad Saad Algahtani (Member)

23 JUL 2011

Dr. Nedal T. Ratrout
Departmental Chairman

Dr. Salam A. Zummo
Dean of Graduate Studies

24/7/11
Date

DEDICATED

TO

MY PARENTS

ACKNOWLEGEMENTS

In the name of Allah, the Beneficent, the Most Merciful. All praises and thanks are due to Allah, the Lord of the world for the successful completion of this research work. May His peace be upon the last messenger, Prophet Muhammad, his family and companions.

Acknowledgement is due to the King Fahd University of Petroleum and Minerals for providing facilities towards this research. I also want to acknowledge Ahmadu Bello University, Zaria for granting me Study fellowship.

My gratitude and acknowledgment are due to Dr. Saeid Aboud Alghamdi, my thesis Advisor, for his constant support, encouragement and inspiration. Also, I am very grateful to Dr. Shamshad Ahmad, my Co-Advisor; and Dr. Mohammed Maslehuddin, my committee member for their guidance and continuous support in all the phases of this work. Similarly, the support and guidance of Dr. Ahmad Saad Algahtani and Dr. Mazen Khaled as committee members are highly appreciated.

I want to particularly acknowledge the tremendous assistance I received from Dr. Mohammed Essa, Engr. Mukarram M. Khan and Engr. Umar Hussein all in the departmental laboratories. Similarly, thanks are due to Engr. Rizwan M. Ali, Engr. Barry M. Salihu and Engr. Mohammed Shameem of University Research Institute for their assistance in all the stages of my experiments.

Special thanks also go to Dr. Idris Abubakar, the Head of Civil Engineering Department, Ahmadu Bello University, Zaria and the entire staff of the Department for their support and encouragement.

My sincere appreciation goes to my parents, brothers, sisters, wife and my entire family for their love, encouragement, patience and prayers.

Finally, I pray to Almighty Allah to reward all those who contributed, either directly or indirectly, towards the success of this work.

TABLE OF CONTENTS

LIST OF TABLES

LIST OF FIGURES

THESIS ABSTRACT

Name: **ADAMU LAWAN**

Title: **ELECTROCHEMICAL AND GRAVIMETRIC STUDIES TOWARDS SERVICE-LIFE PREDICTION AND DURABILITY-BASED DESIGN OF RC STRUCTURES IN CORROSIVE ENVIRONMENTS**

Department: **CIVIL ENGINEERING**

Date: **JULY 2011**

Chloride-induced corrosion of reinforcing steel is a major problem with regard to service-life and structural-durability requirements of reinforced concrete (RC) structures. Under specified chloride exposure conditions, concrete quality and cover-thickness play a pivotal role on initiation and progress of reinforcement corrosion. Therefore, initiation and rate of reinforcement corrosion can be modeled in terms of parameters of concrete quality and cover-thickness. This work presents the results of an experimental investigation carried out on a large number of test specimens designed for this purpose using two types of coarse aggregates collected from two quarries located in eastern province and western province of the Kingdom of Saudi Arabia. The specimens were prepared with three contents (350; 375; and 400 kg/m^3) of cementitious material, three ratios (0.4; 0.45; and 0.5) of water to cement ratio, three ratios (0.35; 0.4; and 0.45) of fine to total aggregate ratio, and three values (25; 37.5; and 50 mm) of concrete cover-thickness.

For a period of three years, the specimens were subjected to three levels of chloride-concentrations (*namely*: 3%, 7% and 12%) experimentally simulating chloride-induced reinforcement corrosion, and the resulting corrosion rates were determined using electrochemical and gravimetric (weight loss) methods to determine the extent of corresponding corrosion.

A numerical analysis of the reinforcement-corrosion rates (determined electrochemically and gravimetrically) was first used to determine statistical-correlation between the corrosion rates obtained by the two methods. Then, the gravimetric reinforcement-corrosion-rate results were utilized for developing regression models for reinforcement corrosion rates in terms of concrete quality parameters, concrete cover-thickness and chloride-salt (NaCl) concentration.

The regression models obtained for reinforcement-corrosion-rates were utilized to develop analysis and design approaches automated using **Microsoft Excel Solver** for service-life prediction and durability-based design of RC structures exposed to chloride environments.

Utilization of the approaches, proposed for analysis and durability-based design of RC structures, is also demonstrated by selected numerical examples for service-life-prediction and durability-based-design of specific structural elements (*namely*: beams and columns) of RC structures.

ملخص الرسالة

الاسم : **ادمو لوان**

العنوان : **دراسات كهروكيميائية و جرافيمترية لتحديد عمر الخدمة وتصميم المباني الخرسانية اعتمادا على اشتراط ديمومة المنشات الخرسانية المسلحة في البيئات التصدئية.**

القسم: **الهندسة المدنية**

تاريخ: **شعبان 1432 هـ**

يعتبر تأكل (تصدء) حديد التسليح الناجم بسبب أملاح الكلورايد مشكلة رئيسة تؤثر على العمر الخدمي والديمومة الهيكلية للمنشات الخرسانية ، وفي البيئة المعرضة للكلورايد، تلعب نوعية الخرسانة وسماكة تغطيتها لحديد التسليح دورا مؤثرا على بداية و تطور تأكل حديد التسليح. ولأهمية نمذجة بداية وسرعة تأكل حديد التسليح بدلالة نوعية الخرسانة و سماكة التغطية، فإن هذا البحث يقدم نتائج دراسات مخبريه أجريت على مجموعة كبيرة من عينات خرسانية صممت لهذا الغرض باستخدام نوعين من الركام (البحص) الخشن تم الحصول عليها من محاجر الركام في المنطقة الشرقية و المنطقة الغربية من المملكة العربية السعودية. صممت العينات الخرسانية باستخدام ثلاث كميات (350 ؛ 375 ؛ 400 كجم / م^3) من مادة الاسمنت مع ثلاث مقادير (0.4 ؛ 0.45 ؛ 0.5) من نسبة الاسمنت إلى الماء ، وثلاث مقادير (0.35؛ 0.4 ؛ 0.45) من نسبة الركام (البحص) الخشن إلى الركام الناعم، وباستخدام ثلاثة مقادير (25 ملم ؛ 37.5 ؛ 50 ملم) من سماكة التغطية الخرسانية في كل العينات.

وفي فترة زمنية مدتها ثلاث سنوات عرضت العينات لثلاثة مقادير (3% ؛ 7% ؛ 12%) من محلول الكلورايد تمثل تشبيها إختباريا للظروف البيئية المتغيرة و المسببة لتأكل (صدأ) حديد التسليح ، وقد تم في هذا البحث تحديد معدل سرعة تأكل حديد التسليح باستخدام الطرق الكهروكيميائية والجرافيمترية (قياس فقدان الوزن) لتحديد مدى التآكل الناجم في كل حالة.

ومن خلال التحليل العددي لقيم سرعة تأكل حديد التسليح التي تم الحصول عليها بالطريقة الكهروكيميائية وبالطريقة الجرافيمترية تم تطوير علاقة إحصائية تربط بين قيم سرعة التأكل باستخدام الطريقتين. ومن ثم استخدمت نتائج معدل سرعة تأكل حديد التسليح باستخدام الطريقة الجرافيمترية في تطوير نموذج لتحديد معدل أو سرعة تأكل الحديد بدلالة كل من نوعية الخرسانة ، و سماكة التغطية - الخرسانية ، و تركيز ملح الكلورايد.

وباستخدام النماذج التي تم الحصول عليها من نتائج الدراسات المخبرية في هذا البحث لتقييم تأكل (صدأ) حديد التسليح، تم تطوير طرق تحليلية وتصميمية برمجت باستخدام الحاسب الآلي (باستخدام مايكروسوفت إكسل سولفر "Microsoft Excel Solver") يمكن من خلالها تقدير العمر الخدمي المتوقع وتصميم الهيكل البنائي لتحقيق اشتراطات ديمومة المنشات الخرسانية المسلحة في البيئات الإنشائية المعرضة للكلورايد.

ولتوضيح طريقة الاستفادة العملية من الطرق المقترحة، يقدم هذا البحث مجموعة مختارة من الأمثلة العددية تبين طريقة تحديد العمر الخدمي وخطوات التصميم الإنشائي الذي يحقق شروط الديمومة - الهيكلية لعينة من عناصر إنشائية محددة (كمرات ؛ و أعمدة) في المباني الخرسانية المسلحة.

CHAPTER 1

INTRODUCTION

1.1 BACKGROUND TO THE PROBLEM

Due to a combination of environmental conditions and construction practices, corrosion of reinforcing steel bars has been known worldwide to be the main cause of accelerated deterioration of many reinforced concrete (RC) structures and some premature structural failures even well-before their intended design service-life [1].

Generally, the deterioration of RC structures in a corrosive environment (taking coastal area of Saudi Arabia as a case study) is mainly attributed to: (i) severe environmental conditions, (ii) substandard quality of materials and (iii) inadequate construction practices. The environmental conditions of the area are characterized by a large variation in the daily and seasonal temperature. During summer season, the ambient temperature may be as high as 45 to 50 $^{\circ}$C and the relative humidity ranges between 40 to 100% over a period of 24 hours [2]. Due to solar radiation, the temperature on the concrete surface may be as high as 70 to 80 $^{\circ}$C and the variation in the day to night temperature may be up to 20 $^{\circ}$C. This variation in the day to night temperature leads to the formation of micro-cracks in the concrete which accelerates the diffusion of aggressive species, such as

chlorides, carbon dioxide, oxygen and moisture, to the steel surface. This provides the required conditions to initiate corrosion of reinforcing steel. The corrosion of embedded steel bar is accompanied with considerable expansive forces. Therefore, reinforced the concrete construction in such environments should be designed for durability as well as for strength [3].

Chloride attack and carbonation are the two main causes of corrosion of steel in concrete. These two mechanisms are uncommon as they do not affect the concrete quality directly, but they are aggressive chemical species that penetrate through the cracks and pores in concrete and attack the steel. Other acids and aggressive ions, such as sulphates, damage the concrete before the steel is affected [4].

However, it has been observed that chloride is mainly responsible for the corrosion of reinforcing steel. In recent times, various reports of occurrence of reinforcement corrosion in structures exposed to chloride ions have really proved this point, and at the same time made the problem particularly well-known. Extensive research on factors contributing to reinforcement corrosion has increased our understanding of the mechanisms of corrosion, especially concerning the role of chloride ions [5].

Chloride ions are common in nature and very small quantities are normal in concrete ingredients. These ions may be intentionally added to the concrete, most often as a constituent of accelerating admixtures. Dissolved chloride ions may also penetrate hardened concrete in structures exposed to marine environments or to deicing salt. Besides, the environment influences the corrosion rate, as it contains *oxygen* and *moisture* which are essential substances in electrochemical corrosion. Macrocell corrosion is

imminent in RC with a significant gradient in chloride ions, especially when subjected to wetting and drying cycles [6].

The presence of chloride ions in the concrete mixture, contributed by its constituents, or due to natural diffusion process has been observed to play a major role in the initiation and progress of reinforcement corrosion in RC structures. The resulting corrosion-products have larger volume and induce stresses and strains that exceed the tensile strength of the concrete, which cause cracking and spalling of concrete cover and also loss of the bond between steel and concrete. A reduction in the rebar diameter and loss of the bond due to reinforcement corrosion cause a significant loss of load-bearing capacity of the corroded reinforced concrete members [7].

Corrosion rate is an important parameter for predicting the service-life of corroded reinforced concrete structures [8]. Various non-destructive techniques based on electrochemical techniques for measuring reinforcement corrosion rate have been used to detect the initiation and rate of corrosion, and to predict residual lives and accordingly decide what preventive or repair systems are to be applied. Both Direct Current (DC) and Alternate Current (AC) methods have been utilized as non-destructive methods for measuring the rate of corrosion in reinforced concrete. The electrochemical polarization methods are used to monitor quantitatively general corrosion and galvanic corrosion. They can also be used qualitatively to monitor localized corrosion (pitting and crevice). The main advantages of electrochemical techniques include: sensitivity to low corrosion rates, short experimental duration, and well-established theoretical understanding. On the other hand, the gravimetric weight loss measurement is a destructive technique for obtaining the corrosion rate [9]. Due to the destructive nature of the gravimetric weight

loss method, the non-destructive linear polarization resistance (LPR) method is commonly utilized for assessing the rate of reinforcement corrosion.

In the LPR measurements, the steel bar is polarized by the application of a small perturbation to the equilibrium potential through a counter electrode. The polarized surface area of the reinforcing steel is assumed to be that area which lies directly below the counter electrode. However, there is considerable evidence that current flowing from the counter electrode is not confined and can spread laterally over an unknown large area of the reinforcing steel, which may lead to the inaccurate estimation of the corrosion rate. On the other hand, gravimetric (weight loss) measurement as a destructive test, when conducted in controlled laboratory conditions serves as the most reliable reference method. It is simple, but is also a time-consuming technique for the determination of corrosion rate [8]. The weight loss measured is converted to a uniform corrosion rate over the exposure period. It has been proposed that the combination of the weight loss method and the polarization resistance method offers means of quantitative corrosion analysis. However, studies on the relationship between the weight loss method and the polarization resistance method are limited and most studies were conducted on different set of specimens [10].

This study is aimed at: 1) measuring corrosion rates, electrochemically as well as gravimetrically, in a large number of reinforced concrete specimens that were designed with various combinations of most influential design variables including: water to cementitious material ratio (w/c), cementitious materials content, fine to total aggregate ratio and cover thickness, and corroded under different chloride exposure concentrations;

2) correlating the electrochemically determined reinforcement corrosion rates with gravimetrically measured reinforcement corrosion rates; 3) developing models for predicting reinforcement corrosion rate using data generated under this study;

4) developing an approach for predicting the service-life of corroded reinforced concrete members demonstrating the use of correlation between electrochemically and gravimetrically measured corrosion rates obtained under the present work; and 5) proposing a methodology for durability-based design of RC structures using the corrosion rate prediction models developed in this study.

1.2 NEED FOR THIS RESEARCH

Analytical models for predicting reinforcement corrosion rate are required to carry out durability-based design of a new reinforced concrete structures. The design of durable RC structure is determined by a host of factors including concrete mixture ingredients and concrete cover to reinforcement in a given corrosive exposure. Also, the models are needed to carry out service-life prediction of reinforced concrete (RC) structures exposed to potential problems of reinforcement corrosion. Many researchers have attempted to derive such reinforcement corrosion models by generating experimental data through electrochemical monitoring of reinforcement corrosion over a reasonable time period. However, the accuracy of the reinforcement corrosion rate measured electrochemically is invariably doubtful because of the difficulties and errors frequently involved in the experimental measurements. Due to this reason, the models developed using the electrochemical techniques lack the accuracy and reliability. Therefore, it is needed to correlate the electrochemically measured corrosion rates with gravimetrically measured

corrosion rates so that the electrochemically measured value of reinforcement corrosion rates can be converted into equivalent more accurate gravimetric reinforcement corrosion rates, needed for service life prediction calculations.

1.3 OBJECTIVES

The primary objective of this work was to conduct electrochemical and gravimetric weight loss studies on a large number of reinforced concrete specimens prepared with varying mixture proportions and covers thicknesses and subjected to experimentally simulated corrosive environments that lead to different degrees of chloride-induced reinforcement corrosion.

The specific objectives of this study are the followings:

i. To develop relationship between corrosion rate measured by electrochemical and gravimetric weight loss methods,

ii. To develop models for the corrosion rate in terms of w/c ratio, fine to total aggregate ratio, cementitious material content, cover thickness, chloride concentration, and types of coarse aggregates.

iii. To utilize the developed correlation for develop models to predict the service-life of RC structures subjected to corrosive environments and outline a practical methodology that may be easily utilized for durability-based design of RC structures.

CHAPTER 2

LITERATURE REVIEW

An extensive literature survey of research issues of most relevance to this research study was carried out. The outcome of the survey is summarized below in the following order:

1. Chloride-induced reinforcement corrosion.
2 Linear polarization resistance (LPR) method versus gravimetric weight loss method for measurement of reinforcement corrosion rate.
3 Factors affecting the service-life of RC structures.
4 Models for predicting service-life of corroded RC structures.
5 Durability-based design of RC structures.

2.1 CHLORIDE-INDUCED REINFORCEMENT CORROSION

As durability of RC structures in harsh (corrosive) environments is of vital consequence, corrosion of steel reinforcement, which is one of the major causes of deterioration of RC structures, has received great attention of researchers in recent years. Chloride-induced corrosion of reinforcing steel is increasingly important in many countries due to increased use of sea sand and heavy construction of marine structures. Although, many

investigators have studied the mechanism of chloride-induced reinforcement corrosion, the chloride ion concentration in concrete that causes the initiation of steel corrosion in concrete, a most important parameter in determining the durability life and/or service life of concrete structures, is still ambiguous and needs further study [11].

It is known that, concrete protection to steel reinforcement bars is provided by: (i) highly alkaline environment which passivates the steel surface and, hence, prevents it from corrosion, and (ii) concrete prevention of ingress of aggressive species, like oxygen, carbon dioxide, water and chloride ions. To keep the reinforcing steel in a passive state, it is essential to maintain a high quality of concrete and minimize the factors which lead to its deterioration, such as quality of mixing water and aggregates. Chloride attack is distinct in that the primary action is the corrosion of reinforcement, and it is only as a consequence of this corrosion that the surrounding concrete is damaged.

Design codes have restricted the amount of chloride that may be introduced from raw materials containing significant amount of chlorides for both reinforced and prestressed concrete structures. The maximum allowed chloride contents according to the European Standard EN 206 are 0.2 to 0.4% by mass of binder for reinforced concrete and 0.1 to 0.2% for prestressed concrete. These limitations are aimed at minimizing corrosion due to chloride in the fresh mix. In the past, chlorides were added to the concrete mix of some structures, deliberately or unknowingly, through contaminated mixing water, aggregates or admixtures. The other main source of chloride is the diffusion from the service environment [12, 13].

2.1.1 Initiation of Corrosion

The chloride ion concentration that causes the initiation of steel corrosion in concrete (known as threshold Cl^- ion concentration) is an important parameter in determining the durability life and/or service life of reinforced concrete structures. When the chloride content at the surface of the reinforcement reaches the threshold value corrosion begins. A particular time is needed from the breakdown of the passive film and the formation of the first pit. From practical point of view, the initiation time can be considered as the time when the reinforcement in concrete that contains substantial moisture and oxygen, is characterized by an average sustained corrosion rate higher than 0.2 $\mu A/cm^2$ [14].

Oh *et al.* [11] conducted an experiment to investigate the threshold chloride concentration for corrosion initiation in reinforced concrete structures. The main objective of their study was to determine the threshold chloride concentration causing depassivation and active corrosion of steel reinforcement in concrete. To assess the threshold concentration of the chloride ion, the half-cell potential, the chemical composition of extracted pore solutions of concrete and the extent of corroded area of the specimens were measured. The test variables considered in the experiment were the added amount of chlorides in concrete, type of binder, and water/binder ratios. The threshold values for total chloride addition, free chloride content and $[Cl^-]/[OH^-]$ were determined for each of the various mixtures. They found that the threshold contents of total chlorides are in the range 0.45 to 0.97% by weight of the cement and the threshold values of free chlorides for all

specimens are in the range of about 0.07% to 0.13% by weight of the cement. Also, they observed that the ratios of threshold values of $[Cl^-]/[OH^-]$ are in the range 0·16 to 0·26 depending upon the type of cement or binder. They concluded that the free chloride values are more reliable to specify a limit value for corrosion initiation of reinforced concrete structures.

For a given structure, the chloride threshold for the initiation of pitting corrosion depends on various factors, which includes the concrete pH (the concentration of hydroxyl ion in the pore solution), the potential of the steel, and the presence of voids at the steel/concrete interface. The concrete pH depends on the type of cement and admixtures. Another factor that affects the threshold value is the electrochemical potential of steel. Indeed, the chloride threshold may increase by more than one order of magnitude as the potential of steel decreases. The chloride threshold has been found to depend on the presence of macroscopic voids in the concrete near the concrete-rebar interface [15].

Voids in concrete are in fact either bubbles of entrapped air or spaces left after excess water has been removed. The volume of the latter depends primarily on the water/cement ratio of the mix and to a lesser extent on concrete voids that may arise from water trapped underneath large particles of aggregate or underneath reinforcement. The air bubbles, which represent ‘accidental’ air, i.e. voids within an originally loose granular material, are governed by the grading of the finest particles in the mix and are more easily expelled from a wetter mix than from a dry one. Hence, for any given method of compaction there may be optimum water content of the mix at which the sum of the volumes of air bubbles and water space will be a minimum [16]. Those voids are normally due to incomplete

compaction and may weaken the layer of cement hydration products deposited at the steel/concrete interface, and would ultimately lead to a local acidification and sustained propagation of corrosion pits. For example, it was found that, if the volume of entrapped air in the steel-concrete interfacial zone decreases from 0.2% to 1.5% by volume, the chloride threshold increases from 0.2% to 2% by mass of cement [17].

The lower values of chloride threshold that are normally found in real structures can be explained by the presence of voids in comparison with those found in the laboratory specimens with similar materials [18]. Numerous other factors, for example temperature, the composition of cement or surface roughness of the steel reinforcement, or polarization with anodic or cathodic current, may affect the chloride threshold. The pitting corrosion has been suggested to take place above a critical ratio of chloride and hydroxyl ion [19].

It is difficult to establish a threshold concentration of chloride ions below which there is no corrosion, as far as chlorides which have ingressed into the concrete are concerned. Moreover, the distribution of chlorides within the hardened cement paste is not uniform, as found in chloride profiles in actual structures. For practical purposes, prevention of corrosion lies in controlling the ingress of chlorides by the thickness of cover to reinforcement and by the penetrability of the concrete in the cover. It is not the total chloride content that is relevant to corrosion. A part of the chlorides are chemically bound, being incorporated in the products of hydration of cement. Another part of the chlorides are physically bound, being adsorbed on the surface of the gel pores. It is only the third part of the chlorides, which is free chloride that is available for the aggressive

reaction with steel. However, the distribution of the chloride ions among the three forms is not permanent as there is an equilibrium situation such that some free chloride ions are always present in the pore water. It follows that only the chloride ions in excess of those needed for this equilibrium can become bound [16].

Practically, total chloride content can be measured more easily than the free chloride concentration; therefore the chloride threshold is expressed as the critical total chloride content. Since the amount of chlorides that can be accepted increases as the cementitious material content in the concrete increases, the critical value is usually given as a percentage of the mass of cement.

2.1.2 Propagation of Corrosion

Breakdown of the protective oxide layer is the necessary prerequisite for the initiation of reinforcement corrosion. Once this layer is destroyed by the ingress of chloride ions, corrosion will occur only in the presence of water and oxygen on the surface of reinforcement [20]. The areas that are no longer protected by the passive film act as anodic (active zones) with respect to the surrounding areas that are still passive and where the cathodic reaction of oxygen takes place. If very high levels of chlorides reach the surface of the reinforcement, the attack may involve larger areas, so that the morphology of pitting will be less evident [21].

Once the corrosion has initiated, a very aggressive environment will be produced inside the pits. In fact, current flowing from anodic areas to surrounding cathodic areas both increases the chloride content (chlorides, being negatively charged ions, migrate to the anodic region) and lowers the alkalinity (increased acidity is produced by the hydrolysis

of corrosion products inside the pits). On the other hand, the current strengthens the protective film on the passive surface since it tends to eliminate the chloride, while the cathodic reaction produces alkalinity.

Much higher level of chloride is required to initiate corrosion in structures immersed in seawater or in zones where the concrete is water-saturated, so that the oxygen supply is hindered and thus, the potential of the reinforcement is rather low [12]. Consequently, both the anodic behavior of active zones and the cathodic behavior of passive zones are stabilized. Corrosion is then accelerated (autocatalytic mechanism of pitting) and it can reach a very high rate of penetration (as high as 1 mm/year) that can quickly lead to a remarkable reduction in the cross-section of the rebars [13].

2.2 LINEAR POLARIZATION RESISTANCE METHOD VERSUS GRAVIMETRIC WEIGHT LOSS METHOD

Pradhan and Bhattacharjee [22] carried out an experimental investigation on large number of concrete specimens in order to assess by means of corrosion rate techniques, the performance of different types of rebar in chloride contaminated concrete made with different cement types. They prepared reinforced concrete specimens with three different types of steel, three types of cement, three w/c ratios and four admixed chloride contents. The corrosion rate measurement techniques considered in their work were LPR with guard ring arrangement, gravimetric (weight loss) method and AC impedance spectroscopy technique. The researchers found that the variation of corrosion current density values obtained by LPR method and that of the corresponding corrosion current density values determined by gravimetric method is very negligible as evident from a relationship given as I_{corr}(LPR) = 0.99I_{corr}(gravimetric) with corresponding regression

coefficient (R^2) of 0.989 as indicated in Figure 2.1. It is then concluded that chloride content has the strongest effect on corrosion rate followed by cement type, steel type and w/c ratio for the specimens made and tested.

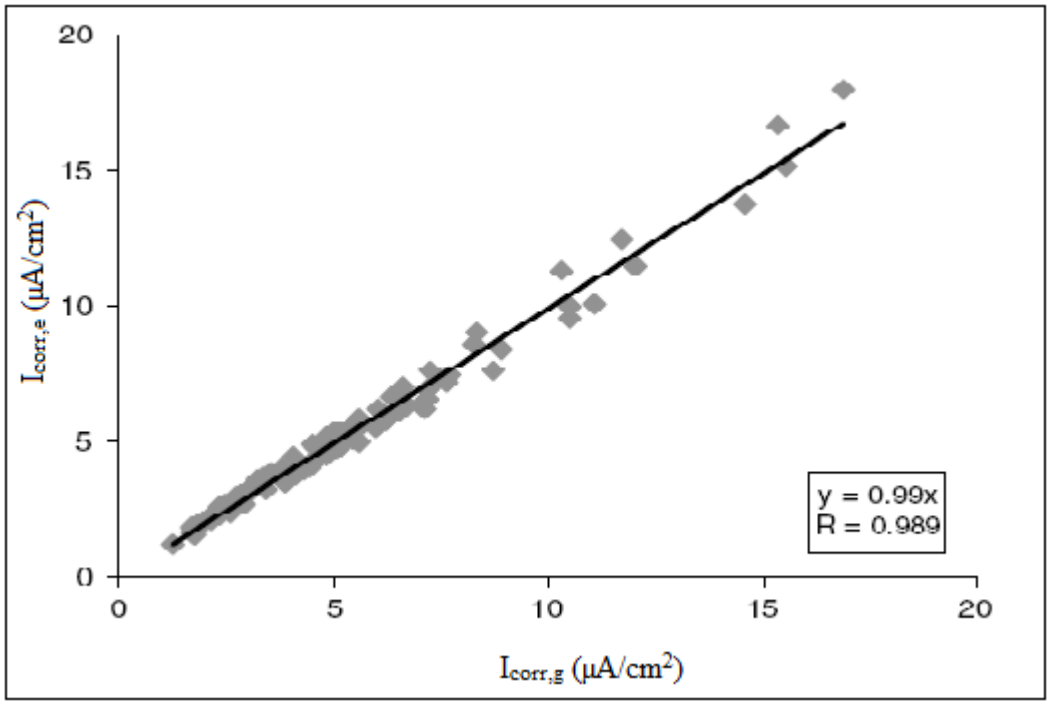

Figure 2.1: Variation between $I_{corr,e}$ and $I_{corr,g}$ [22].

Sathyanarayanan *et al*. [23] conducted an experiment to study the corrosion of steel in concrete using different corrosion rate measurement techniques. They evaluated the performance of the galvanostatic pulse technique for monitoring the corrosion of steel in concrete by comparing the corrosion rate values found by the gravimetric weight loss method and LPR technique. The steel bars were embedded in concrete of grades 15, 20, 30, and 35 MPa exposed to chloride ion concentration values of 0 to 5%. They reported that the corrosion rate values of steel in concrete depend on the strength of concrete and the chloride concentration. They also observed that the corrosion rate values obtained by

the LPR method are found to be one order of magnitude lower than that of the gravimetric weight loss method due to the inclusion of resistance of the concrete in the measured polarization resistance R_p values.

Vedalakshmi *et al*. [24] studied the long-term corrosion performance of steel bars embedded in blended cement concrete under macro cell corrosion condition. Corrosion rate values of the rebars embedded in concrete made with Portland pozzolana cement (PPC) and Portland slag cement (PSC) were compared with the one embedded in concrete made with Ordinary Portland cement (OPC). Concrete having grades of 20, 30 and 40 MPa were considered for the studies and the corrosion rate values of the rebar were determined by the gravimetric weight loss method. They reported that in the Grade 20 concrete, the corrosion rate of rebar in PPC and PSC concretes was 9 and 10 times lower than the value in OPC concrete, respectively, while in the case of Grade 30 and 40 concrete, it was 17, 6, and 1.6, 2.5 times less in PPC and PSC concretes, respectively, than in OPC concrete. Also, they observed that the reduction of corrosion rate by improved microstructure was more pronounced in 20 and 30 MPa concrete compared to OPC than in 40 MPa concrete. They concluded that improved performance of blended cement concrete in terms of corrosion rate and chloride ion penetration was attributed by the improved physical structure of concrete matrix characterized by reduced permeability to chloride and water.

Ganesan *et al.* [25] conducted an experiment to evaluate the feasibility of using bagasse ash as corrosion resisting admixture for carbon steel in concrete. They prepared baggase ash by burning boiler-fired ash at a controlled temperature of 650 ^{o}C for 1 hour. The ash

was grounded to fineness as Pozzolanic material and blended in concrete in different levels of cement replacement. The corrosion rate of steel in bagasse ash blended cement concretes exposed to alternate dry-wet cycles in 3% sodium chloride (NaCl) solution for 18 months was obtained using gravimetric weight loss, linear polarization resistance and electrochemical impedance spectroscopy techniques. It is reported that the corrosion rate of reinforcing steel and chloride penetration was slightly lowered and compressive strength was increased with the addition of bagasse ash up to 20 % replacement of cement in concrete. Also, the corrosion rate of rebar studied using gravimetric weight loss method showed a 3.6 times reduction for bagasse ash concrete with 10 % cement replacement level compared to the reference concrete. However, for all of the specimens, the corrosion rates measured by weight loss method on the rebar coupon were higher than those estimated on the basis of the I_{corr} measured by the LPR and impedance methods. Nevertheless, they concluded that the corrosion rate measured using LPR method, impedance method and weight loss method gave the same trends in the corrosion performance of reinforcing steel in bagasse ash concretes.

Hsieh *et al*. [26] studied the instantaneous corrosion rates for metals and metal alloys in industrial cooling-water systems using the gravimetric weight loss and the electrochemical polarization resistance methods. They exposed metal and metal-alloy samples to synthetic cooling water in a bench-scale recirculating system. The values obtained by both methods were related through a coefficient, *B*, defined as the constant of proportionality between weight loss and time-integrated polarization resistance. They reported that with the knowledge of *B* for a particular system, polarization resistance measurements can be used to get an accurate instantaneous corrosion rate. Hence, a

combination of both the gravimetric and the electrochemical polarization resistance methods are of particular value in the evaluation of instantaneous corrosion rates.

Zou *et al*. [27] carried out experiment to estimate the corrosion rates of mild steel for long-term immersion by electrochemical and weight loss methods. They reported that the corrosion rate values obtained using electrochemical technique coincided with that of gravimetric weight loss method during the initial immersion period while great *deviations resulted after long-term immersion*, which showed that the data obtained by electrochemical measurement was unreliable in this period. But, after calibration the electrochemical measurement result was corresponding to that of gravimetric weight loss method.

2.3 FACTORS AFFECTING SERVICE-LIFE OF RC STRUCTURES

The appearance of premature and unexpected corrosion damage in RC structures, which at the time of construction were considered of almost unlimited duration, led to the introduction of the concepts of service life and durability. The service life of a structure can be defined as the period of time in which it is able to comply with the given requirements of safety, stability, service-ability and function, without requiring extraordinary costs of maintenance and repair [28]. In an aggressive environments of coastal regions (for example the Arabian Gulf region), the useful service-life of RC structures is considerably reduced due to the severe climatic and geomorphic conditions that cause noticeable accelerated structural deterioration, the degree of which is often extensive and beyond repair [29].

Durability of concrete can be improved by many options, such as: application of coating over concrete, utilizing coated reinforcement and/or good quality concrete. Utilizing quality concrete is the cheapest option compared to other measures. A high performance or good quality concrete can be produced by using appropriate mix design, quality and grading of aggregates, good consolidation and curing, and reducing the water to cementitious materials ratio.

Therefore, in a new structure with good quality concrete, the concrete can protect the steel reinforcing bars from corrosion for the service-life of the structure. For steel embedded in uncarbonated concrete or in sound un-cracked concrete with little or no chloride, the steel is passivated, and only very low corrosion can be expected. Any corrosion-induced concrete deterioration is not likely to reach a point where repair or rehabilitation will be required during the expected service-life of the structure.

In aggressive corrosive regions, deterioration of RC structures is predominately exhibited in the form of reinforcement corrosion accompanied by severe spalling of cover concrete. For that reason, concrete structures should be designed with design requirements for structural durability specified as a priority to ensure an acceptable useful service-life of a RC structure in view of the factors affecting the service-life [3].

Additional material and design parameters to be considered include: fine aggregate, coarse aggregate, cement type, mineral admixture and water-to-cementitious materials ratio. Research studies on the effects of these design parameters with regard to service-life assessment of RC members are briefly discussed in the following sections.

2.3.1 Water-to -Cementitious Materials Ratio (w/c)

Primarily, the water to cementitious materials ratio controls the strength, durability and impermeability of concrete. When RC structures are exposed to aggressive solution, it is the permeability of concrete, which is a function of w/c ratio that affects the corrosion of rebars. The capillary porosity is in turn dependent on the water to cementitious materials ratio and the degree of hydration. Concrete permeability plays an important role in the deterioration of concrete when it is exposed to aggressive agents. Changes in the w/c do not significantly influence the resistivity at an earlier stage. The electrical resistance of concrete at 28 days with w/c varying from 0.30 to 0.50 has been found to be similar, but significantly altered at 90 days. The resistivity of concrete with a w/c of 0.3 is much more than that of concretes with w/c of 0.4 or 0.5 at 90 days [30].

A number of studies have been conducted to investigate the effect of w/c ratio of concrete on the service life of reinforced concrete structures. Park *et al* [31] conducted an experiment to investigate the influence of w/c on chloride ingress of reinforcing steel in concrete. Ordinary Portland cement, river sand, and crushed stone with a maximum size of 25 mm were used to produce concrete mixtures. Densities of fine and coarse aggregates were 2.60 and 2.65g/cm^3, respectively. A sulfonate naphthalene superplasticizer (SP) was used to get a workable fresh concrete. The mix proportions for concrete mixtures were prepared with w/c ratios of 31%, 42%, and 50% and the target slumps were 180 ± 20 mm to 210 ± 20 mm. Chlorides were added in series in the mixtures of test specimens with different contents 0.3, 0.6, and 0.9 kg/m^3. They found that the critical chloride content for steel corrosion and the diffusion coefficient for chloride ion were influenced by the w/c ratio. Specifically, they observed that the

diffusion coefficient for chloride ions decreased with decreasing w/c ratio. Also, as expected, the compressive strength of concrete cylinders increased with decreasing w/c ratio. Life-365 program was used to predict the service life of RC structures exposed to chloride environment. It was found that the service life increases with decreasing w/c ratio. Therefore, they concluded that w/c ratio as well as concrete cover greatly influenced the service life of RC structures.

Chalee *et al* [32] studied the effect of w/c ratio on cover depth required against the corrosion of embedded steel in the fly ash cement concrete in marine environment. Fly ash was used to partially replace Type I cement at 0%, 15%, 25%, 35%, and 50% by weight of the cementitious material. Water to cementitious material ratios (w/c) of fly ash cement concretes were varied at 0.45, 0.55, and 0.65. 200-mm concrete cube specimens were cast and steel bars with 12-mm diameter and 50 mm in length were inserted in the concrete with a cover depth of 10, 20, 50, and 75 mm. The specimens were cured in water for 28 days, and then placed in the tidal zone of marine environment. Subsequently, the concrete specimens were tested for the compressive strength, chloride penetration profile and corrosion of embedded steel bar after being exposed to tidal zone for 2, 3, and 4 years. The results showed that the Type I cement concrete exhibited higher rate of chloride penetration than fly ash cement concrete. It was found that a decrease in the w/c ratio reduced the cover depth required for the initial corrosion of the steel bar, as shown in Figure 2.2.

Oh *et al* [33] reported that free chloride content increases with an increase in the w/c ratio, as indicated in Figure 2.3. It was noted that w/c influences greatly the chloride binding properties of concrete.

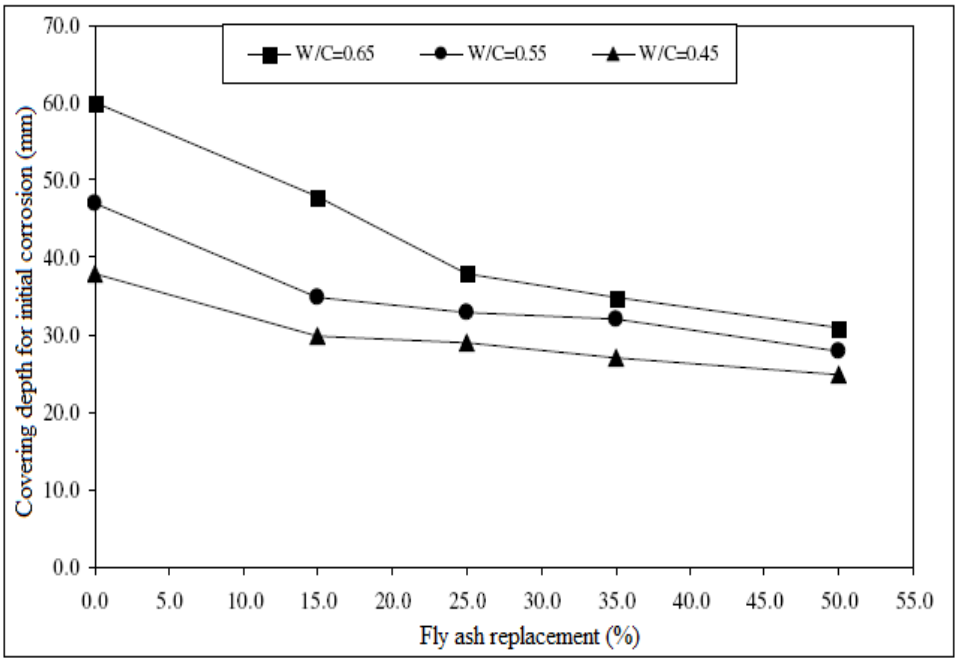

Figure 2.2: Variation of required cover depth (for initial corrosion of embedded steel bar in concrete) with fly ash and w/c ratios [32].

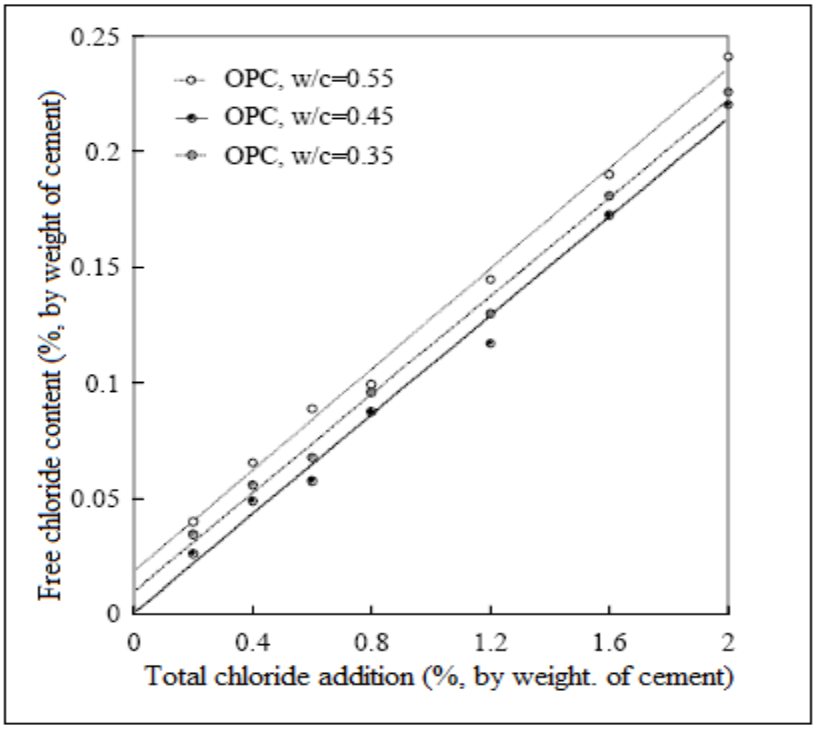

Figure 2.3: Relation between total chloride content and free chloride content for different w/c ratios [33].

2.3.2 Cementitious Materials Content

The water to cementitious materials ratio alone does not determine the resistance of concrete to chloride penetration, but the type of cementitious material used greatly affects the chloride penetrability of the resulting concrete. The nature of the cementitious materials to be used is of vital importance under the conditions of exposure. The cementitious materials content in concrete has a significant effect on its durability. Insufficient quantities of cement may result in loss of strength and the development of honeycombs within the concrete microstructure as a result of improper bonding of the concrete constituents. The honeycombs consequently lead to deeper penetration and diffusion of corrosion-causing agents, i.e., Cl^-, H_2O, O_2, CO_2, etc., in concrete [34]. This results in initiating reinforcement corrosion due to the formation of differential cells. In addition, the concrete with low cement content lacks plastic consistency and alkalinity. The formation of a stable passive layer against corrosion on the surface of the reinforcing bars is thus retarded [35].

Oh *et al.* [33] reported that the free chloride content is higher in the case of Type V sulfate-resisting portland cement (SRPC) compared to Type I ordinary Portland cement (OPC) at the same total chloride addition. This indicates that the chloride binding capacity of SRPC is lower than that of OPC. This is due to the different binding of chloride ions by tricalcium aluminate (C_3A) in cements. Figure 2.4 shows the influence of cement content on the chloride binding capacity.

Furthermore, the cement paste formed by the hydration reactions contains pores of different sizes. These include: the gel and capillary pores. The interlayer spacing within

the calcium silicate hydrate (C-S-H) has a volume equal to about 28% of the gel and dimensions ranging from a few fractions of a nanometer (nm) to several millimeters (mm). These effects do not affect the durability of concrete and its protection of the reinforcement, because they are too small to allow the significant transport of aggressive species.

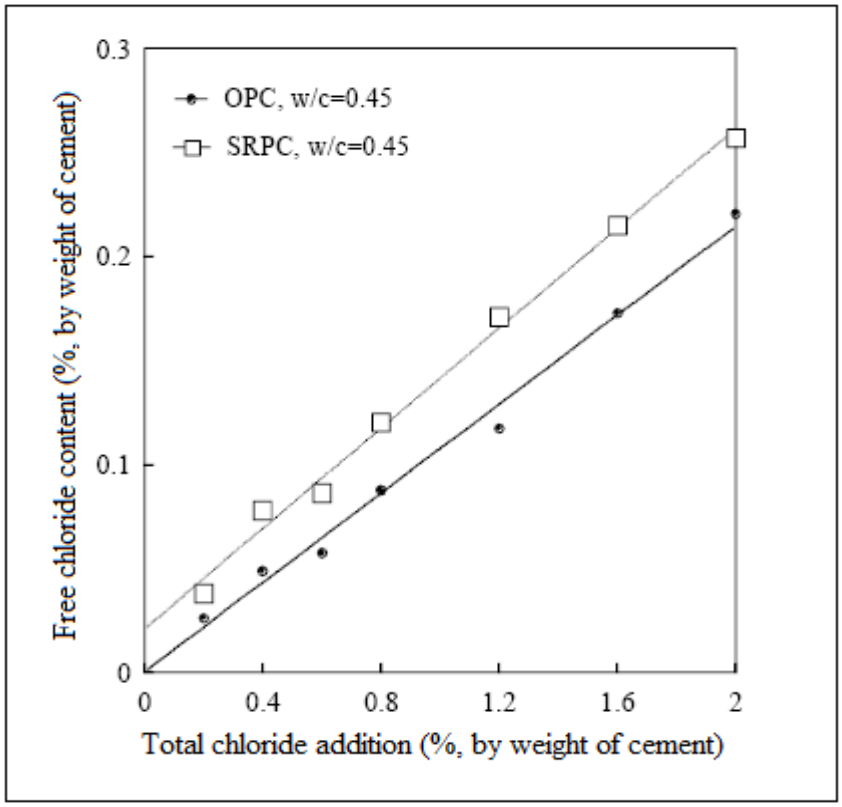

Figure 2.4: Effect of cement content on chloride binding with w/c = 0.45 [33].

The capillary pores are voids not filled by the solid products of hydration of hardened cement paste. They have dimensions of 10-50 nm if the cement paste is well hydrated and produced with low water-cementitious material ratios but they can reach to 3-5 μm if the concrete is made with high water-cementitious material ratios or is not well hydrated. Capillarity is relevant to the durability of concrete and its protection of the rebars [28].

There is an increasing evidence to show that the reaction of C_3A with chloride is only one of the several mechanisms for effective removal of chloride ions from the solution. This reaction removes chlorides from the pore water, and it reduces the amount of free chlorides available to participate in the unfavorable depassivation mechanism and corrosion processes. The amount of free chloride ions in the pore water is more important than the amount of total chloride ions [30]. In ordinary Portland cements (OPC), there is no direct relationship between the concentration of chloride ions and C_3A content. There is, however, a qualitative relationship with the combination of both tricalcium aluminate (C_3A) and tetra calcium alumino ferrite content (C_4AF) and pH of the pore solution [36].

Mehta [37] has cited several examples of concrete sea structures built with high C_3A cements that showed excellent durability performance because they were prepared with rich mixes in conjunction with attendant low w/c ratio. On the other hand, structures prepared with lean mixes deteriorated prematurely. Therefore, due to the beneficial role of C_3A in binding chlorides and reducing the chloride ion diffusivity, as stated above, cement with high C_3A content is preferred from the durability point of view. Page *et al.* [38,39] reported 2.5 times higher diffusivity of chloride ions in hardened cement paste prepared with Type V cement compared to that prepared with Type I cement. Thus, the conjoint effect of higher chloride complexing ability and of the reduced chloride ion diffusivity of high C_3A cements enables them to perform better than low C_3A cements in terms of corrosion protection.

While high C_3A cements are preferred from the reinforcement corrosion point of view, such cements are susceptible to sulfate damage when exposed to soil and ground water contaminated with chloride/sulfate soils [40]. In such situations, the use of Type V

cement does usually provide adequate protection against sulfate attack, but it would fail to remove free chlorides to any extent, for the simple reason that up to 8% C_3A in the cement is preferentially consumed by the 4 to 5% gypsum typically added to all Portland cements to regulate the setting time. In such situations, a useful approach would be to generally specify, for both substructures and superstructures, a moderate C_3A (8 to 9%) cement modified with suitable supplementary cementing materials. Such cement would be simultaneously resistant to sulfate attack and chloride-induced reinforcement corrosion.

2.3.3 Supplementary Cementing Materials

An admixture can be defined as a chemical product which, except in special cases, is added to the concrete mix in quantities no more than 5% by mass of cement during mixing or during an additional mixing operation prior to the placing of concrete, for the purpose of achieving a specific modification to the normal properties of concrete. Admixtures may be organic or inorganic in composition but their chemical character, as distinct from material from mineral, is their essential feature [16].

Fly ash as a cementitious material is used extensively all across the world and is known to enhance the *sustainability of concrete* by alleviating concerns related to environmental pollution and green house gas emissions. Incorporation of fly ash as a mineral admixture in concrete directly, facilitates reduction in water demand for the same workability, and, achieves improvement in microstructure through pozzolanic reactivity. However, pozzolanic reaction of fly ash with lime (CH) liberated from reactions of dicalcium silicate (C_2S) and tricalcium silicate (C_3S) with water may result in a small reduction in

alkaline content of concrete. Alkalinity of concrete, together with other factors, is known to contribute to protection capacity of concrete against rebar corrosion [41].

Amleh *et al* [42] reported that the concrete with supplementary cementitious material exhibited a lower level of corrosion because of its lower permeability. However, Oh *et al* [33] pointed out that the effect of mineral admixtures on the chloride binding is not large at early ages, as indicated in Figure 2.5.

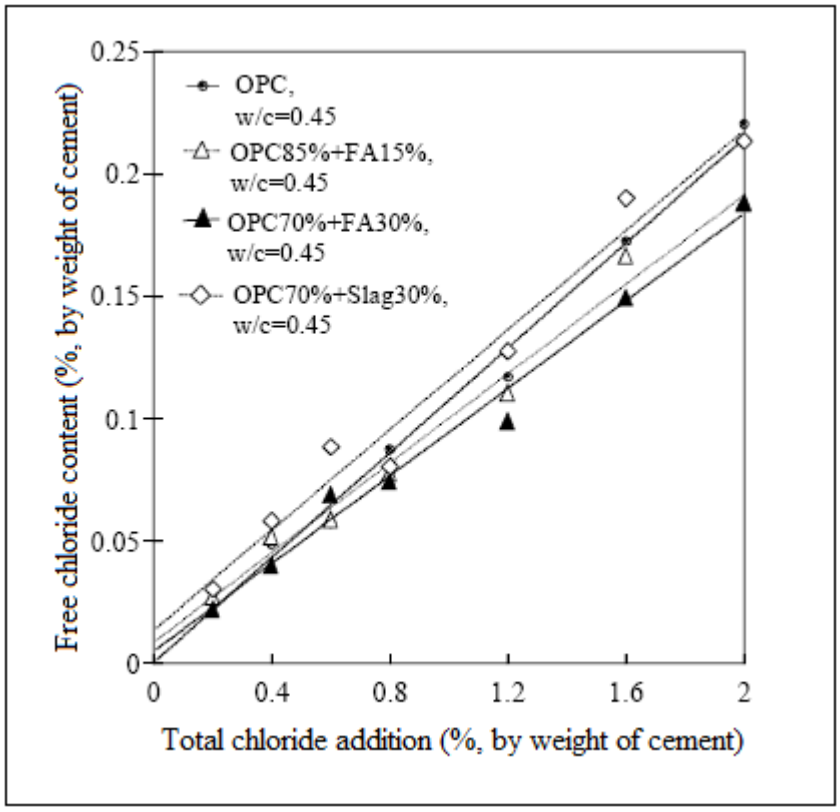

Figure 2.5: Relation between total chloride content and free chloride content for different types of mineral admixture [33].

According to Shekarchi and Moradi [43], if modified concrete with additional silica-fume cures well, it will have a positive effect on the corrosion of steel in concrete by increasing the electrical resistivity. Bhattacharjee [41] also reported that for the same grade of concrete, long term permeability of un-cracked fly ash concrete is lower and resistance to

moisture penetration is significantly higher compared to OPC concrete. In addition, for the same exposure conditions the electrical resistivity of fly ash cement concrete is 3-5 times more than that of OPC concrete. He concluded that RC members cast with concrete incorporating fly ash, has much longer service life against rebar corrosion, even for flexural members with micro-cracks in the tension zone, compared to OPC concrete members.

Chalee *et al.* [44] carried out an experiment to investigate the utilization of fly ash concrete in marine environment for long-term design life analysis. The specimens used were 200 mm cubes containing 0%, 15%, 25%, 35%, and 50% fly ash as a replacement of Type I cement. Concrete had w/c ratios of 0.45, 0.55, and0.65. Reinforcing bars with a diameter of 12 mm and a length of 50 mm were embedded in the concrete specimens at cover depths of 10, 20, 50, and 75 mm. After curing for 28 days, the concrete specimens were exposed to two wet-dry conditions daily. After exposure to this environment for 2, 3, 4, 5 and 7 years, the specimens were dry-cored and tested to determine the chloride penetration profile and chloride content at the position of the embedded steel bar. Chloride concentrations were determined using the acid-soluble chloride method, resulting in the total chloride content (by weight of binder) in concrete. Besides, the concrete cubes were cored to obtain cylindrical concretes of 50 mm in diameter and100 mm in length. The compressive strength of the cored concretes was determined and the result was the average of 3 specimens. Finally, the 200 mm concrete specimens were then crushed, and the corrosion of the embedded steel bars was measured in terms of the percentage of the rusted area. They found that, an increase in fly ash replacement in concrete clearly reduced the chloride penetration, chloride penetration coefficient, and

steel corrosion. Figure 2.6 indicates the chloride penetration profiles of Type I and fly ash cement concretes with w/c ratio of 0.45 after 7-year exposure in a marine environment. It shows that the chloride content in the fly ash cement concrete is less than in the plain cement concrete.

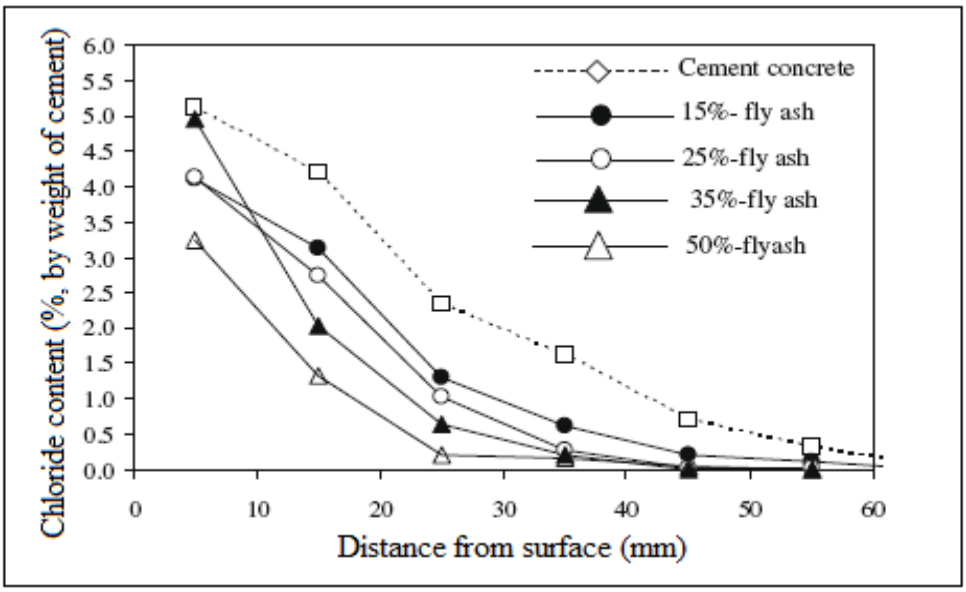

Figure 2.6: Chloride penetration profiles of fly ash concretes with a w/c of 0.45 at 7-year exposure in a marine environment [44].

2.3.4 Concrete Cover over Reinforcing Bars

Cover thickness is one of the major factors affecting the service life of RC structures. To reduce or delay the initiation and corrosion time in RC structures in an aggressive environment, the concrete must be of good quality. Besides concrete quality, a minimum value of the concrete cover also has to be specified. The cover depth of concrete required to protect against the initial corrosion of embedded steel bar is defined by the penetration depth of threshold chloride in concrete. The threshold chloride values were determined from the amount of chloride required to cause the initial corrosion of the steel bars embedded in the concrete specimens. By implication, it will take a longer time for the

aggressive substances, such as chloride, moisture or carbon dioxide, to migrate to the rebar surface. In RC structural members, exposed to chlorides and subjected to intermittent wetting, the degree of protection against corrosion is determined primarily by the depth of concrete cover to the reinforcing steel and the permeability of concrete [45]. The concrete cover depth has a significant effect on corrosion either due to carbonization or penetration of chlorides [46].

The concrete cover significantly influences the time-to-corrosion of the steel reinforcing bars, and its quality influences the diffusion rate of chloride ions through the concrete. As this diffusion is non-linear with increasing cover thickness, there is a significant increase in the time required for chloride ions to reach the steel reinforcing bars [30]. David and Kenneth [47] performed a sensitivity analyses for the time to corrosion of reinforced concrete structures exposed to early, continuous, and constant chloride ion exposure conditions. They found that the concrete cover is the most sensitive parameter for each of the three exposure conditions. Also, increasing the concrete cover will have the largest impact on increasing the time to corrosion initiation and service life of the concrete structure, as shown in Figure 2.7. However, practical increases in cover likely limit the increase in time to corrosion to approximately 70% to 80%. Park *et al.* [31] found that the effect of chloride content in concrete and concrete cover on the critical chloride content was insignificant, as evidenced in Figure 2.8. On the other hand, they observed that concrete cover greatly influenced the service life of RC structures. Moreover, cover depth (CD) of concrete required to protect against the initial corrosion of embedded steel bar is defined by the penetration depth of threshold chloride in concrete. In their studies, Chalee *et al.* [44] established a relationship between the required cover depth to protect

against the initial corrosion of embedded steel bar and the exposure period of fly-ash concrete using a logarithm function.

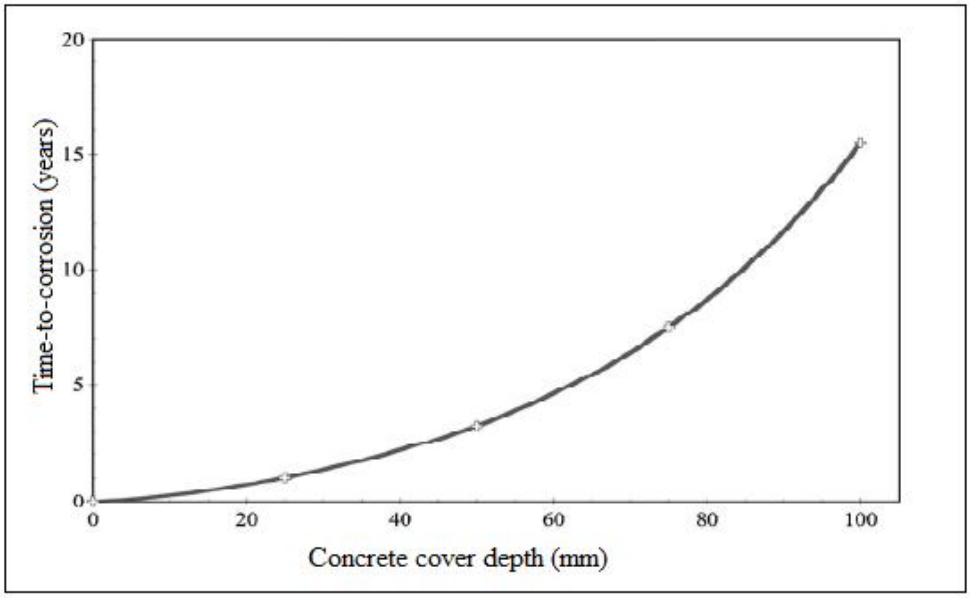

Figure 2.7: Influence of concrete cover on time to corrosion [47].

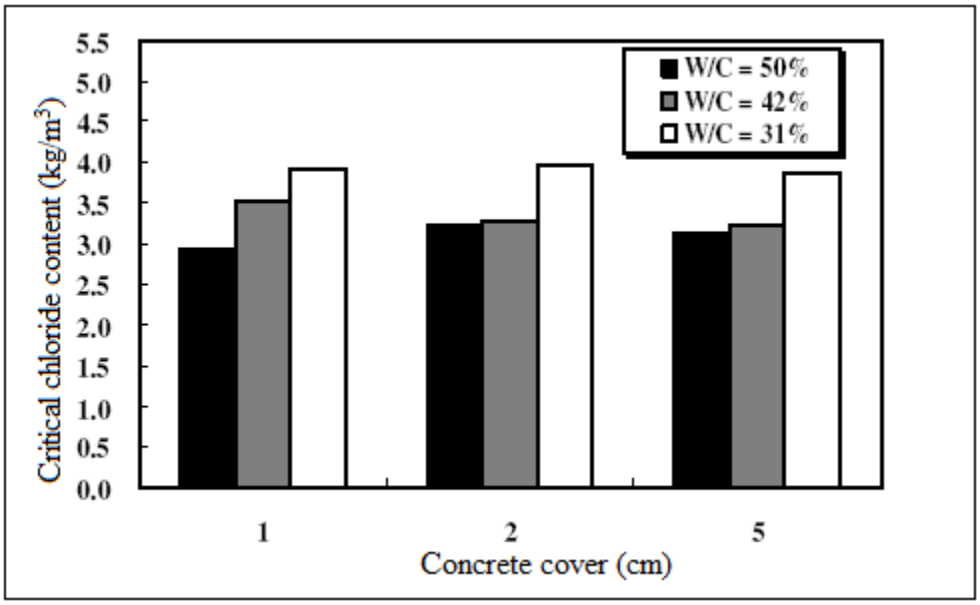

Figure 2.8: Effect of concrete cover on critical chloride content of concrete [31].

Typical values of reported minimum concrete cover thickness for concrete durability are listed Table 2.1 (Bertolini *et al.* [28]).

Table 2.1: Recommended minimum values of concrete cover thickness [28].

Exposure condition		Minimum cover thickness, mm	
		Reinforced concrete	Prestressed concrete
No risk of corrosion or other attacks		10	10
Carbonation-induced corrosion	Dry or permanent wet	15	25
	Wet, rarely dry, moderate humidity	25	35
	Cyclic wet and dry	30	40
Chloride-induced corrosion	Exposed to air borne salt but not in direct contact with sea water, moderate humidity	35	45
	Permanently submerged, wet. Rarely dry	40	50
	Tidal, splash and spray zones, cyclic wet and dry	45	55

2.3.5 Aggregate Quality, Size and Gradation

Aggregates occupy 60% to 75% of the concrete volume; therefore, it is not surprising that its quality is of considerable importance to strength and durability of concrete structures. The aggregate may not only limit the strength of concrete, but the properties of aggregate greatly affect the durability and structural performance of concrete [16]. Aggregates must conform to certain standards for optimum engineering use. They must be clean, hard, strong, durable, and free of absorbed chemicals, coating of clay and other fine materials in amounts that could affect hydration and bond with the cement paste. Aggregate particles that are friable or capable of being split are undesirable. The essential

requirement of an aggregate for concrete is that it remains stable within the concrete and in the particular environment throughout the design life of the concrete.

Aggregate characteristics can be divided into two groups: physical features (particle size, shape and texture) and quality features (strength, density, porosity, hardness, elastic moduli, chemical and mineral composition, etc.). Smaller size aggregates produce high strength concrete, and the particle shape and texture affect the workability of fresh concrete and the strength of hardened concrete. Properties, such as the particle size and shape, which are influenced by selective crushing and the use of the appropriate type of crusher for the particular rock type, as well as the cleanliness in terms of fines and clay content, have great influence on the water requirement of the concrete. The strength and durability properties of hardened concrete may also be affected by any change in the water demand. The aggregates in concrete mainly affect its workability, unit weight, elasticity and strength to a large extent; these properties depend on the grading and the proportions of fine and coarse aggregates. The chemical or mineralogical characteristics of the aggregates are less important than the physical characteristics, such as shape and size of particles, and distribution of voids within a particle. But with regard to concrete durability and reinforcement corrosion, the behavior of the interface between concrete and aggregate is of major concern [4].

The aggregate shape also influences the concrete permeability. The use of elongated and flaky aggregates significantly increases the permeability and thereby producing very porous under-aggregate fissures and zones. This results in a weak transition zone, in which micro-cracks can easily form. These micro-cracks are influential contributing

factors that unfavorably increase the permeability of concrete. Both the aggregate size and grading affect concrete durability. The maximum size of the aggregate is of considerable significance, as the mix water decreases with the increase of aggregate due to a reduction in the surface area [6]. Therefore, theoretically, owing to different binding capacity at aggregate and cement paste interface, physical characteristics, such as size, shape and surface roughness, have a great effect on concrete durability and reinforcement corrosion [4].

2.4 SERVICE-LIFE PREDICTION MODELS FOR RC STRUCTURES

The residual service life for an RC structure in corrosive environments at any time may be taken as the *time remaining for the crack to develop* at concrete surface due to rust expansion. There are various models [48-52] available in the literature for service-life prediction. In addition to these models, experimental techniques are also available for predicting the service-life. Some of the models and experimental techniques available for service-life prediction are summarized in the following subsections.

2.4.1 Models for Time of corrosion initiation due to chloride penetration

The time to corrosion initiation due to chloride penetration (t_p) can be obtained from Fick's second law of non-stationary diffusion as follows:

$$t_p = \frac{1}{12D_{app}}\left[\frac{C_v}{1-\left(C_{th}/C_s\right)^{0.5}}\right]^2 \tag{2.1}$$

where C_v = cover thickness (mm)

C_{th} = threshold chloride concentration (%)

C_s = chloride concentration at the concrete surface (%)

D_{app} = apparent diffusion coefficient for chloride (m^2/s)

The following range of values may be used as C_{th}, C_s and D_{app}:

C_{th} = 0.05 to 0.07 % of Cl^- by weight of concrete

C_s = 0.3 to 0.4 % of Cl^- by weight of concrete

$D_{app} = 10^{-12}$ to 10^{-11} m^2/s

2.4.2 Models for Time to Cracking

Due to the importance of modeling on initiation and progress of cracking process of RC structures, the following key studies on the subject have been reported in the literature:

i) Bazant's Mathematical Models

Bazant [48] proposed a simplified mathematical model for predicting time-to-cracking of concrete cover for corrosion of reinforcement exposed to seawater. The model considered various chemical and physical phenomena regarding chloride-induced reinforcement corrosion, and the model is based on the following basic assumptions:

i) One-dimensional oxygen and chloride transport through concrete cover.

ii) Steady-state corrosion and rust production after depassivation.

iii) Density of original steel versus the rust product.

The model also defines the time-to-cracking in terms of electrochemical properties: corrosion rate, dimensional properties: cover depth, bar spacing, physical properties:

density of steel and density of rust product, and mechanical properties of concrete: tensile strength, modulus of elasticity, Poisson's ratio, and creep coefficient.

Based on Bazant's model, the formula for time of concrete cover cracking is given by:

$$t_{cor} = \rho_{cor} \frac{D\,\Delta D}{pJ_r} \tag{2.2}$$

In which $\rho_{cor} = \left[\frac{1}{\rho_r} - \frac{0.583}{\rho_{st}}\right]^{-1} \frac{\pi}{2} = 3.6\ \text{g/cm}^3$, and (2.3)

p is the perimeter of bar

D is the diameter of the bar

ΔD is the change in diameter of the bar

J_r is the rate of rust production

ρ_{cor} is a function of the mass densities of steel and rust.

ρ_r is the density of rust

ρ_{st} is the density of steel

ii) Morinaga's Model

Based on field and laboratory data, empirical equations, suggested by Morinaga [50], can be used for predicting the time to cracking. It is assumed that cracking of concrete will first occur when there is a certain quantity of corrosion product that is formed on the reinforcement. The amount is given by:

$$Q_{cr} = 0.602\left(1+\frac{2C_v}{D}\right)^{0.85} D \quad (2.4)$$

in which Q_{cr} is the critical mass of corrosion products (10^{-4} g/cm^2);

C_v is the cover to the reinforcement (mm)

D is the diameter of reinforcing bar (mm).

The time for cracking to take place is then given by

$$t_{cor} = \frac{Q_{cr}}{J_r} \quad (2.5)$$

in which $J_r = \left(\frac{W}{F}\right) I_{corr}$ (2.6)

where J_r (g/cm^2/day) is the instantaneous corrosion rate. The electrochemically measured value of I_{corr} can be converted to the instantaneous corrosion rate, J_r, using Faraday's equation with the equivalent weight of steel, *W*=27.925 g and Faraday's constant, *F*=96487 Coulombs (or Amp-sec). According to Morinaga's equations, the time to cracking is a function of the corrosion rate, concrete cover and bar size.

iii) Wang and Zhao's model

Wang and Zhao [51] have suggested a step method of using finite element analysis to determine the thickness Δ of the corrosion product, corresponding to the time duration when the surface concrete cracks. Further, by analyzing a large number of rebar corrosion data collected from laboratory and comparing them with the results of finite element analysis, the authors have established an empirical expression to determine the ratio of thickness Δ of corrosion product, to the depth H of rebar penetration, corresponding to

the cracks in cover concrete. The ratio (Δ/H) is termed as expansion coefficient, γ and has been expressed as a function of cube strength of concrete, f_{cu}, as:

$$\frac{\Delta}{H} = \gamma = 0.33\left(\frac{D}{C_v}\right)^{0.565} f_{cu}^{1.436} \tag{2.7}$$

Using the value of Δ obtained through the finite element model, the value of H corresponding to cracks in cover concrete can be obtained. Further, the value of H can be used to determine the time necessary for longitudinal cracking of concrete cover, t_{cor} as:

$$t_{cor} = \frac{H}{P_r} \tag{2.8}$$

where P_r is corrosion penetration rate in mm/yr.

This model can be used only in conjunction with the finite element model requiring the determination of Δ.

iv) Dagher and Kulendran's model

Dagher and Kulendran [52] have also carried out a finite element modeling of corrosion damage in concrete structures. This numerical model is rather versatile for estimating the radial bar expansion Δ, as it includes:

- options for modeling crack formation and propagation,
- options to accept any shape of corrosion around the rebars,
- ability to incorporate dead and live load stress and initial shrinkage and temperature cracks in the analysis, and

- pre-and post-processing modules which offer automatic mesh generation and visual representation of crack propagation.

In the context of service life prediction of RC structures subjected to rebar corrosion, this model can be used more reliably to determine the radial bar expansion Δ, at which the cracks in cover concrete would occur.

2.4.3 Experimental Methods for Service-life Prediction

Oslakovic *et al.* [53] conducted an experiment to evaluate the service life design models on concrete structures exposed to marine environment. The structure considered in their study is Krk Bridge which has been exposed to a very aggressive marine environment for over 25 years. Based on collected materials data and the exposure conditions, the service life of this structure is estimated using three currently available predictions models, two deterministic models, the North American Life-365 model and Croatian CHLODIF model, and the DuraCrete probabilistic method. A chloride analysis was performed on the bridge structure and then a statistical analysis was done based on the collected data to determine the dependence of structural serviceability on the exposure zone and material's parameters.

Chloride contents (total amount of chlorides) which depend on the mass of cement were determined experimentally by standard laboratory method. Concrete powder was sampled on site and in the laboratory from concrete cores. Samples were taken from horizontal and vertical surfaces on the structure by18-mm diameter drill, minimum of three holes were drilled at each location and the samples were pulverized for chloride determination.

The measured chloride profiles have been analyzed to derive the chloride surface concentration (C_S values) and these computed data have been used as a basis for the further analysis. The surface chloride concentration is determined by adjusting representative chloride profiles along with the Crank's solution of Fick's second law of diffusion using error function and then extrapolating the curve to the surface. After determining the chloride profiles, the chloride diffusion coefficient was calculated for the representative chloride profiles by curve fitting along with the defined solution of Fick's second law by means of inverse error function.

It was found that Life-365 model gives higher chloride concentration comparing to the experimental values of chloride concentrations, but this is mainly due to the input of design value of chloride surface concentration, which includes dissipation of results and safety coefficient. However, *CHLODIF* model gives very close or lower values of chloride concentrations compared to the experiment alones in the atmospheric zone, while in the splash zone the calculated chloride profiles are mostly close to or above the experimental ones.

For the probabilistic performance-based service life design according *DuraCrete* model, theoretical values of input parameters showed greater deviations for the concrete types of good quality. Specifically, the predicted reliability of the structure was higher than that actually found. This was clearly due to the unrealistic prediction of a large reduction in diffusion coefficient with time for the type of cement used, which clearly does not correspond to the real in-field situation. The theoretical value of the age factor is 0.65 and 0.85, respectively. It is, therefore, suggested that this parameter should be further investigated and compared with the actual condition of structures in operation after a

longer period of time. Experimental input parameters correspond very well to the results of calculation when the age factor was set to the values of 0.20 and 0.25. The authors conclude that service life design models should be further calibrated against empirical data. In the case when experimental input parameters were used in calculations, the results obtained using mathematical models showed much better match with the real state after 25 years in operation for all the zones of the environmental influences.

Vu and Steward [54] carried out an experiment to determine the service life of RC slab exposed to aggressive environment by the probability of cracking and spalling of concrete cover. The time to corrosion cracking/spalling is investigated from accelerated corrosion testing of RC slabs with the emphasis on the relationship between concrete quality (w/c ratio, or strength), concrete cover, crack propagation and time. The probability of cracking and spalling of concrete cover is calculated by using a structural deterioration life-cycle reliability model. Experimental studies were conducted, where typical RC specimens (slabs) were subject to accelerated levels of corrosion. The accelerated corrosion experimental program is designed to simulate the corrosion of a section of a typical bridge deck structure. The tests consisted of two series. The first series of tests comprised of four specimens (two specimens had 25 mm cover; the other two had 50mm cover). All specimens had the same water-cement ratio (w/c=0.5), but differences in mix designs resulted in different concrete strengths. The second series of tests isolated the effect of w/c ratio and cover. These specimens had w/c = 0.45 and w/c = 0.58 and 25 mm and 50 mm covers. All specimens were 700 mm x 1000 mm rectangular slab with thickness of 250 mm. The top mat of the slab contained four steel reinforcing bars, which were covered with electroplating tape to give exposed (bare steel) lengths of

1000 mm. Ordinary Portland cement was used in the mix and 3% of $CaCl_2$ by weight of cement were added to the concrete mix in order to induce corrosion along the length of exposed bars. The active accelerated corrosion process was achieved by applying an electrical current to the bars. The soffit of the specimen was immersed in a 5% NaCl solution. A current was then supplied to the bar (the anode) by a power supply *via* a current regulator and the cathode was a stainless steel plate submerged in the NaCl solution. After testing, the weight loss of the reinforcement bars due to corrosion was measured according to the gravimetric weight loss method. The weight loss corresponded closely to that expected from I_{corr} measurements.

All of the experimental slabs had been designed for the purpose of studying the effect of concrete cover, with the cover being either 25 mm or 50 mm. As expected, it is observed that concrete cover influenced crack propagation for experimental slabs at 25mm and 50mm at different w/c ratios (i.e. 0.45; 0.5; 0.58). It is noted that the cracking patterns at the cross sections were quite similar for both 25 mm and 50 mm cover. It was observed that the time length (in years) of crack propagation (t_{ser}) at 50 mm cover is about 1.15; 1.2; 1.4 times that observed for 25 mm cover slabs at 0.45; 0.5; 0.58 w/c ratios, respectively. However, it was observed that the effect of concrete cover was not significant when crack widths were less than 0.15 mm to 0.25 mm. The influence of w/c ratio was studied by keeping slabs at the same cover but having different w/c ratios. It was observed that increasing w/c ratio resulted in increased crack propagation rates by up to 30% and 40% for 25 mm and 50 mm cover respectively. On the other hand, as was observed for concrete cover, the w/c ratio appears to mostly influence crack propagation when the crack width exceeds 0.15 mm to 0.3 mm.

2.4.4 Prediction of Residual Load Bearing Capacity of RC Members

Several studies on the prediction of residual load bearing capacity of corroded reinforced concrete members have been reported in literature. The models suggested in the literature can be used to predict the residual flexural strength and to estimate the remaining service life of a given RC structures in corrosive environments. Some of the models are discussed below:

Azad and Ahmad [55] proposed a procedure to predict the residual strength of a corroded beam. The moment capacity M_{thu} of the beam, the corrosion penetration rate P_r and alpha (α-factor) are determined from the following equations:

$$M_{thu} = f_y \times A_s \times \left[d - \frac{0.5 f_y A_s}{0.85 b f_c^{'}} \right] \tag{2.9}$$

$$P_r = \frac{W}{F \gamma_{st}} I_{corr} \tag{2.10}$$

$$\alpha = \frac{2 P_r T}{D} \tag{2.11}$$

Then the theoretical moment capacity $M_{th,c}$, correction factor C_f, predicted residual strength M_{res} and the percentage residual flexural strength R of the beam are determined from the following expressions:

$$M_{th,c} = f_y \times A_s (1-\alpha)^2 \times \left[d - \frac{0.5 f_y A_s (1-\alpha)^2}{0.85 b f_c^{'}} \right] \tag{2.12}$$

$$C_f = \frac{5.0}{D^{0.54} (I_{corr} T)^{0.19}} \leq 1.0 \tag{2.13}$$

$$M_{res} = C_f M_{th,c} \tag{2.14}$$

$$R = \left(M_{res} \Big/ M_{th,c} \right) \times 100 \tag{2.15}$$

where f_y = tensile strength of steel (N/mm^2)

A_s = area of steel (mm^2)

d = depth of the beam (mm)

b = width of the beam (mm)

f_c = concrete compressive strength (N/mm^2)

F = 96500 A-s, W = 27.925 g

$\gamma_{st} = 7.85 g / cm^3$

T = corrosion period (year)

P_r = corrosion penetration rate (μm/year)

D = diameter of rebar (mm)

Jin and Zhao [56] developed an empirical model for determining the percentage residual flexural strength of the corroded beams in terms of the percentage reinforcement corrosion.

Castel *et al.* [57] studied the mechanical behavior of corroded reinforced concrete beams. They reported that the concrete cracking created by corrosion of compressive reinforcement does not significantly influence the mechanical characteristics of the reinforced concrete beams in service. Therefore, they proposed two factors to explain the mechanical behavior of corroded reinforced concrete beams (for a typical example of

35% loss of stiffness and unsymmetrical behavior) considering the reduction in the steel cross-section and the reduction in the local steel-concrete bond strength in the tensile zone. Analysis of the state of corrosion of tensile reinforcements showed that the maximum degree of corrosion (20%), located in the central part of the beam, was not enough to explain the loss of stiffness (35%) recorded on the beam strength, according to current standard reinforced concrete structural calculations. The deterioration of steel-concrete bond strength in the tensile zone may contribute greatly to the deterioration in the behavior of corroded structural elements in service. Hence, results obtained on ultimate behavior of some typical corroded reinforced concrete beams show that the loss in steel-concrete bond strength has no influence on flexural capacity of reinforced concrete and the residual bearing capacity can be assessed by taking into account *only* the reduction in the tensile steel cross-section (when the corrosion of the compressive reinforcements does not lead to significant damage). Finally, a ductility reduction by about 70% was observed. This effect is at least as unfavorable to the safety of the reinforced concrete structures as is the reduction in ultimate strength. This loss of ductility could be attributed to a loss of ductility of the tensile steels due to corrosion damage.

Aziz [58] conducted an experiment on slabs, each having dimensions of 305×711×63.5 mm, with a center-to-center span of 610 mm and reinforced with 6 mm diameter bars at 57 mm center-to-center spacing and with a 9.5 mm clear cover. The main objective of the work is to find out the effect of reinforcement corrosion on the flexural capacity of the slab. The specimens were partially immersed in a 5% sodium chloride solution and subjected to a constant electrical current of 2 Amperes. He found that there is sharp

reduction in the ultimate flexural strength of slabs with up to 20% reinforcement corrosion; thereafter, with further increase in reinforcement corrosion, the strength decreased more slowly. The reduction in the ultimate flexural strength of slabs with 5% reinforcement corrosion was 25%, while it was 60% in the slabs with 25% reinforcement corrosion.

Mangat and Elgarf [59] researched the developing relationship between the degree of reinforcement corrosion and the residual strength of flexural members through an experimental scheme. They induced a different degree of accelerated reinforcement corrosion in concrete beams reinforced with longitudinal bars, without representing countervailing interactions with stirrup (shear) reinforcement since shear reinforcement was provided externally. They found that reinforcement corrosion in concrete has a marked effect on both the flexural load capacity and deflection of beams and the reduction in residual strength is primarily due to the loss or breakdown of the steel/concrete interfacial bond.

Uomoto and Misra [60] studied the relationship between the corrosion and the load carrying capacity of the concrete structures. They conducted an accelerated corrosion test by immersing the concrete members in a solution of sodium chloride and applying a constant electrical current density to the reinforcement of about 280 - 380 $\mu A/cm^2$ for a period of 7 to 14 days. They tested a set of beams with dimensions of 100×100×700 mm and reinforced with 2 - 10 mm diameter bottom bars. They found that most of the beams failed in shear. Also, they tested another set of beams each with dimensions of 200×100×2100 mm and reinforced with 2 to 6 mm diameter top bars, 2 to 16 mm diameter bottom bars and 6 mm diameter shear reinforcement at 170 mm spacing. The

beams failed in compression of concrete with buckling of the top bars (no links existed at the constant moment span). The reduction of the load-carrying capacity of this beam was not caused simply by the reduction of the effective area or the reduction in strength of reinforcing bars, but by the cracks formed by the corrosion process. Weight loss of about 1% to 2.4% in the main reinforcing bars (16 mm diameter) corresponded to approximately 4% to 17% of reduction in the load carrying capacity.

2.5 STRUCTURAL DURABILITY-BASED DESIGN OF RC STRUCTURES

For carrying out structural durability design of a reinforced concrete member, two main effects of degradation in concrete and steel should be considered:

- loss of concrete cover leading to reduced cross-sectional area of the concrete due to surface deterioration caused by different types of weathering mechanisms in outdoor conditions, such as fluctuations in temperature and moisture, leaching of minerals from concrete, and physical salt weathering.
- loss of steel cross-sectional area, bond between steel and concrete, and loss of concrete cover in spalling due to reinforcement corrosion caused by a combination of concrete carbonation and chloride penetration.

Sarja and Vesikari [61] have proposed the following *two approaches for structural durability design* of reinforced concrete members:

(1) Separated design method:

In this method, the ordinary mechanical design (i.e., calculation of width *b*, depth *h*, and rebar diameter *D* considering only the dead and live loads) of the member is first performed separately using a conventional design method. The design is then finalized by

calculating *final dimensions* b_o, h_o, and D_o by simply adding the durability parameters, i.e., values of $c'(t_d)$ and $d'(t_d)$ to b, h, and D, as follows:

$$b_o = b + 2c'(t_d) \tag{2.16}$$

$$h_o = h + 2c'(t_d) \tag{2.17}$$

$$D_o = D + 2d'(t_d) \tag{2.18}$$

(2) Combined design method:

In this method, set the expression for reduced width, $b'(t_d)$ and reduced depth, $h'(t_d)$ of the concrete member (in terms of the final dimensions b_0 and h_0) by substituting $c'(t_d)$ in Eqs. 2.19 and 2.20, respectively. Set the expression for reduced rebar diameter, $D'(t_d)$ (in terms of the final rebar diameter D_0) by substituting $d'(t_d)$ in Eq. 2.21. This way the durability parameters are combined before the final dimensions b_0, h_0, and D_0 would be calculated using a conventional design method considering the given dead and live loads.

$$b'(t) = b_o - 2c'(t) \tag{2.19}$$

$$h'(t) = h_o - 2c'(t) \tag{2.20}$$

$$D'(t) = D_o - 2d'(t) \tag{2.21}$$

Anoop *et al*. [62] have also proposed a methodology for durability-based design of reinforced concrete flexural members that ensures acceptable performance under service loads. The performance measures considered are safety (or collapse) and serviceability (or cracking) of the RC member with respect to chloride-induced corrosion of reinforcement. In the proposed methodology, the uncertainties arising due to the use of linguistic terms for describing the exposure conditions and quality of construction are

taken into account by considering the time for corrosion initiation and the variables affecting the rate of corrosion as fuzzy variables. The efficacy of the proposed methodology in predicting the corrosion damage to the structural members has been demonstrated through a practical case study.

2.5.1 Determination of the Rate of Loss of Concrete and Steel

a) Model for rate of loss of concrete

The model for evaluating the rate of deterioration of surface concrete subjected to aggressive exposure conditions, excluding frost attack, is given as follows [63];

$$C_r = \frac{c_{env}\, c_{cur}}{f_{ck}^{3.3}} \tag{2.22}$$

where:

C_r = the rate of loss of structurally effective concrete (mm/year)

c_{env} = the environmental coefficient

c_{cur} = the curing coefficient

f_{ck} = the characteristic cubic compressive strength of concrete at 28 days (MPa)

The c_{env} in the Gulf region within latitude 10^0 – 30^0 can be assumed to be within the range of 10,000 to 500,000 [63]. The curing coefficient, c_{cur}, may be calculated by using the following equation [64].

$$c_{cur} = \frac{1}{0.85 + 0.17 \log_{10}(d)} \tag{2.23}$$

where d = the curing time (days).

The rate of loss of structurally effective concrete, C_r, is calculated by using Eq. (2.22). Then loss of surface concrete, $c'(t)$, leading to reduced cross-sectional area of concrete, at any exposure time, t, may be calculated by using Eq. (2.24), as follows:

$$c'(t) = C_r\, t \tag{2.24}$$

By using $c'(t)$ calculated from Eq. (2.24), the residual width $b'(t)$ and the residual depth $h'(t)$ of the concrete member at any exposure time, t, may be calculated by using Eqs. (2.19) and (2.20), where b_o and h_o are the original width and depth of the member, respectively.

b) Model for calculating reinforcement corrosion penetration rate

The value of corrosion penetration rate P_r can be calculated by using Eq. (2.10); the loss of the rebar diameter $d'(t)$ leading to a reduced cross-sectional area of steel at any exposure time t may be calculated using Eq. (2.25).

$$d'(t) = P_r t \tag{2.25}$$

By using $d'(t)$ calculated from Eq. (2.25), the reduced diameter of rebar $D'(t)$ at any exposure time t may be calculated using Eq. (2.26),

$$D'(t) = D_o - 2d'(t) \tag{2.26}$$

where D_o is the original diameter of rebar.

CHAPTER 3

METHODOLOGY OF RESEARCH

The present work was carried out in four steps. Firstly, reinforcement corrosion rates were measured electrochemically and gravimetrically on a total number of 486 reinforced concrete specimens corroded under different chloride exposures over a period of about three years. Reinforcement corrosion rates measured electrochemically and gravimetrically were used to examine the correlation between the results obtained using these two different methods (one of these is non-destructive but lacks accuracy and other is accurate but destructive). Secondly, using the corrosion rate data, models were developed statistically for the prediction of reinforcement corrosion. Thirdly, a step-by-step procedure for predicting the service-life of corroded RC structures was developed demonstrating the use of correlation for converting electrochemically measured reinforcement corrosion rate into more accurate equivalent gravimetric rate before using it for service life prediction. Finally, an approach for durability-based design of RC structures is outlined illustrating the use of corrosion rate models developed in terms of concrete mixture key variables, cover thickness, and chloride exposure concentration.

3.1 MATERIALS

3.1.1 Cementitious Materials

ASTM C 150 Type I Portland Cement was used for this study. Silica fume was added to all the mixtures. The chemical composition of the Portland cement and silica fume used in the preparation of the concrete mixtures is shown in Table 3.1.

Table 3.1: Chemical composition of Portland cement and silica fume.

Constituent (wt %)	Type I cement	Silica fume
Silica (SiO_2)	19.92	98.7
Alumina (Al_2O_3)	6.54	0.21
Ferric oxide (Fe_2O_3)	2.09	0.046
Lime (CaO)	64.70	0.024
Magnesia (MgO)	1.84	-
Silicate (SO_3)	2.61	0.015
Potassium Oxide (K_2O)	0.56	0.048
Sodium Oxide(Na_2O)	0.28	0.085
Tri calciumsilicate (C_3S)	55.9	-
Dicalcium silicate (C_2S)	19	-
Tricalcium aluminate (C_3A)	7.5	-
Tetracalciumaluminoferrite (C_4AF)	9.8	-

3.1.2 Aggregates

The concrete mixtures were prepared with aggregates obtained from two geographically distant quarries in Abu-Hadriyah and in Taif regions of the Kingdom of Saudi Arabia. The aggregates from Abu-Hadriyah and Taif were designated as H-type and T-type, respectively. The specific gravity and water absorption were determined as per ASTM

C 128 [65] and abrasion resistance was determined as per ASTM C 131. These values are given in Table 3.2. Dune sand was used as fine aggregate. The specific gravity and absorption of fine aggregate were 2.6 and 0.57%, respectively.

Table 3.2: Specific gravity, absorption and abrasion test results of the coarse aggregates.

Aggregate source	Specific gravity	Water absorption (%)	Abrasion loss (%)
Abu-Hadriyah (H)	2.55	1.75	28.86
Taif (T)	2.82	1.27	37.84

3.2 DETAILS OF TEST SPECIMENS

Cylindrical concrete specimens with a centrally placed reinforcing bar of height 150 mm and diameters 66 mm, 91 mm and 116 mm, with three different cover thicknesses of 25 mm, 37.5 mm and 50 mm were prepared for the determination of corrosion rate. Epoxy coating was applied to the steel bar at the bottom and at the interface between the concrete and air to avoid the initiation of corrosion at those critical places as shown in Figure 3.1 [66].

3.3 PREPARATION OF TEST SPECIMENS

3.3.1 Mix Design

The absolute volume method [16] was used for the concrete mix design and the quantity of each constituent was calculated on the basis of weight. All the concrete mixtures were prepared with 8% silica fume. The following mix design variables were used to prepare the concrete mixtures:

i) Cementitious materials content: 350, 375 and 400 kg/m^3

ii) Water to cementitious materials ratio: 0.40, 0.45 and 0.5

iii) Fine-to-total aggregate ratio: 0.35, 0.4 and 0.45

iv) Types of course aggregates (Abu Hadriyah (H) type and Taif (T) type)

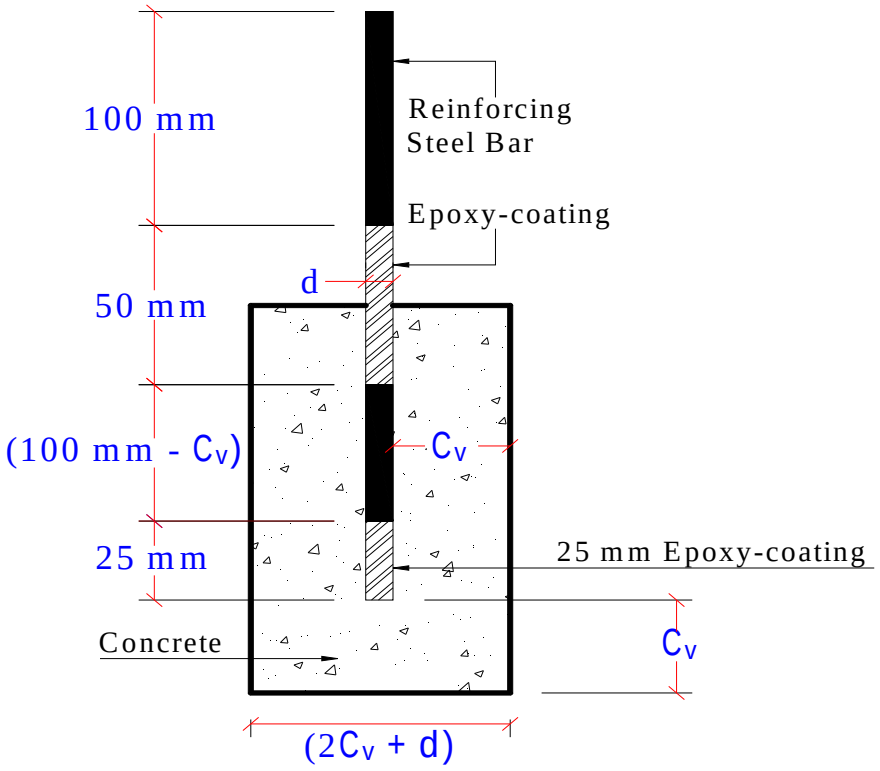

Figure 3.1: Details of test specimens used for corrosion rate measurements.

A superplasticizer was used in low water-cement ratio concrete mixtures to enhance the workability. Design parameters used for preparing concrete test specimens to determine corrosion rates are shown in Table 3.3. The total number of the cylindrical concrete test specimens was 486.

3.3.2 Mixing and Casting of Test Specimens

Preparation of concrete mixtures proceeded as follows: *Firstly*, fine and coarse aggregates were mixed individually. *Afterward*, cement and silica fume were mixed separately. A homogenous concrete was obtained with all the constituents mixed together with the addition of potable water and with a superplasticizer mixed uniformly with the constituents to enhance the workability. Then, to achieve uniform consistency and cohesiveness without segregation, the concrete constituents were mixed in a revolving drum type mixer for one minute.

Table 3.3: Parameters for reinforced concrete specimens for corrosion rate measurements.

Parameter	Levels	No. of case studies
Effective water/cementitious materials ratio (by mass)	0.4, 0.45, 0.50	3
Cementitious materials content	350, 375, 400 kg/m^3	3
FA/TA ratio (by mass)	0.35, 0.40, 0.45	3
Aggregate types	2 (H and T aggregates)	2
Cement type	1 (Type-1)	1
Mineral admixtures	1 (8% silica fume by weight of cement) (28, 30, 32 kg/m^3)	1
Cover thickness	25 mm, 37.5 mm, 50 mm	3
Chloride concentration	3%, 7% and 12% NaCl	3

The moulds were oiled and the reinforcing steel bars were placed in their position in the moulds, the concrete was then poured into the cylindrical moulds in three layers and the concrete was consolidated by vibrating the molds over a vibrating table. This procedure was used to prepare all the 486 test specimens.

3.3.3 Curing and Exposure of specimens

The test specimens were demolded after 24 hours of casting. All the specimens were then cured for a period of 28 days in water tanks under laboratory conditions and the specimens were then partly submerged in chloride solution to allow corrosion to take place**.** The specimens were exposed to 3%, 7% or 12% NaCl solution. Some of the test specimens exposed to the chloride solution are shown in Figure 3.2.

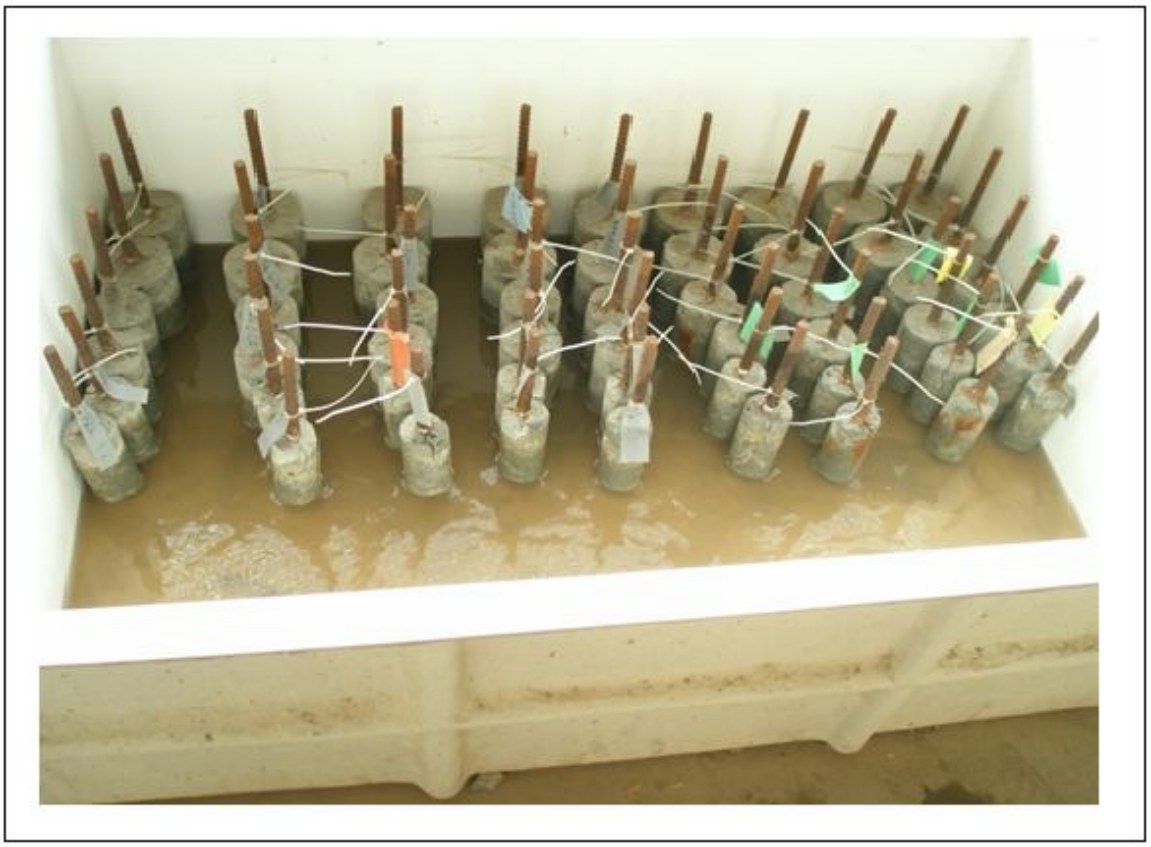

Figure 3.2: Some of the concrete specimens exposed to the chloride solution.

3.4 EXPERIMENTAL TECHNIQUES

3.4.1 Electrochemical Technique (LPRM)

The most commonly used electrochemical technique for measuring rate of reinforcement corrosion, i.e., linear polarization resistance method (LPRM), was utilized to determine the corrosion current density (I_{corr}). The test equipment used was PARSTAT 2273 potentiostat that was manufactured by PRINCETON (USA) [67]. The experimental set-up for LPR measurements is shown in Figure 3.3.

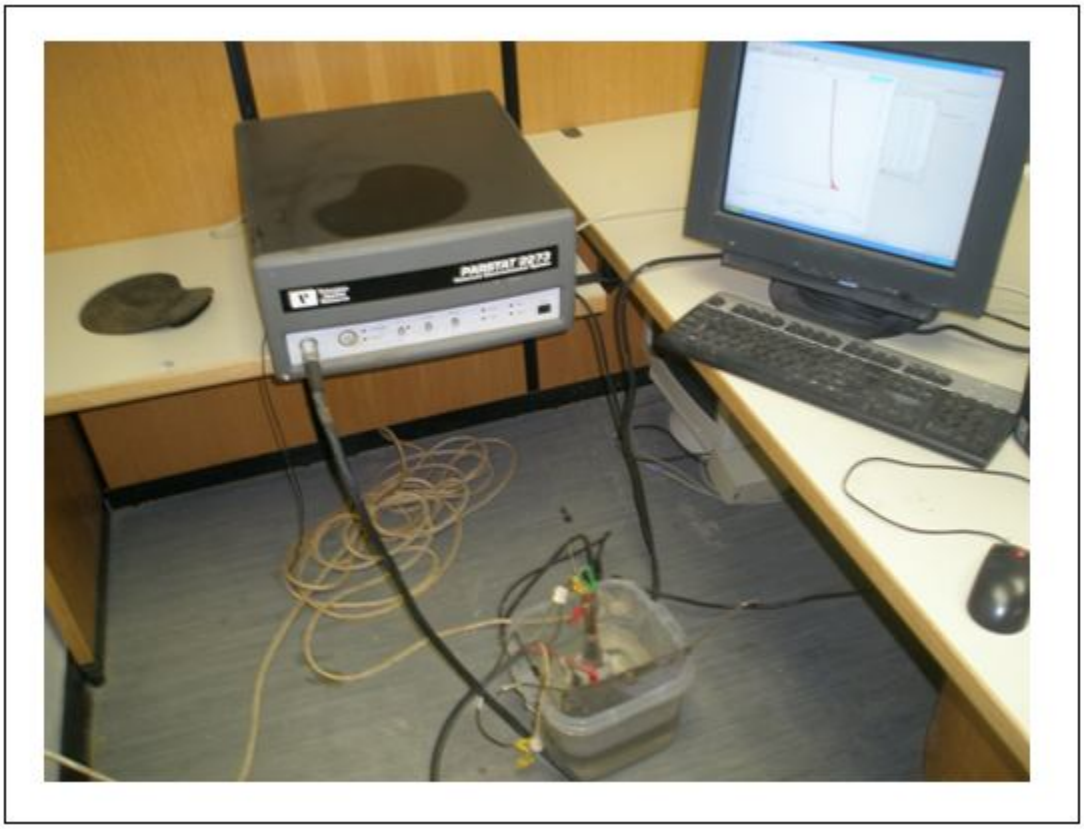

Figure 3.3: Experimental set-up for the LPR measurements [67].

LPRM has been developed from the Stern-Geary theory [35, 67] as a method of evaluating the instantaneous corrosion rate of a metal. In case of reinforced concrete, the

method is restricted mainly because of a concrete resistance, unknown area of the polarized reinforcement and non-uniform corrosion. The measurement of corrosion current density was performed using a three-electrode system: i) reference electrode (which is used as another half-cell forming thereby a complete cell), ii) counter electrode (which is used to apply the external electrical signal) was connected to the respective terminals of the potentiostat, iii) steel reinforcement in the concrete specimen (often known as the working electrode). The working electrode was polarized to ±20 mV from its equilibrium potential at a scan rate of 0.166 mV per second. After a suitable initial delay, typically 60 seconds, the steel was polarized.

The slope of the applied potential versus measured current plot is used to determine the linear polarization resistance, R_p. The corrosion current density is then calculated using the following relationship:

$$I_{corr} = \frac{B}{R_p} \tag{3.1}$$

where:

I_{corr} = corrosion current density ($\mu A/cm^2$)

R_p = polarization resistance ($k\Omega\ cm^2$)

$$B = \frac{\beta_a \beta_c}{(\beta_a + \beta_c)2.303} \tag{3.2}$$

β_a = anodic Tafel constant

β_c = cathodic Tafel constant

The Tafel constants are generally obtained from a Tafel plot [35], but, in the absence of the plot, a value of B equal to 52 mV for steel in passive state and a value equal to 26

mV for steel in active state can be used. For steel in aqueous media, equal values of β_a and β_c of 120 mV have been used. The value of '*B*' used in this test was 26 mV. Details of the governing equations of electrochemistry (namely: Butler-Volmer equations) utilized to derive the polarization curve are given in Appendix A.

3.4.2 **Gravimetric Weight Loss Method** (GWLM)

Following the electrochemical (LPRM) test, the concrete specimens were broken for the determination of corrosion rate by gravimetric weight loss method. The set-up used for breaking of specimens is shown in Figure 3.4.

Figure 3.4: Set-up for breaking of test specimens.

Preparation, cleaning and estimation of the weight loss were done according to ASTM G1-03 [68]. The cleaning solution used was 1,000 ml of hydrochloric acid with 20 g of antimony trioxide and 50 g of stannous chloride.

The weight loss W_l was calculated as:

$$W_l = W_i - W_f \tag{3.3}$$

where:

W_i = initial weight of the bars before corrosion (g), and

W_f = weight of the bars after cleaning all rust products (g)

The corrosion rate was determined using the following equation:

$$P_r = \frac{1.116 \times 10^7 \times W_l}{A \times T} \tag{3.4}$$

where:

P_r = corrosion penetration rate (μm/year)

W_l = weight loss (g)

A = exposed surface area of rebar (cm^2)

T = exposure time (hours)

The corrosion penetration rate was then converted to I_{corr} using the following formula:

$$I_{corr} = {}^{P_r}\!/_{11.7} \, (\mu A/cm^2) \tag{3.5}$$

It is noted here that P_r was computed for all test specimens based on a reference value of W_i for a steel bar segment with L_i = 5 cm.

Samples of the corroded steel bars obtained from the test specimens before and after cleaning are shown in Figures 3.5 and 3.6.

3.4.3 **Scanning Electron Microscopy** (SEM)

SEM was performed on the concrete specimens of varying w/c ratio of 0.4, 0.45 and 0.5 in order to study the effect of w/c ratio on the concrete morphology. The following procedure was followed:

1) Fractured samples were obtained from the concrete specimens with w/c ratio of 0.4, 0.45, and 0.5 and they were coated with gold.
2) Using SEM machine (JEOL SEM JSM-5800 LV) shown in Figure 3.7, the images of the concrete samples were captured. Images were carried out at 10,000 magnification using secondary electron mode.

Figure 3.5: Samples of corroded rebars before cleaning.

Figure 3.6: Samples of corroded rebars after cleaning (L_i = 5 cm) for all pieces

Figure 3.7: Scanning Electron Microscope (SEM) machine [69].

CHAPTER 4

RESULTS AND DISCUSSION

4.1 COMPILATION OF REINFORCEMENT CORROSION RATE DATA

The values of reinforcement corrosion rate measured in terms of corrosion current density using the electrochemical and gravimetric methods are presented in Tables 4.1 and 4.2 for Abu Hadriyah (H) aggregates and in Tables 4.3 and 4.4 for Taif (T) aggregates.

4.1.1 Compiled Experimental Data for H-type aggregates

Table 4.1 shows the corrosion current density determined by LPRM for concrete specimens prepared with H-type aggregates. The highest and lowest values of the corrosion current density were noted to be 15.80 $\mu A/cm^2$ and 0.39 $\mu A/cm^2$, respectively. It is observed that there is an increase in the corrosion current density with an increase in the water/cementitious materials ratio. It was also observed from the results that, corrosion current density decreases with an increase in the cover thickness. Another point to be noted is that there is a significant decrease in the rate of corrosion when the cover is increased from 25 to 37.5 mm while the decrease in I_{corr} is not that significant when the cover is increased from 37.5 to 50 mm. The average percentage decrease in I_{corr} when the cover was increased from 25 to 37.5 mm was 37% while it was only 17% when the cover was increased from 37.5 to 50 mm for 3% NaCl solution exposure. For 7% NaCl solution

Table 4.1: Corrosion Current Density for H- Specimens by LPR Method

Mix	w/cm ratio (by mass)	Cementitious material content (kg/m^3)	FA/TA ratio (by mass)	Corrosion current density, I_{corr}($\mu A/cm^2$)								
				3% NaCl solution exposure			7% NaCl solution exposure			12% NaCl solution exposure		
				25mm cover	37.5mm cover	50mm cover	25mm cover	37.5mm cover	50mm cover	25mm cover	37.5mm cover	50mm cover
H1	0.40	350.00	0.35	7.85	1.61	0.92	5.99	2.08	0.92	6.21	1.83	2.21
H2	0.40	350.00	0.40	7.86	2.52	1.15	6.45	2.80	2.86	7.64	3.06	0.39
H3	0.40	350.00	0.45	7.01	3.41	2.60	7.58	3.26	0.48	8.07	3.37	1.18
H4	0.40	375.00	0.35	8.48	4.47	2.49	9.02	4.57	2.04	8.59	3.53	2.11
H5	0.40	375.00	0.40	8.71	4.37	2.50	10.69	5.27	2.87	9.52	4.57	3.39
H6	0.40	375.00	0.45	9.57	5.13	3.86	10.30	5.21	4.68	10.12	4.07	5.15
H7	0.40	400.00	0.35	9.68	5.26	5.73	11.61	6.55	4.84	10.98	4.10	4.57
H8	0.40	400.00	0.40	10.79	5.91	5.70	11.35	5.45	5.35	11.68	6.96	5.84
H9	0.40	400.00	0.45	11.72	7.69	5.36	12.01	7.33	5.35	12.85	5.87	6.19
H10	0.45	350.00	0.35	10.39	5.20	5.18	12.00	7.35	5.71	12.37	8.00	6.76
H11	0.45	350.00	0.40	9.80	4.40	5.44	11.03	4.66	5.52	13.60	8.59	6.91
H12	0.45	350.00	0.45	9.68	5.74	6.36	11.99	5.50	6.69	12.03	7.52	6.03
H13	0.45	375.00	0.35	9.30	6.26	6.86	12.45	6.49	5.20	13.04	7.90	6.76
H14	0.45	375.00	0.40	10.20	8.19	5.96	12.84	6.16	5.79	13.18	7.88	6.88
H15	0.45	375.00	0.45	10.20	8.87	5.66	12.10	6.59	5.58	13.32	8.55	7.05
H16	0.45	400.00	0.35	9.74	8.42	6.88	13.14	7.65	6.14	13.69	8.43	7.14
H17	0.45	400.00	0.40	13.51	7.33	6.83	13.58	7.21	5.48	14.01	8.70	7.99
H18	0.45	400.00	0.45	12.78	8.86	6.07	13.21	8.41	6.43	14.55	8.61	7.50
H19	0.50	350.00	0.35	12.17	7.67	7.11	14.41	8.12	5.15	14.48	7.76	6.21
H20	0.50	350.00	0.40	12.08	7.34	6.74	14.49	9.33	7.07	15.50	9.23	7.20
H21	0.50	350.00	0.45	10.73	8.15	6.71	14.96	9.39	7.25	14.21	9.35	7.13
H22	0.50	375.00	0.35	10.07	8.66	7.97	14.33	9.17	7.37	14.42	9.88	7.42
H23	0.50	375.00	0.40	11.11	9.77	7.37	14.62	10.16	7.30	15.45	10.85	8.71
H24	0.50	375.00	0.45	12.87	9.48	8.09	13.39	10.34	8.76	15.80	10.86	8.83
H25	0.50	400.00	0.35	11.42	8.00	8.34	14.16	10.25	8.08	14.42	11.83	8.94
H26	0.50	400.00	0.40	12.26	8.61	8.27	13.61	11.97	8.26	15.23	12.11	8.80
H27	0.50	400.00	0.45	12.81	10.52	7.04	15.22	10.86	7.96	14.58	11.99	9.17

Table 4.2: Corrosion Current Density for H- Specimens by Gravimetric method

Mix	w/cm ratio (by mass)	Cementitious material content (kg/m^3)	FA/TA ratio (by mass)	Corrosion current density, $I_{corr}(\mu A/cm^2)$								
				3% NaCl solution exposure			7% NaCl solution exposure			12% NaCl solution exposure		
				25mm cover	37.5mm cover	50mm cover	25mm cover	37.5mm cover	50mm cover	25mm cover	37.5mm cover	50mm cover
H1	0.40	350.00	0.35	6.83	2.11	1.11	6.36	2.70	1.60	6.57	2.00	1.36
H2	0.40	350.00	0.40	7.34	2.28	0.48	7.60	1.32	1.75	7.85	2.16	0.98
H3	0.40	350.00	0.45	7.14	2.67	1.42	6.84	2.25	1.61	7.93	3.22	1.90
H4	0.40	375.00	0.35	7.46	2.67	1.40	7.63	3.65	2.76	8.83	3.56	3.33
H5	0.40	375.00	0.40	7.40	3.02	3.30	8.38	3.69	3.10	8.80	4.27	3.34
H6	0.40	375.00	0.45	8.13	4.27	3.90	8.33	3.67	4.58	8.06	4.15	4.35
H7	0.40	400.00	0.35	8.06	4.41	4.18	8.78	5.05	4.61	8.03	5.38	4.40
H8	0.40	400.00	0.40	8.80	4.25	4.23	8.98	5.40	5.22	9.84	5.84	5.75
H9	0.40	400.00	0.45	8.97	5.71	4.09	9.21	7.31	5.07	9.98	7.06	5.98
H10	0.45	350.00	0.35	9.21	5.76	4.70	9.80	7.43	6.01	11.10	7.74	6.29
H11	0.45	350.00	0.40	9.26	5.43	4.94	8.31	6.09	5.39	12.44	7.50	6.35
H12	0.45	350.00	0.45	9.77	5.16	5.03	8.35	7.96	6.50	11.40	9.07	5.02
H13	0.45	375.00	0.35	10.21	5.90	5.89	10.79	6.51	6.36	11.36	7.20	5.84
H14	0.45	375.00	0.40	9.46	6.27	5.73	9.70	7.40	7.20	12.53	11.02	6.46
H15	0.45	375.00	0.45	9.42	6.11	4.89	9.97	6.83	5.61	11.16	7.47	6.62
H16	0.45	400.00	0.35	10.74	6.21	5.48	12.58	6.18	5.59	13.06	7.12	5.56
H17	0.45	400.00	0.40	10.79	5.33	5.76	9.93	6.03	3.26	11.98	7.14	7.04
H18	0.45	400.00	0.45	11.13	6.73	4.77	10.67	6.85	5.36	10.63	5.82	4.80
H19	0.50	350.00	0.35	11.28	6.84	5.83	10.92	6.86	5.46	8.99	6.00	5.31
H20	0.50	350.00	0.40	8.53	6.38	4.52	11.53	6.80	6.70	8.44	8.09	7.53
H21	0.50	350.00	0.45	9.84	6.09	4.08	11.79	9.50	8.64	9.20	7.91	6.98
H22	0.50	375.00	0.35	11.45	8.30	7.81	10.23	9.44	8.42	10.03	8.14	5.57
H23	0.50	375.00	0.40	10.32	6.76	7.03	10.64	6.72	5.95	13.68	6.68	8.85
H24	0.50	375.00	0.45	11.13	8.44	7.50	12.48	10.48	8.44	8.72	8.83	7.27
H25	0.50	400.00	0.35	11.49	7.05	7.63	12.34	9.70	6.96	10.43	7.99	7.07
H26	0.50	400.00	0.40	11.63	7.89	6.49	10.56	9.18	7.83	10.82	6.10	6.73
H27	0.50	400.00	0.45	10.52	8.56	6.80	11.32	8.39	7.63	10.16	9.34	7.20

Table 4.3: Corrosion Current Density for T-Specimens by LPR Method

Mix	w/cm ratio(by mass)	Cementitious material content (kg/m^3)	FA/TA ratio(by mass)	Corrosion current density, $I_{corr}(\mu A/cm^2)$								
				3% NaCl solution exposure			7% NaCl solution exposure			12% NaCl solution exposure		
				25mm cover	37.5mm cover	50mm cover	25mm cover	37.5mm cover	50mm cover	25mm cover	37.5mm cover	50mm cover
T1	0.40	350.00	0.35	5.04	1.06	1.17	6.20	2.45	1.16	6.65	2.68	1.55
T2	0.40	350.00	0.40	6.05	2.48	1.85	6.26	3.23	2.50	6.55	2.22	1.26
T3	0.40	350.00	0.45	6.45	2.73	2.17	6.62	2.56	2.18	5.25	3.35	2.24
T4	0.40	375.00	0.35	7.77	2.72	2.56	7.76	2.86	2.36	7.13	2.89	1.48
T5	0.40	375.00	0.40	6.43	3.56	2.94	8.07	3.34	3.73	8.73	4.20	4.12
T6	0.40	375.00	0.45	7.17	3.74	3.19	8.15	3.93	3.54	8.15	3.80	3.76
T7	0.40	400.00	0.35	8.64	3.81	2.86	7.97	4.58	2.28	8.98	4.79	3.00
T8	0.40	400.00	0.40	8.72	4.49	3.66	8.20	4.55	3.59	9.19	4.83	4.16
T9	0.40	400.00	0.45	9.31	4.75	3.35	9.01	5.10	3.73	9.29	4.93	4.33
T10	0.45	350.00	0.35	9.08	4.16	3.84	10.60	5.71	3.80	10.23	5.64	4.41
T11	0.45	350.00	0.40	9.16	4.91	4.15	10.05	6.02	4.08	10.89	6.59	5.04
T12	0.45	350.00	0.45	9.50	5.30	4.38	10.16	6.81	4.60	10.51	6.97	5.46
T13	0.45	375.00	0.35	8.39	5.31	4.31	10.74	6.58	5.13	11.52	7.07	5.97
T14	0.45	375.00	0.40	8.04	5.18	4.59	9.40	5.57	5.16	10.34	7.28	5.71
T15	0.45	375.00	0.45	8.69	5.69	5.15	9.84	6.83	5.74	11.28	7.78	6.54
T16	0.45	400.00	0.35	9.97	6.64	4.69	10.41	6.52	5.22	11.57	7.25	6.70
T17	0.45	400.00	0.40	10.87	5.58	4.05	11.99	6.78	6.09	12.24	6.19	6.41
T18	0.45	400.00	0.45	11.01	6.73	4.81	13.35	7.22	6.72	13.48	7.62	7.12
T19	0.50	350.00	0.35	11.40	6.78	5.10	13.29	7.65	6.58	13.11	8.82	6.93
T20	0.50	350.00	0.40	12.20	5.17	5.51	13.60	7.46	6.97	14.38	8.32	7.31
T21	0.50	350.00	0.45	12.29	6.49	5.85	14.66	7.00	7.76	15.00	8.10	8.35
T22	0.50	375.00	0.35	13.59	6.63	5.30	14.83	7.76	8.05	15.95	8.76	9.22
T23	0.50	375.00	0.40	14.02	7.32	6.72	15.59	8.65	7.10	16.37	9.30	9.42
T24	0.50	375.00	0.45	15.02	8.39	6.81	15.31	8.55	7.19	16.25	9.43	10.95
T25	0.50	400.00	0.35	15.70	8.52	7.07	15.00	8.88	7.60	16.71	9.54	10.29
T26	0.50	400.00	0.40	16.28	7.74	6.29	16.55	9.81	8.39	17.26	10.44	9.60
T27	0.50	400.00	0.45	16.71	7.43	6.52	17.04	8.36	8.19	16.63	9.76	10.88

Table 4.4: Corrosion Current Density for T-Specimens by Gravimetric method

Mix	w/cm ratio (by mass)	Cementitious mateial content (kg/m^3)	FA/TA ratio (by mass)	Corrosion current density, $I_{corr}(\mu A/cm^2)$								
				3% NaCl solution exposure			7% NaCl solution exposure			12% NaCl solution exposure		
				25mm cover	37.5mm cover	50mm cover	25mm cover	37.5mm cover	50mm cover	25mm cover	37.5mm cover	50mm cover
T1	0.40	350.00	0.35	5.24	0.74	0.54	6.27	2.01	1.08	6.51	2.03	1.95
T2	0.40	350.00	0.40	5.85	1.40	0.52	6.60	3.02	2.63	5.85	2.31	1.34
T3	0.40	350.00	0.45	6.01	2.13	1.96	6.53	2.41	2.09	4.92	2.62	3.00
T4	0.40	375.00	0.35	6.52	2.94	1.50	6.36	2.56	1.50	7.31	2.93	0.99
T5	0.40	375.00	0.40	5.80	2.52	1.59	6.76	4.35	3.01	8.28	5.73	3.27
T6	0.40	375.00	0.45	6.31	2.76	2.19	6.18	2.63	2.10	7.44	3.69	2.17
T7	0.40	400.00	0.35	6.34	3.51	2.84	8.39	3.10	1.76	7.90	3.34	2.91
T8	0.40	400.00	0.40	7.01	3.73	2.94	8.61	3.78	2.37	8.74	5.67	5.67
T9	0.40	400.00	0.45	7.99	4.36	3.06	8.14	2.44	2.33	8.59	4.67	4.53
T10	0.45	350.00	0.35	8.43	2.80	3.22	8.50	5.77	3.58	8.74	5.54	4.05
T11	0.45	350.00	0.40	7.88	3.65	3.41	8.50	4.81	3.15	8.84	7.47	6.00
T12	0.45	350.00	0.45	8.83	4.81	4.16	8.68	6.43	4.08	9.44	7.58	6.97
T13	0.45	375.00	0.35	7.69	6.24	3.71	8.51	6.69	4.23	9.47	7.26	4.65
T14	0.45	375.00	0.40	7.65	6.37	4.17	7.98	6.36	3.40	9.76	7.42	3.79
T15	0.45	375.00	0.45	9.77	6.48	3.48	8.07	6.01	5.25	9.04	7.53	5.34
T16	0.45	400.00	0.35	9.89	6.53	4.16	9.01	6.42	5.38	10.10	6.56	5.20
T17	0.45	400.00	0.40	9.57	6.09	4.22	9.92	6.12	3.39	11.49	8.21	4.88
T18	0.45	400.00	0.45	9.50	7.21	5.05	10.54	8.11	5.44	11.58	8.40	6.01
T19	0.50	350.00	0.35	10.17	7.44	5.30	8.89	8.77	6.85	12.26	8.68	7.23
T20	0.50	350.00	0.40	10.46	6.94	5.04	10.76	7.35	5.84	10.92	8.05	6.39
T21	0.50	350.00	0.45	10.76	7.18	5.35	10.99	7.69	2.69	10.99	6.75	4.70
T22	0.50	375.00	0.35	11.09	7.29	5.85	11.67	7.47	4.02	10.86	7.76	5.85
T23	0.50	375.00	0.40	11.84	7.71	5.97	13.20	8.08	2.51	13.48	7.82	5.94
T24	0.50	375.00	0.45	12.56	8.11	6.20	12.84	8.05	6.16	12.18	8.62	5.70
T25	0.50	400.00	0.35	13.13	8.23	6.24	12.39	8.25	6.90	13.51	10.09	6.64
T26	0.50	400.00	0.40	13.63	8.17	6.05	14.04	8.95	7.36	14.30	10.88	7.06
T27	0.50	400.00	0.45	14.38	7.52	5.94	14.92	7.57	6.08	14.09	7.91	7.12

exposure, the average percentage decrease in I_{corr} when the cover was increased from 25 to37.5 mm was 43% while it was only 23% when the cover was increased from 37.5 to 50 mm. The average percentage decrease in I_{corr} when the cover is increased from 25 to 37.5 mm was 42% while it was only 19% when the cover was increased from 37.5 to 50 mm for 12% NaCl solution exposure. The corrosion current density was generally observed to increase Also, as the chloride concentration increased from 3 to 12%. There is no clear trend in the values of corrosion current density when the cementitious materials content increased from 350 to 400 kg/m^3. This may be attributed to the fact that the increase in the cementitious materials content from 350 to 400 kg/m^3 does not significantly affect the quality of concrete. It was also observed that fine to total aggregate ratio does not have a significant influence on the corrosion current density, which may be attributed to the fact that the increase in fine to total aggregate ratio from 0.35 to 0.45 does not significantly improve the quality of concrete.

Table 4.2 summarizes the corrosion current density determined by the gravimetric weight loss method (GWLM) based on Eqn. 3.5, for concrete specimens prepared with H-type aggregates. The highest and lowest values of the corrosion current density were to be 13.68 μA/cm^2 and 0.48 μA/cm^2, respectively. There was an increase in the corrosion current density as the water/cementitious content increases. Also, the corrosion current density decreased with an increase in the concrete cover from 25 to 50 mm. However, it was noted that there was a significant decrease in the rate of corrosion when the cover was increased from 25 to 37.5 mm whereas when the cover was increased from 37.5 to 50 mm, the decrease in I_{corr} was insignificant. The average percentage decrease in I_{corr} when the cover is increased from 25 to 37.5 mm was 43% while it was only 17% when

the cover was increased from 37.5 to 50 mm for specimens exposed to 3% NaCl solution. For 7% NaCl solution exposure, the average percentage decrease in I_{corr} when the cover was increased from 25 to 37.5 mm was 36% while it was only 14% when the cover was increased from 37.5 to 50 mm. The average percentage decrease in I_{corr} when the cover was increased from 25 to 37.5 mm was 36% while it was only 17% when the cover was increased from 37.5 to 50 mm for 12% NaCl solution exposure. It was also noted that, there is no clear trend in the values of corrosion current density when the cementitious materials content was increased from 350 to 400 kg/m^3 and when the fine to total aggregate ratio was increased from 0.35 to 0.45. This may be due to the fact that the increase in the cementitious materials content from 350 to 400 kg/m^3 and the increase in fine to total aggregate ratio from 0.35 to 0.45 do not significantly improve the concrete quality.

4.1.2 Compiled Experimental Data for T-type aggregates

The corrosion current density determined by LPR method for concrete specimens prepared with T-type aggregates is presented in Table 4.3. The lowest and highest values of the corrosion current density were observed to be 1.06 μA/cm^2 and 17.26 μA/cm^2, respectively. It can be deduced from the results obtained that cover thickness has a great influence on the corrosion current density, as the increase in cover thickness decreases the corrosion current density. However, it was observed that there is no significant decrease in the rate of corrosion when the cover was increased from 37.5 to 50 mm but when the cover was increased from 25 to 37.5 mm, the decrease in I_{corr} is significant. The average percentage decrease in I_{corr} when the cover is increased from 25 to 37.5 mm was 49% while it was only 16% when the cover was increased from 37.5 to 50 mm for 3%

NaCl solution exposure. For 7% NaCl solution exposure, the average percentage decrease in I_{corr} when the cover is increased from 25 to 37.5 mm was 46% while it was only 17% when the cover was increased from 37.5 to 50 mm. The average percentage decrease in I_{corr} when the cover is increased from 25 to 37.5 mm was 44% while it was only 13% when the cover was increased from 37.5 to 50 mm for 12% NaCl solution exposure. Also, the corrosion current density increased with an increase in the water-cementitious materials ratio. Also, it was noted that the fine to total aggregate ratio does not have a significant effect on the corrosion current density, since there is no clear trend in the values of corrosion current density as the fine to total aggregate ratio increased. This may be attributed to the fact that an increase in the fine to total aggregate ratio from 0.35 to 0.45 does not significantly enhance quality of concrete.

The experimental data compiled in Table 4.4 shows the corrosion current density determined by gravimetric weight loss method for concrete specimens prepared with T-type aggregates. The lowest and highest values of the equivalent corrosion current density are noted to be 0.52 $\mu A/cm^2$ and 14.92 $\mu A/cm^2$, respectively. Two important observations can be made from the trend of the values obtained. Firstly, the corrosion current density was observed to increase linearly with an increase in the water-cementitious materials ratio and chloride concentration. Secondly, the corrosion current density was observed to decrease with an increase in the concrete cover. However, it was noted that there was significant decrease in the rate of corrosion when the cover was increased from 25 to 37.5 mm and when the cover was increased from 37.5 to 50 mm. The average percentage decrease in I_{corr} when the cover is increased from 25 to 37.5 mm was 43% while it was only 27% when the cover was increased from 37.5 to 50 mm for

3% NaCl solution exposure. For 7% NaCl solution exposure, the average percentage decrease in I_{corr} when the cover is increased from 25 to 37.5 mm was 40% while it was 31% when the cover was increased from 37.5 to 50 mm. The average percentage decrease in I_{corr} when the cover is increased from 25 to 37.5 mm was 36% while it was only 25% when the cover was increased from 37.5 to 50 mm for 12% NaCl solution exposure. In addition, there was no clear trend in the values of corrosion current density when the cementitious materials content increased from 350 to 400 kg/m^3 and as the fine to total aggregate ratio was increased from 0.35 to 0.45. This may be attributed to the fact that the increase in the cementitious materials content from 350 to 400 kg/m^3 and the increase in fine to total aggregate ratio from 0.35 to 0.45 do not significantly improve the concrete quality. The I_{corr} values determined using the gravimetric method are presented in Figures C1 through C27 of Appendix C.

4.2 STATISTICAL ANALYSIS OF TEST RESULTS

4.2.1 *Chi-square* analysis of corrosion rate data

A *chi-square test* is a measure of the correspondence between theory and observation [70]. One important of this statistical test is that, it allows testing for deviations of observed frequencies from expected frequencies. To perform a chi-square test, a *null hypothesis* (H_o) must first be established. In this case-study, the values of corrosion current density (I_{corr}) for water-cementitious materials ratio ($R_{W/C}$) of 0.4 from Table 4.2 are taken as the observed or experimental values (O_i). H_o is assumed as $R_{W/C}$ is *insignificant* in predicting corrosion current density (I_{corr}). As an illustrative example of typical calculations assuming a *uniform* probability distribution, the expected values are determined as:

$$E_i = \frac{\sum O_i}{n} = \frac{408}{81} = 5.037$$

where n = number of data points

Then, $(O_i - E_i)^2$ and $(O_i - E_i)^2 / E_i$ are computed and listed in Table 4.5.

For the assumed distribution function, the chi-square (χ^2) computed coefficient is determined as:

$$\chi^2_{comp.} = \sum_{i=1}^{n} \left[\frac{(O_i - E_i)^2}{E_i} \right] = 105.98$$

Then with the degree of freedom (d.f.) = n – 1 = 81 – 1 = 80, for 5% level of significance (probability), the $\chi^2_{tab.}$ is 101.88 from the table of *chi-square statistics* [71]. Since the *calculated* value of $\chi^2_{comp.}$ = 105.98 is greater than the *tabulated* value, H_o is rejected. That is, $R_{W/C}$ is significant in predicting I_{corr}.

Due to the multivariate nature of the data obtained in the present study, an extensive statistical analysis test (*namely*: analysis of variance "ANOVA") was performed on the data as discussed in the next sub-section.

4.2.2 Analysis of variance of corrosion rate data

Analysis of variance (ANOVA) of the test results was carried out using the software MINITAB [72] to evaluate the effect of independent variables on the dependent variable being the corrosion current density, I_{corr}. Analysis of variance is used as a means to

Table 4.5: Example case-study of *chi-square analysis*.

Number of samples, n	Observed Value, O_i	Expected Value, E_i	$(O_i - E_i)^2$	$(O_i - E_i)^2 / E_i$
1	6.83	5.04	3.20	0.64
2	2.11	5.04	8.58	1.70
3	1.11	5.04	15.44	3.06
4	6.36	5.04	1.74	0.35
5	2.70	5.04	5.48	1.09
6	1.60	5.04	11.83	2.35
7	6.57	5.04	2.34	0.46
8	2.00	5.04	9.24	1.83
9	1.36	5.04	13.54	2.69
10	7.34	5.04	5.29	1.05
11	2.28	5.04	7.62	1.51
12	0.48	5.04	20.79	4.13
13	7.6	5.04	6.55	1.30
14	1.32	5.04	13.84	2.75
15	1.75	5.04	10.82	2.15
16	7.85	5.04	7.90	1.57
17	2.16	5.04	8.29	1.65
18	0.98	5.04	16.48	3.27
19	7.14	5.04	4.41	0.88
20	2.67	5.04	5.62	1.11
21	1.42	5.04	13.10	2.60
22	6.84	5.04	3.24	0.64
23	2.25	5.04	7.78	1.54
24	1.61	5.04	11.76	2.33
25	7.93	5.04	8.35	1.66
26	3.22	5.04	3.31	0.66
27	1.9	5.04	9.86	1.96
28	7.46	5.04	5.86	1.16
29	2.67	5.04	5.62	1.11
30	1.4	5.04	13.25	2.63
31	7.63	5.04	6.71	1.33
32	3.65	5.04	1.93	0.38
33	2.76	5.04	5.20	1.03
34	8.83	5.04	14.36	2.85
35	3.56	5.04	2.19	0.43
36	3.33	5.04	2.92	0.58
37	7.4	5.04	5.57	1.11
38	3.02	5.04	4.08	0.81
39	3.3	5.04	3.03	0.60
40	8.38	5.04	11.16	2.21
41	3.69	5.04	1.82	0.36

(continued)

Table 4.5 (contd.)

42	3.1	5.04	3.76	0.75
43	8.8	5.04	14.14	2.81
44	4.27	5.04	0.59	0.12
45	3.34	5.04	2.89	0.57
46	8.13	5.04	9.55	1.89
47	4.27	5.04	0.59	0.12
48	3.9	5.04	1.30	0.26
49	8.33	5.04	10.82	2.15
50	3.67	5.04	1.88	0.37
51	4.58	5.04	0.21	0.04
52	8.06	5.04	9.12	1.81
53	4.15	5.04	0.79	0.16
54	4.35	5.04	0.48	0.09
55	8.06	5.04	9.12	1.81
56	4.41	5.04	0.40	0.08
57	4.18	5.04	0.74	0.15
58	8.78	5.04	13.99	2.78
59	5.05	5.04	0.00	0.00
60	4.61	5.04	0.18	0.04
61	8.03	5.04	8.94	1.77
62	5.38	5.04	0.12	0.02
63	4.4	5.04	0.41	0.08
64	8.8	5.04	14.14	2.81
65	4.25	5.04	0.62	0.12
66	4.23	5.04	0.66	0.13
67	8.98	5.04	15.52	3.08
68	5.4	5.04	0.13	0.03
69	5.22	5.04	0.03	0.01
70	9.84	5.04	23.04	4.57
71	5.84	5.04	0.64	0.13
72	5.75	5.04	0.50	0.10
73	8.97	5.04	15.44	3.06
74	5.71	5.04	0.45	0.09
75	4.09	5.04	0.90	0.18
76	9.21	5.04	17.39	3.45
77	7.31	5.04	5.15	1.02
78	5.07	5.04	0.00	0.00
79	9.98	5.04	24.40	4.84
80	7.06	5.04	4.08	0.81
81	5.98	5.04	0.88	0.18
$E_i = \frac{\sum O_i}{n}$	5.04	$\sum_{i=1}^{n}\left[\frac{(O_i - E_i)^2}{E_i}\right]$		105.98

determine whether an independent variable (predictor) has an effect on the dependent variable (response) or not. The notations for the variables are as follows:

$I_{corr,e}$ = Electrochemically measured corrosion current density in $\mu A/cm^2$

$I_{corr,g}$ = Gravimetrically measured corrosion current density in $\mu A/cm^2$

$R_{W/C}$ = Water to cementitious materials ratio by mass

$R_{F/T}$= Fine to total aggregate ratio by mass

C_C = Cementitious material content in kg/m^3

C_V = Cover thickness in mm

C_L = Chloride concentration in percentage

The results obtained from ANOVA analysis for I_{corr} determined by electrochemical and gravimetric weight loss methods are presented in Tables 4.6 through 4.9.

Table 4.6: ANOVA for electrochemically measured corrosion rate, $I_{corr,e}$, of concrete specimens prepared with H-type aggregates.

Factor	**Type**	**Levels**	**Values**		
$R_{W/C}$	Fixed	3.00	0.40	0.45	0.50
C_C	Fixed	3.00	350.00	375.00	400.00
$R_{F/T}$	Fixed	3.00	0.35	0.40	0.45
C_L	Fixed	3.00	0.03	0.07	0.12
C_V	Fixed	3.00	25.00	37.50	50.00
Source	**DF**	**SS**	**Adj MS**	**F**	**P**
$R_{W/C}$	2	882.27	**441.13**	**393.40**	0.000
C_C	2	195.69	97.85	87.26	0.000
$R_{F/T}$	2	20.71	10.36	9.24	0.000
C_L	4	54.14	27.07	24.14	0.000
C_V	4	1560.62	**780.31**	**695.87**	0.000

Table 4.7: ANOVA for gravimetrically measured corrosion rate, $I_{corr,g}$, of concrete specimens prepared with H-type aggregates.

Factors	**Type**	**Levels**	**Values**		
$R_{W/C}$	Fixed	3.00	0.40	0.45	0.50
C_C	Fixed	3.00	350.00	375.00	400.00
$R_{F/T}$	Fixed	3.00	0.35	0.40	0.45
C_L	Fixed	3.00	0.03	0.07	0.12
C_V	Fixed	3.00	25.00	37.50	50.00
Source	**DF**	**SS**	**Adj MS**	**F**	**P**
$R_{W/C}$	2	527.20	**263.60**	**218.16**	0.000
C_C	2	79.20	39.60	32.77	0.000
$R_{F/T}$	2	4.58	2.29	1.90	0.152
C_L	4	25.70	12.85	10.64	0.000
C_V	4	930.69	**465.35**	**385.14**	0.000

Table 4.8: ANOVA for electrochemically measured corrosion rate, $I_{corr,e}$, of concrete specimens prepared with T-type aggregates.

Factors	**Type**	**Levels**	**Values**		
$R_{W/C}$	Fixed	3.00	0.40	0.45	0.50
C_C	Fixed	3.00	350.00	375.00	400.00
$R_{F/T}$	Fixed	3.00	0.35	0.40	0.45
C_L	Fixed	3.00	0.03	0.07	0.12
C_V	Fixed	3.00	25.00	37.50	50.00
Source	**DF**	**SS**	**Adj MS**	**F**	**P**
$R_{W/C}$	2	1293.71	**646.85**	**770.50**	0.000
C_C	2	140.20	70.10	3.50	0.000
$R_{F/T}$	2	18.05	9.03	10.75	0.000
C_L	4	81.71	40.86	48.67	0.000
C_V	2	1607.43	**803.72**	**957.35**	0.000

Table 4.9: ANOVA for gravimetrically measured corrosion rate, $I_{corr,g}$, of concrete specimens prepared with T-type aggregates.

Factors	**Type**	**Levels**	**Values**		
$R_{W/C}$	Fixed	3.00	0.40	0.45	0.50
C_C	Fixed	3.00	350.00	375.00	400.00
$R_{F/T}$	Fixed	3.00	0.35	0.40	0.45
C_L	Fixed	3.00	0.03	0.07	0.12
C_V	Fixed	3.00	25.00	37.50	50.00
Source	**DF**	**SS**	**Adj MS**	**F**	**P**
$R_{W/C}$	2	862.75	**431.37**	**498.87**	0.000
C_C	2	102.99	51.49	59.55	0.000
$R_{F/T}$	2	8.83	4.42	5.11	0.007
C_L	4	41.82	20.91	24.18	0.000
C_V	2	1164.89	**582.45**	**673.58**	0.000

where:

DF is the number of observations that can be varied independently of each other.

SS is the squared distance between each data point and the sample mean, summed for all *n* data points.

Adj MS is the measure of the variability of group mean around the grand mean.

F-ratio is a statistical measure calculated by ANOVA, which reveals the significance of the hypothesis that dependent variable depends on independent variable.

P-value is a measure of *acceptance* or *rejection* of a statistical significance based on a standard that no more than 5 % (0.05 level) of the difference is due to chance or sampling error.

These statistical terminologies of ANOVA are further described in Appendix D.

From the ANOVA results, it can be *observed* (by close inspection of the values of adj. MS and F-ratio) that the water to cementitious materials ratio ($R_{W/C}$) and cover thickness (C_V) have higher values of adjusted mean square (MS) and F-ratio (F) in all the four cases compared to other factors, this shows that $R_{W/C}$ and C_V have major effect on reinforcement corrosion rate. The other variable factors, such as cementitious materials content (C_C), fine to total aggregate ratio ($R_{F/T}$), and chloride concentration (C_L) have minor effects. The reason behind minor effect of C_C is that, the variation of this factor is in a narrow range of 350 to 400 kg/m^3 (close to the value used in practice). Also, $R_{F/T}$ was found to have minor effect on corrosion rate, because its variation is in the range of 0.35 to 0.45, which is close to the optimum value of $R_{F/T}$ (around 0.40) corresponding to which the aggregates have least voids (i.e., maximum density). C_L has minor impact on reinforcement corrosion rate although widely varied (3% to 12%) because the chloride level mainly affects initiation of reinforcement corrosion and its effect on the rate of corrosion is minimal. The progress of reinforcement corrosion after initiation (i.e., reinforcement corrosion rate) depends on many other factors such as the availability of moisture and oxygen, and resistivity of concrete.

However, considering the P-values shown in Tables 4.6 through 4.9, it can be observed that all the factors ($R_{W/C}$, C_C, $R_{F/T}$, C_L, and C_V) were found with significant effects on the corrosion current density I_{corr}. Therefore, all the factors were considered for obtaining the regression model for I_{corr}.

4.3 EFFECT OF $R_{W/C}$ AND C_V ON CORROSION RATE

In order to show the effect of the major factors ($R_{W/C}$ and C_V) on reinforcement corrosion rate, the values of gravimetrically measured reinforcement corrosion rates, $I_{corr,g}$, were plotted against $R_{W/C}$ for all the three values of C_V, separately for each type of aggregate, neglecting the effect of minor factors, as shown in Figures 4.1 and 4.2. The gravimetrically determined values of reinforcement corrosion rates, $I_{corr,g}$, were used to show the effect of $R_{W/C}$ and C_V on corrosion rate because they are more reliable than the electrochemically measured corrosion rates.

It can be observed from Figures 4.1 and 4.2 that the corrosion rate increased with an increase in the $R_{W/C}$ almost linearly. It can also be observed that the increase in cover thickness is causing a substantial decrease in the corrosion rate. The decrease in corrosion rate is more when the cover is increased from 25 mm to 37.5 mm than when the cover is increased from 37.5 mm to 50 mm.

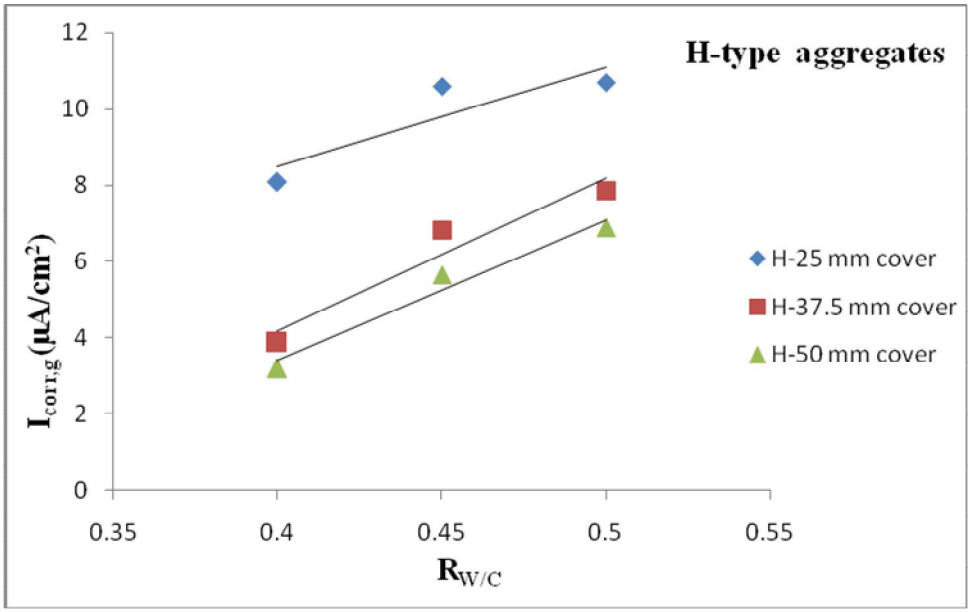

Figure 4.1: Variation of $I_{corr,g}$ with $R_{W/C}$ at different cover thickness for concrete with H-type aggregates.

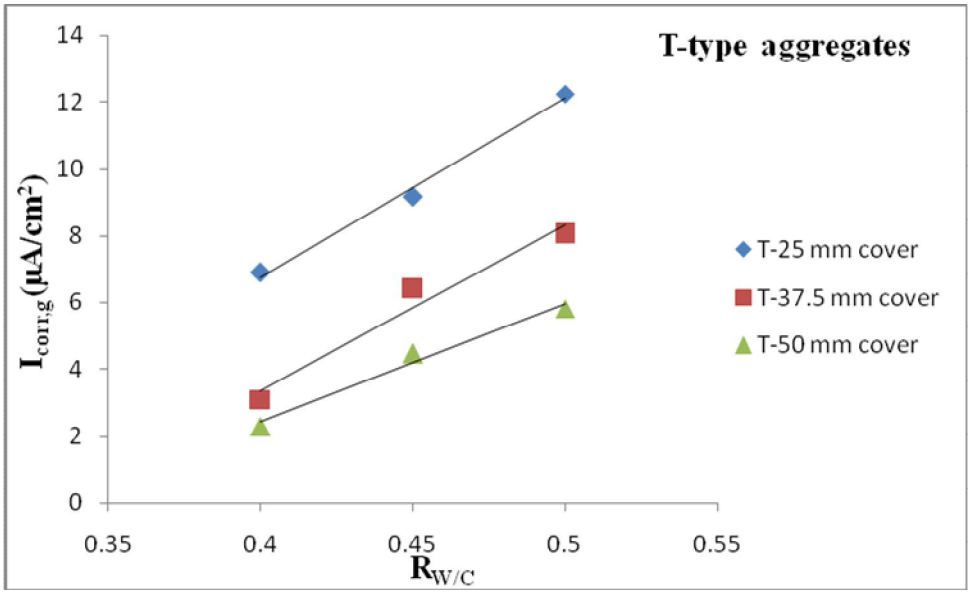

Figure 4.2: Variation of $I_{corr,g}$ with $R_{W/C}$ at different cover thickness for concrete with T-type aggregates.

A condensed summary of the average percentage decrease in corrosion current density, ΔI_{corr} with the concrete cover C_V increased from 25 mm to 37.5 mm and from 37.5 mm to 50 mm is presented in Figures 4.3 through 4.5.

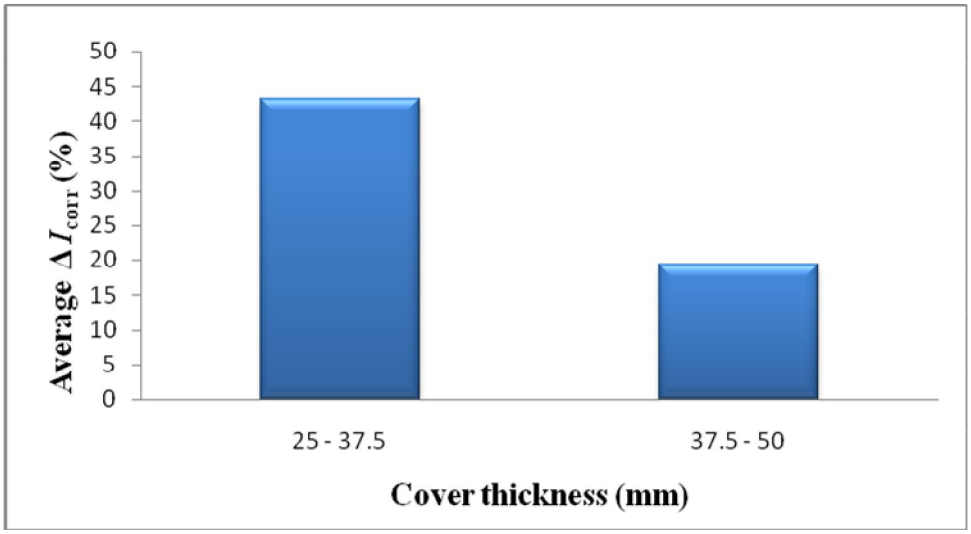

Figure 4.3: Average percentage decrease in I_{corr} when the cover thickness is increased from 25 to 37.5 mm and from 37.5 to 50 mm (3% NaCl solution exposure).

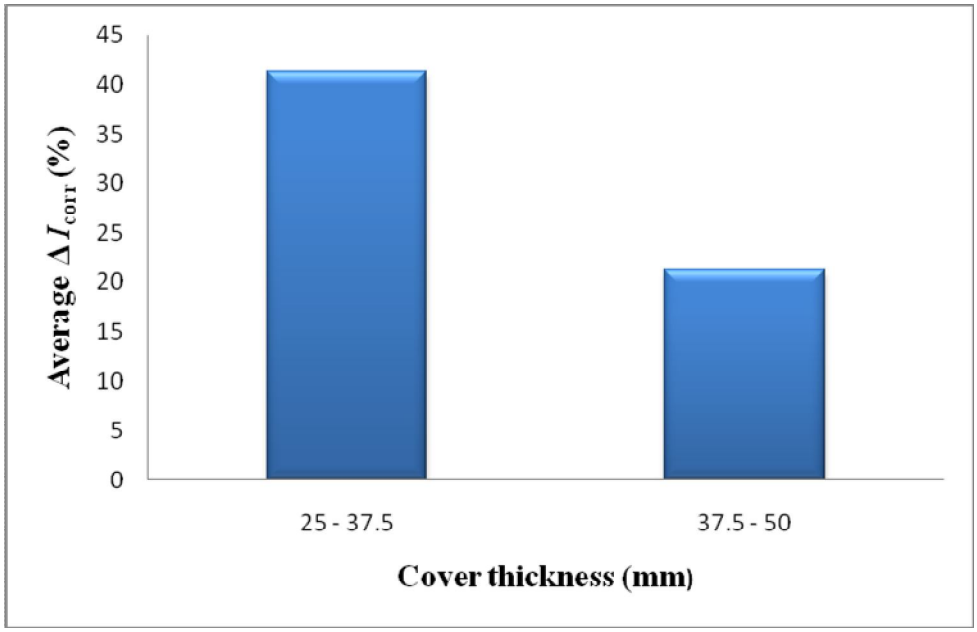

Figure 4.4: Average percentage decrease in I_{corr} when the cover thickness is increased from 25 to 37.5 mm and from 37.5 to 50 mm (7% NaCl solution exposure).

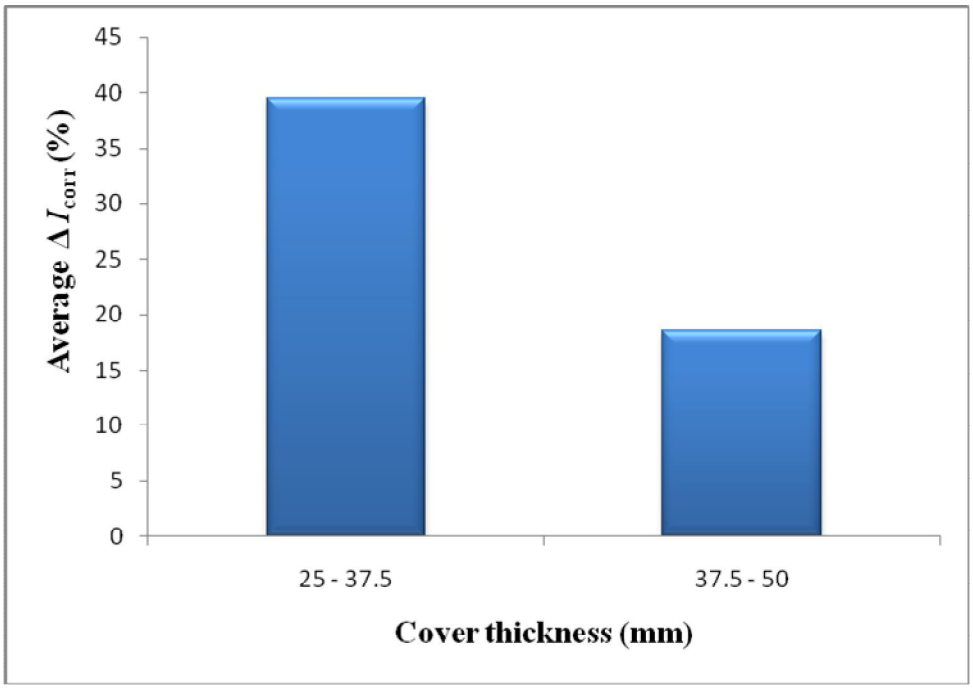

Figure 4.5: Average percentage decrease in I_{corr} when the cover thickness is increased from 25 to 37.5 mm and from 37.5 to 50 mm (12% NaCl solution exposure).

4.4 EFFECT OF AGGREGATE TYPE ON CORROSION RATE

From the plots of corrosion current density shown in Figures 4.1 and 4.2, it was observed that at lower w/c ratio, the corrosion current density values for concrete specimens prepared with H-type aggregates were generally more than that prepared with T-type aggregates. But, at higher w/c ratio, the corrosion current density values for H-type aggregate were either lower or nearly the same compared to that of T-type aggregate. This shows that, at lower w/c ratio the concrete specimens prepared with T-type aggregates performed better than those prepared with H-type aggregates. This may be attributed to the properties of the aggregates, which includes water absorption and abrasion loss. It is to be noted that at higher values of w/c ratio, the difference in I_{corr} for the concretes prepared with the two types of aggregates was more apparent compared to lower values of w/c ratio. This shows that the influence of aggregate quality is more at higher values of w/c ratio.

4.5 EFFECT OF TIME ON CORROSION RATE

The variation of I_{corr} with time for the concrete specimens exposed to NaCl solution of 3%, 7% or 12% were plotted to study the effect of time on the rate of reinforcement corrosion. A summary of the variations of corrosion current density with time for concrete specimens prepared with H-type aggregates is compiled in Appendix B (Figures B1 through B9). The I_{corr} values determined using LPR method by Yusuf [6] during two rounds of corrosion monitoring and the I_{corr} values obtained using LPR method in this study on the same concrete specimens were used to plot the variation over the exposure period. In almost all the concrete specimens, the I_{corr} values increased with time. At early exposure period of 78 to 216 days, the I_{corr} in all the concrete specimens was less than

2 $\mu A/cm^2$. This indicates that the corrosion damage in the concrete specimens at that period was not severe. After 1,368 days, there was severe corrosion damage especially in the concrete specimens with lowest cover, because the I_{corr} values were in the range of 5.99 to 15.80 $\mu A/cm^2$.

A summary of the variations of corrosion current density with time for concrete specimens prepared with T-type aggregates is compiled in Appendix B (Figures B10 through B18). Generally, the I_{corr} values increased with an increase in the time of exposure. It can be observed that, in the initial period of exposure, i.e. 117 to 316 days, the I_{corr} values were less than 4 $\mu A/cm^2$. This shows that there was significant corrosion damage in the concrete specimens, though it was not that severe. But, in the later stage of exposure i.e., 1189 to 1196 days, the I_{corr} values were in the range of 5.99 to 17.26 $\mu A/cm^2$ for the concrete specimens with cover of 25 mm. This indicates that corrosion damage was severe in those specimens. It is also noted that the rate of reinforcement corrosion at the early stage of exposure increased slowly, whereas at the later period of exposure, it increased rapidly.

A close inspection and study of the summarized data (compiled in Figure B1 to B18) indicate that cover over reinforcing steel has a significant effect on the rate of reinforcement corrosion. The rate of reinforcement corrosion decreased with cover. However, the concentration of chloride solution did not have that significant effect on the rate of corrosion. In fact, the rate of corrosion for specimens exposed to solutions with varying chloride concentration was almost the same in most of the cases.

4.6 EFFECT OF W/C RATIO ON CONCRETE PORE STRUCTURE

When the microstructure of a high and low w/c concrete are observed under scanning electron microscope (SEM), it is possible to visualize the drastic consequence of the reduction in w/c on concrete microstructure and consequently on concrete durability [73]. Scanning electron images of concrete specimens prepared with w/c ratios of 0.4, 0.45 and 0.5 (shown in Figure 4.6 through 4.8) highlight the effect of water-cementitious materials ratio on concrete morphology and chemical composition.

Figure 4.6 shows the SEM of concrete specimens prepared with a w/c ratio of 0.4. A dense morphology of calcium silicate hydrate (C-S-H) overlaid by calcium hydroxide crystals is noted. The energy dispersive X-ray analysis (EDAX) shows mainly the presence of Si, Ca, Al, Fe and Cl. The SEM of concrete specimens prepared with a w/c ratio of 0.45 is presented in Figure 4.7. The C-S-H structure is shallow and the presence of ettringite crystals is more evident. The EDAX shows mainly the presence of Mg, Al, Si, Ca, Fe and Cl. The SEM of concrete specimens prepared with a w/c ratio of 0.50 is shown in Figure 4.8. The structure of the C-S-H is porous and the presence of ettringite crystals and calcium hydroxide was noted in the pores of the C-S-H. The EDAX analysis shows mainly the presence of Mg, Al, Si, Ca, Fe and Cl. A comparison of the SEM-based results in Figures 4.6 through 4.8 indicates that the C-S-H becomes *more porous* with an increase in the w/c ratio. The elemental composition noted from the EDAX analysis is summarized in Table 4.10. From these data, it is evident that the chloride concentration increases with an increase in the w/c ratio. The percentage increase in chloride concentration when the w/c ratio increased from 0.4 to 0.45 was 4.2% while it was only 0.58% when the w/c ratio was increased from 0.45 to 0.50. This could be

attributed to the increase in the porosity as highlighted by the SEM summary due to an increase in the w/c ratio.

Table 4.10: Spectrum of concrete specimens of varying w/c ratio

w/c ratio	Spectrum (%)							
	O	Na	Mg	Al	Si	Cl	Ca	Fe
0.40	50.57	3.31	1.10	7.16	18.51	2.09	15.77	1.49
0.45	39.25	_	1.96	2.69	15.25	6.29	32.52	2.03
0.50	32.53	_	1.63	6.48	8.54	6.87	39.75	4.22

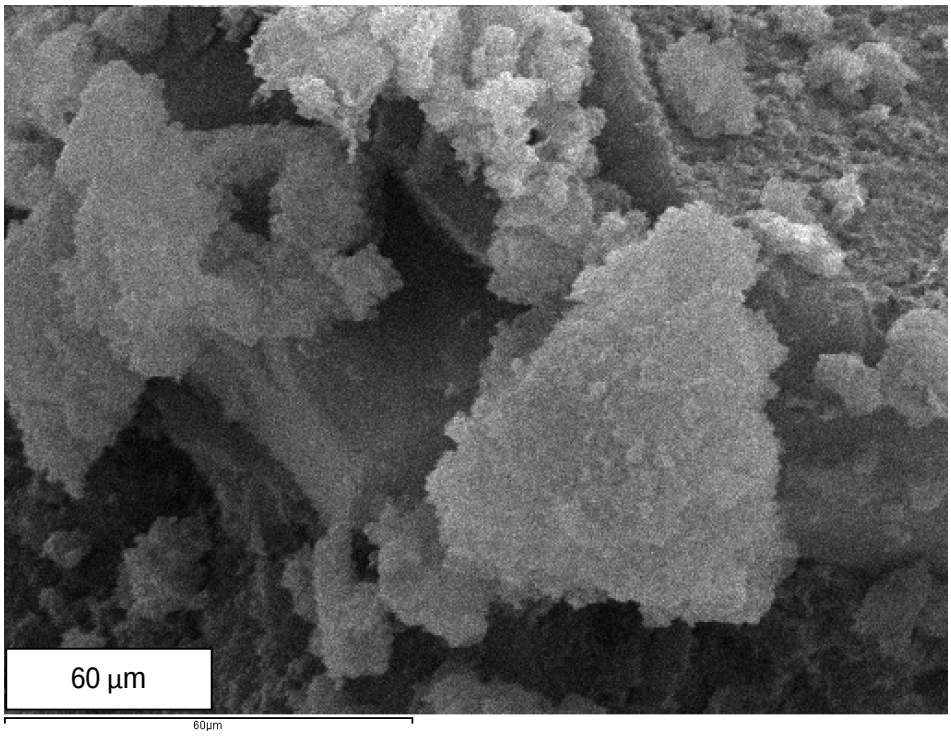

Figure 4.6: Pore structure and spectrum for concrete specimen of 0.40 w/c ratio.

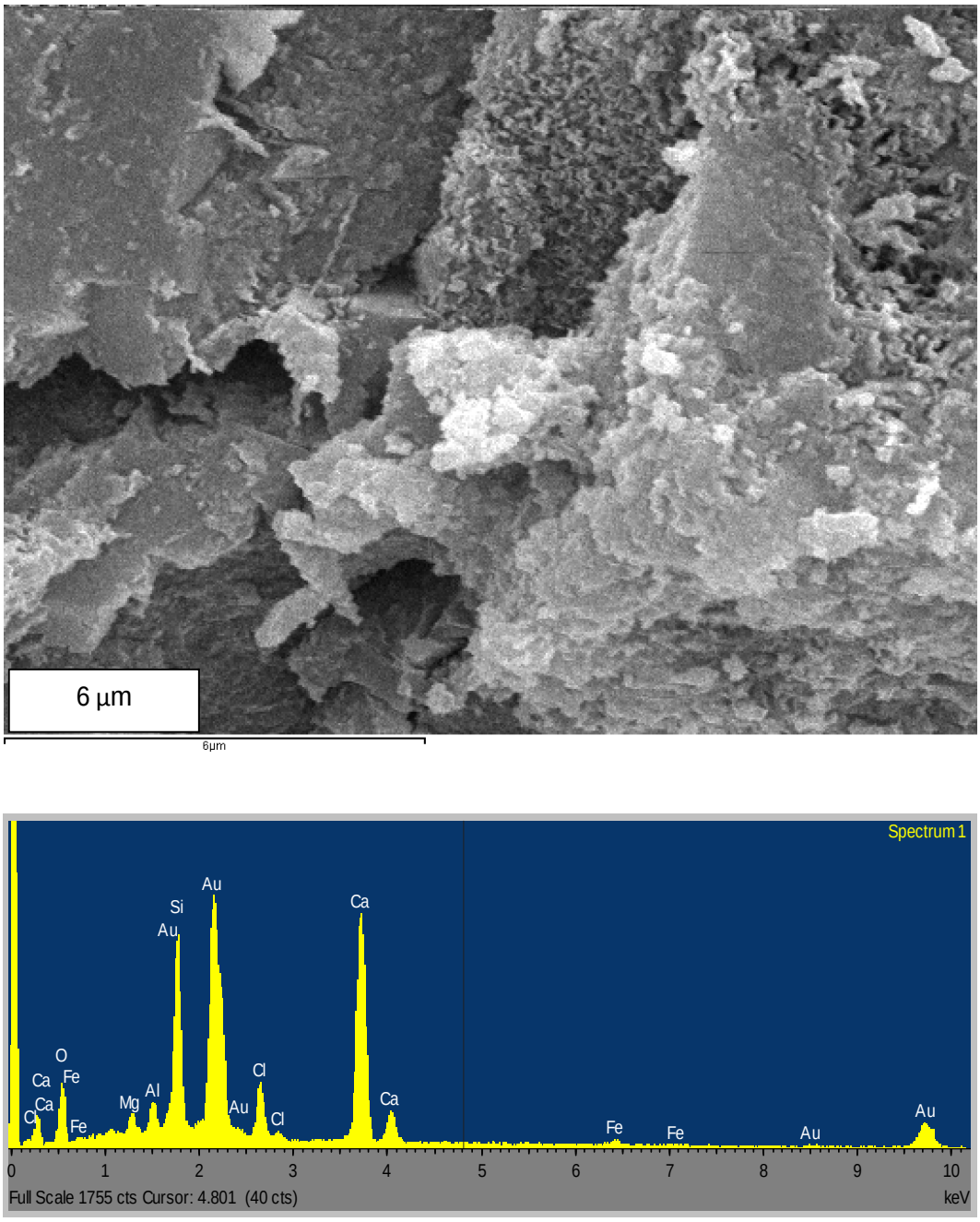

Figure 4.7: Pore structure and spectrum for concrete specimen of 0.45 w/c ratio.

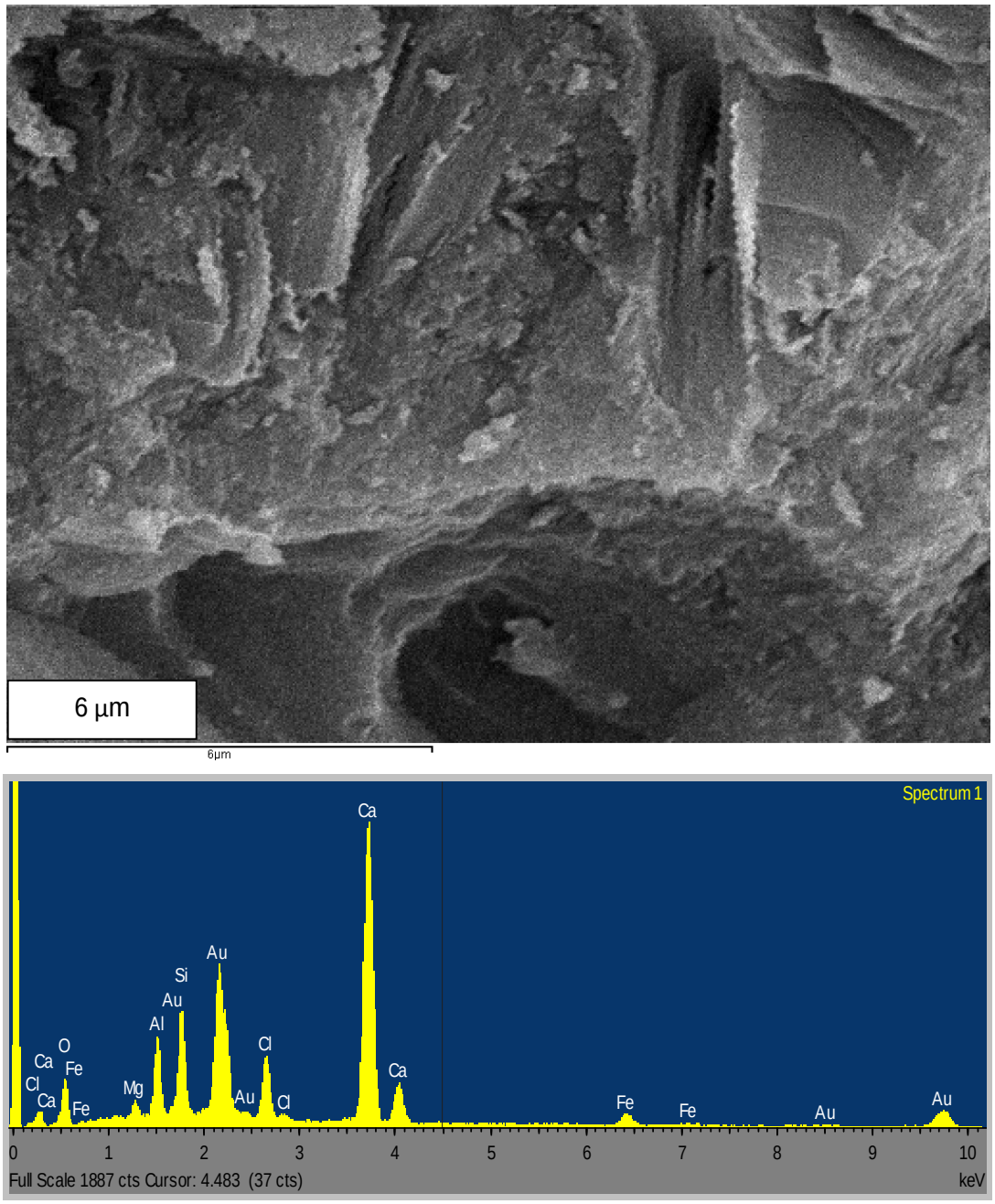

Figure 4.8: Pore structure and spectrum for concrete specimen of 0.50 w/c ratio.

CHAPTER 5

REGRESSION ANALYSIS OF CORROSION RATE DATA

Regression analysis of experimental data obtained through the present work is first used to study correlation between electrochemically and gravimetrically measured reinforcement corrosion rates. The regression models for predicting reinforcement corrosion rate obtained utilizing the gravimetrically measured reinforcement corrosion rate are presented and discussed.

5.1 CORRELATION BETWEEN $I_{corr,g}$ and $I_{corr,e}$

The data compiled from the experimental program using the LPRM and GWLM were regressed to develop the correlation between corrosion current density determined electrochemically and gravimetrically. In order to examine the effects of the concrete mixture variables, cover thickness, and chloride concentration on correlation between $I_{corr,g}$ and $I_{corr,e}$, corrosion rate data were regressed in various groups as described in the following sub-sections:

5.1.1 Effect of aggregate quality on correlation between $I_{corr,g}$ and $I_{corr,e}$

The relationship between corrosion current density determined using the LPRM and GWLM for the two types of aggregates is shown in Figures 5.1 and 5.2 for H-type aggregates and T-type aggregates, respectively.

Figure 5.1 shows the correlation between corrosion current density determined by the LPRM and GWLM for H-type aggregates. It is observed that the relationship between I_{corr} values determined by the two methods is nearly linear with regression coefficient, R^2 of 0.80. It is estimated (from regression analysis) that I_{corr} measured by the gravimetric weight loss will be approximately 84% the value obtained by the LPRM.

The correlation between corrosion current density determined by LPRM and GWLM for T-type aggregates is shown in Figure 5.2. It is observed from the plot that there is agreement of results obtained from the two methods as evident from the relationship shown i.e. I_{corr} determined by GWLM is 86% of LPRM and corresponding value of regression coefficient, R^2 is 0.88.

From these plots, it is observed that the relationship of the corrosion current density from the two methods for H-type aggregates and T-type aggregates are respectively 0.84 and 0.86, which are very close to the average value of the two i.e. 0.85. The results indicate that the aggregate type does not have a profound effect on the relationship between the corrosion current density determined using LPRM and GWLM.

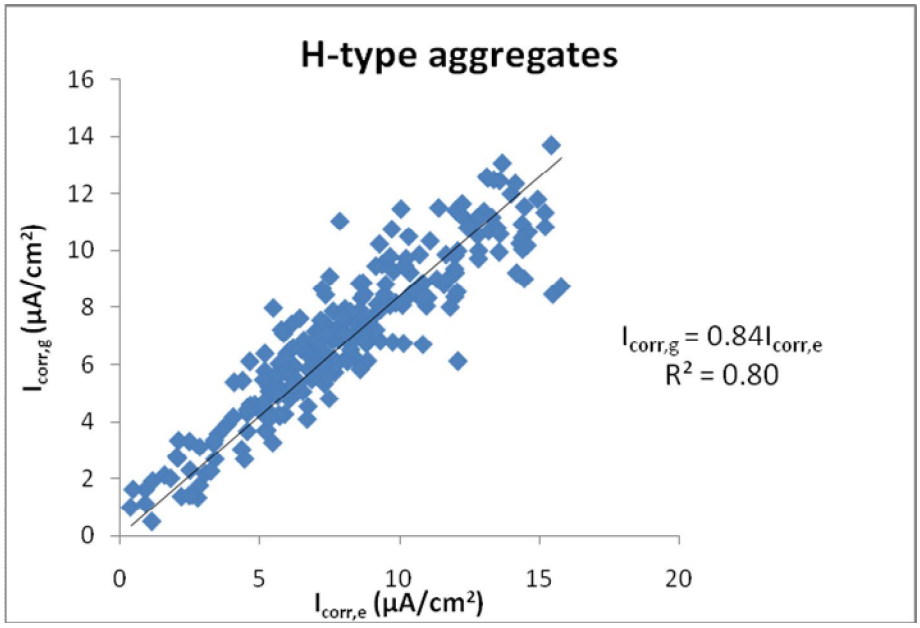

Figure 5.1: Correlation between $I_{corr,g}$ and $I_{corr,e}$ for H-type aggregates

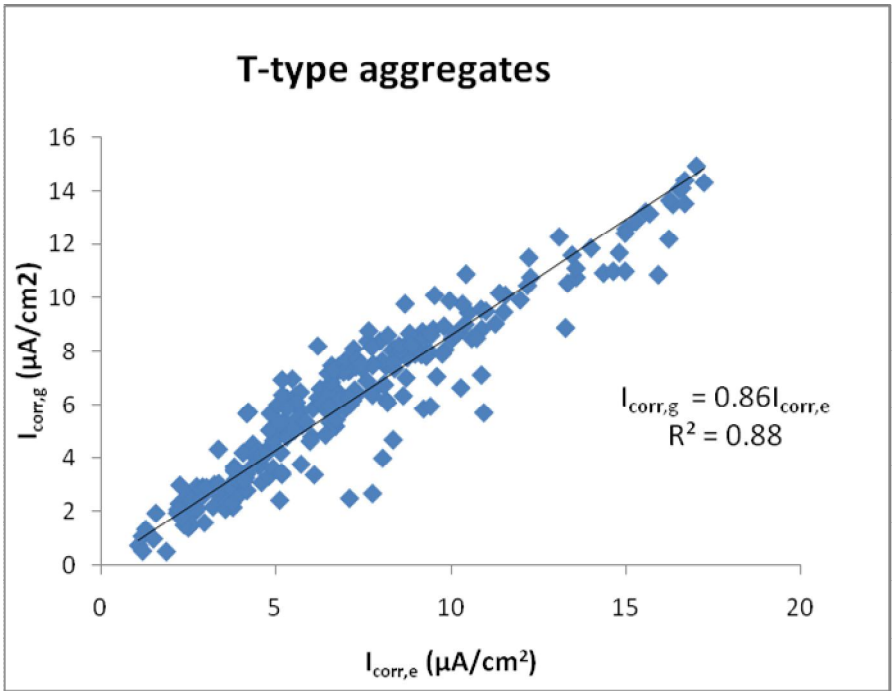

Figure 5.2: Correlation between $I_{corr,g}$ and $I_{corr,e}$ for T-type aggregates.

5.1.2 Effect of concrete cover, C_V, on correlation between $I_{corr,g}$ and $I_{corr,e}$

Figures 5.3 through 5.5 show the correlation of corrosion current density determined using LPRM and GWLM for 25 mm, 37.5 mm and 50 mm cover thickness, C_v. The correlation between corrosion current density determined from LPRM and corrosion current density determined by GWLM for 25 mm thickness is shown in Figure 5.3. It is observed that there is agreement of results obtained from the two methods as evident from the relationship, $I_{corr,g} = 0.84 I_{corr,e}$ and the regression coefficient of 0.82.

Figure 5.4 shows the correlation between corrosion current density determined by the LPRM and corrosion current density determined by GWLM for 37.5 mm cover. It is observed that there is close agreement of results obtained from the two methods as evident from the relationship, $I_{corr,g} = 0.91 I_{corr,e}$ and regression coefficient value of 0.84.

The correlation between values of corrosion current density I_{corr} determined by LPRM and corrosion current density I_{corr} determined by GWLM for 50 mm cover is shown in Figure 5.5. Similar agreement of results obtained from the two methods is evident from the relationship $I_{corr,g} = 0.87 I_{corr,e}$ and the regression coefficient value of 0.86.

It was observed from the three plots that the correlation between the corrosion current density obtained from LPRM and GWLM are 0.84, 0.91 and 0.87 for the 25 mm, 37.5 mm and 50 mm cover thickness, respectively. These values are not far from the average value of 0.87. In addition, there is no clear trend in the variation, as the variation increases when the cover is increased from 25 mm to 37.5 mm, it then decreases when the cover is increased 37.5 mm to 50 mm. This indicates that the effect of concrete cover

on the relationship between the corrosion current density obtained using LPRM and GWLM is also insignificant.

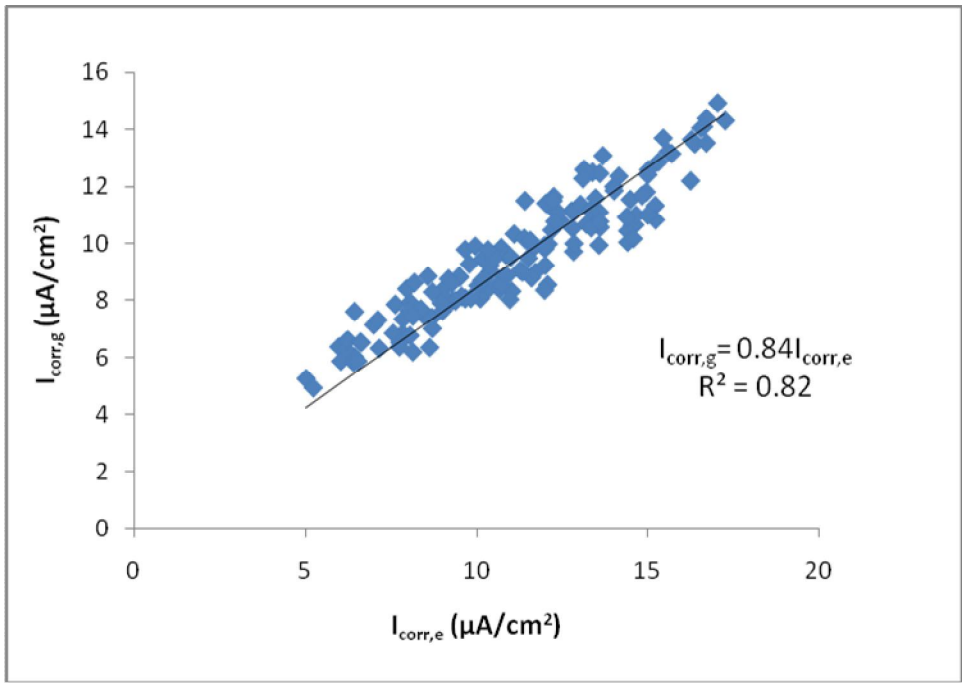

Figure 5.3: Correlation between $I_{corr,g}$ and $I_{corr,e}$ for 25mm cover.

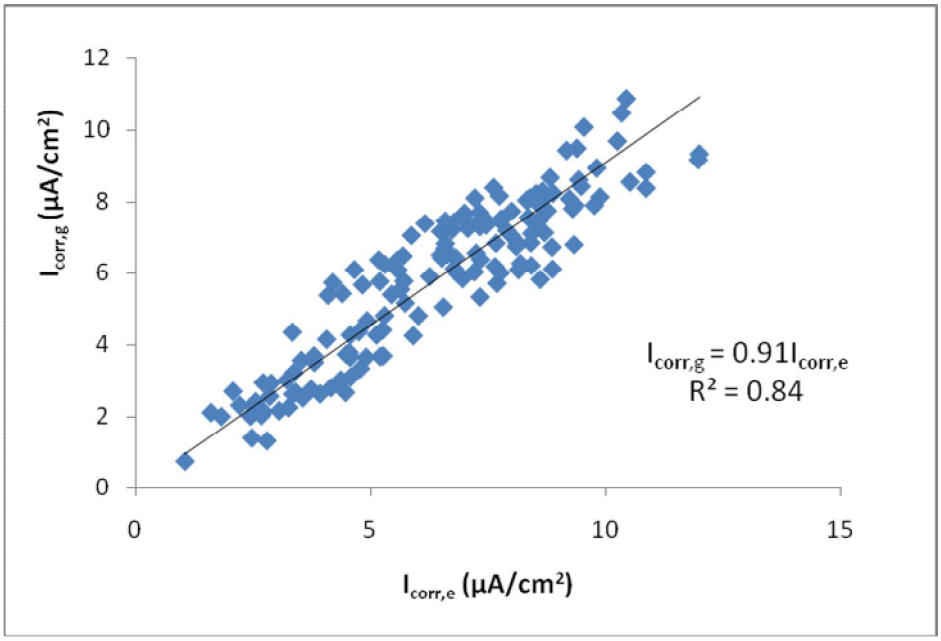

Figure 5.4: Correlation between $I_{corr,g}$ and $I_{corr,e}$ for 37.5 mm cover.

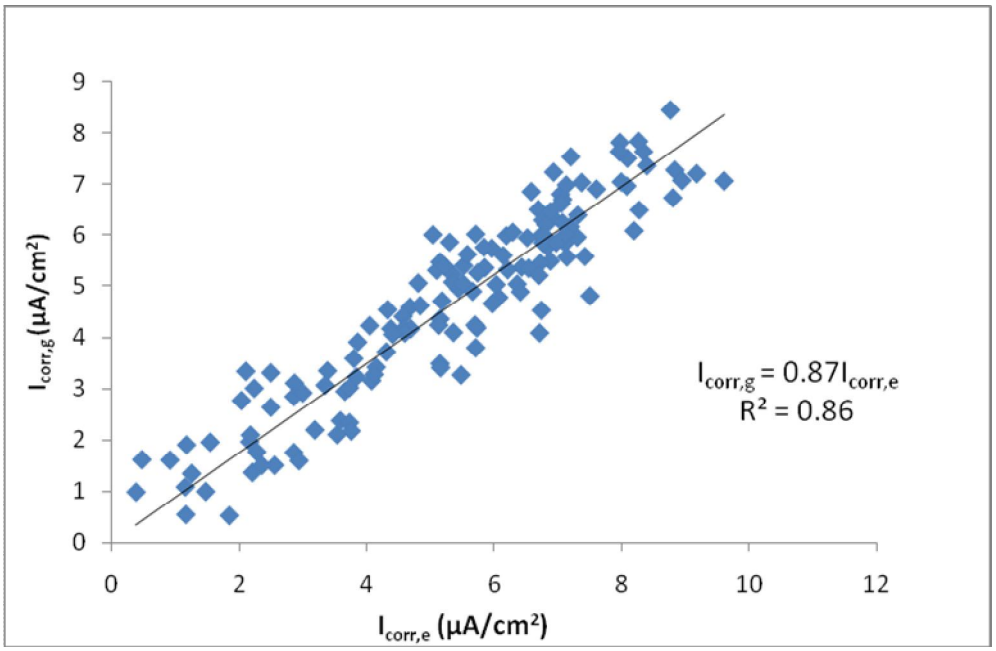

Figure 5.5: Correlation between $I_{corr,g}$ and $I_{corr,e}$ for 50 mm cover.

5.1.3 Effect of chloride concentration on correlation between $I_{corr,g}$ and $I_{corr,e}$

For the purpose of examining the effect of chloride concentration on the variation of corrosion current density obtained using LPRM and GWLM, plots of corrosion current density determined by LPRM and GWLM for 3%, 7% and 12% NaCl concentration are shown in Figures 5.6 through 5.8.

The correlation between corrosion current density determined by LPRM and corrosion current density determined by GWLM for 3% NaCl concentration is shown in Figure 5.6. It is observed that there is close agreement of results obtained from the two methods as evident from the relationship $I_{corr,g} = 0.88I_{corr,e}$and the regression coefficient value of 0.91.

Figure 5.7 shows the correlation between corrosion current density determined by LPRM and corrosion current density determined by GWLM for 7% NaCl concentration. It is

observed that there is close agreement of results obtained from the two methods as evident from the relationship $I_{corr,g} = 0.84I_{corr,e}$ and regression coefficient value of 0.85.

The correlation between corrosion current density determined by LPRM and corrosion current density determined by GWLM for 12% NaCl concentration is shown in Figure 5.8. It is observed that there is relative agreement of results obtained from the two methods as evident from the relationship $I_{corr,g} = 0.83I_{corr,e}$ and the regression coefficient value of 0.78.

It is also observed from the plots (Figures 5.6 through 5.8) that the correlation between the corrosion current density obtained from LPRM and GWLM for the three chloride concentration exposures were 0.88, 0.84, and 0.83, which are close to the average value of 0.85. This implies an insignificant effect of chloride concentration on correlation between corrosion current density determined by LPRM and GWLM.

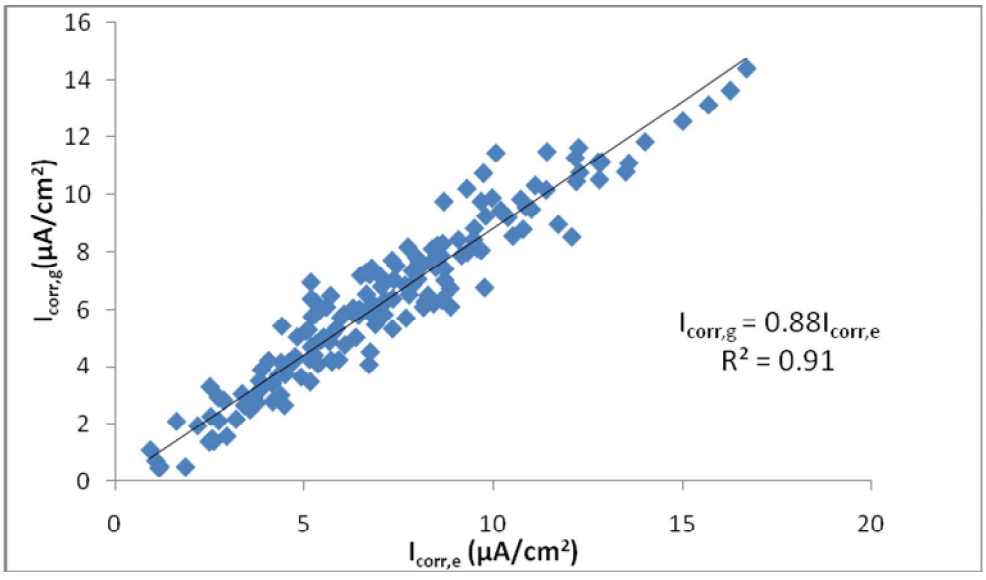

Figure 5.6: Correlation between $I_{corr,g}$ and $I_{corr,e}$ for 3% chloride concentration.

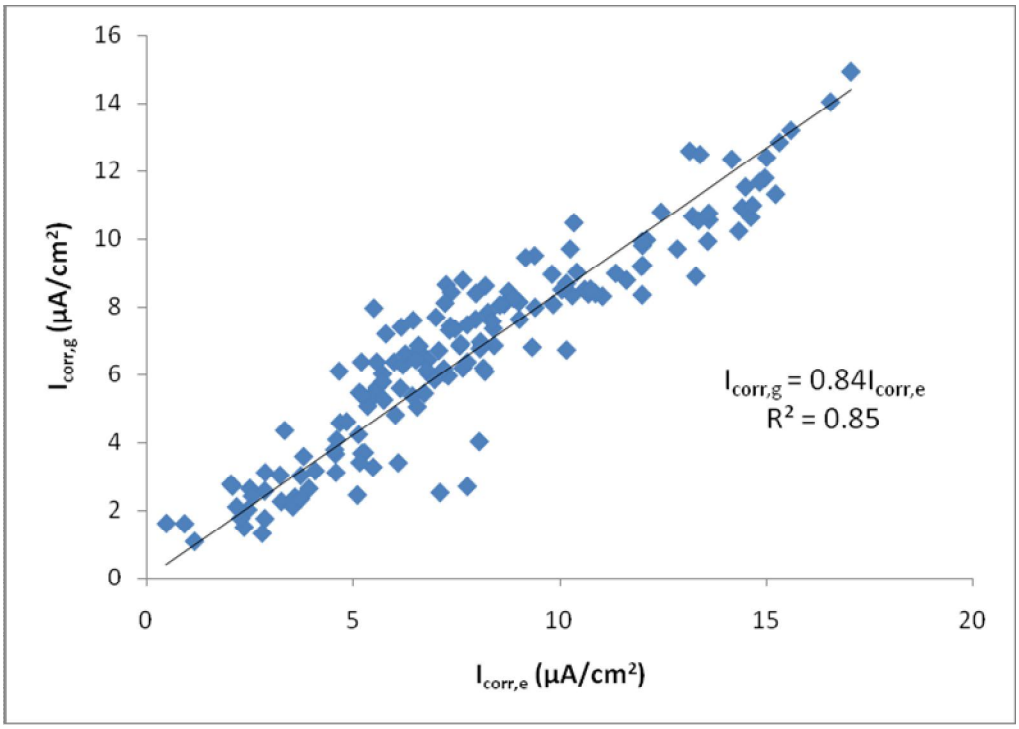

Figure 5.7: Correlation between $I_{corr,g}$ and $I_{corr,e}$ for 7% chloride concentration.

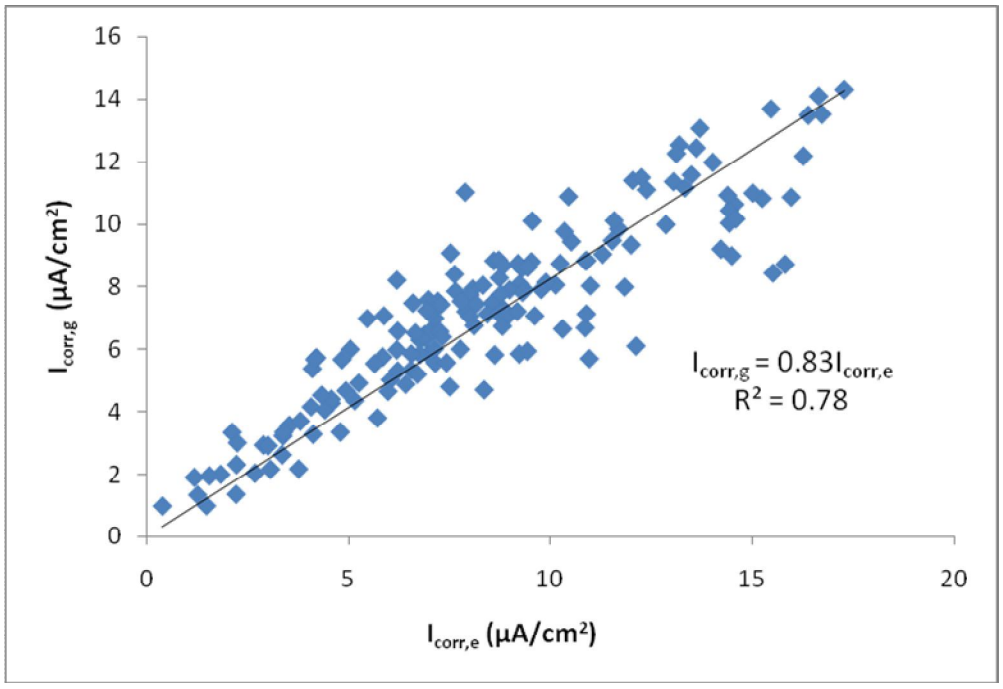

Figure 5.8: Correlation between $I_{corr,g}$ and $I_{corr,e}$ for 12% chloride concentration.

A close inspection of the results summarized above indicates that the effect of aggregate type, cover thickness and chloride concentration on the correlation between the corrosion current density determined by LPRM and GWLM are practically insignificant. Hence, a single plot of corrosion current density values determined by LPRM against corresponding corrosion current density values determined by GWLM for all the 486 specimens is shown in Figure 5.9. It is observed that a good correlation exists between the $I_{corr,g}$ and $I_{corr,e}$ as evident from a higher value of 'R^2'. From the correlation equation (shown in the Figure), the value of gravimetric corrosion current density can be taken, on an average, as 86% of the value of electrochemical corrosion current density.

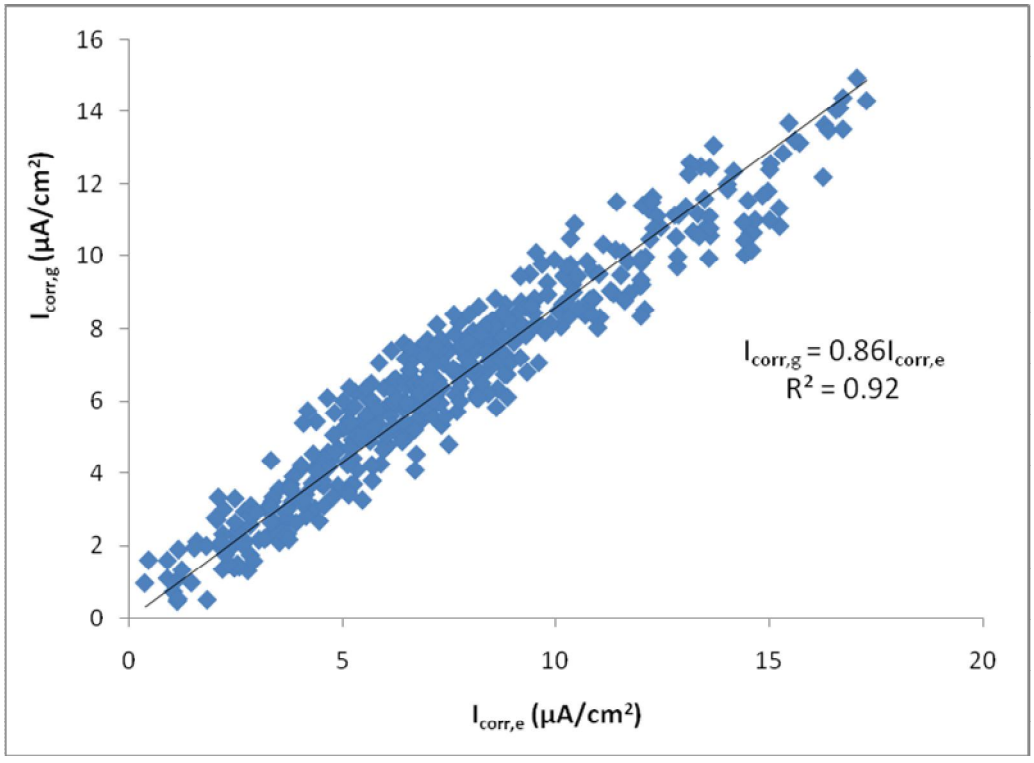

Figure 5.9: Correlation between $I_{corr,g}$ and $I_{corr,e}$ for all the specimens.

5.2 REGRESSION MODELS FOR CORROSION RATE

Since the gravimetrically computed reinforcement corrosion rates are found to be more accurate and reliable, the models for predicting corrosion current density in terms of water-cementitious materials ratio (w/cm ratio), fine to total aggregate ratio, cover thickness, cementitious materials content and chloride concentration were developed separately for the two types of aggregate using the gravimetric data. A linear form of the regression model was selected considering the linear variation of corrosion rate with major factors ($R_{W/C}$ and C_V) affecting corrosion rate**,** as observed from Figures 4.1 and 4.2. The regression models for corrosion current density obtained for both types of aggregates are presented in Table 5.1.

Table 5.1: Regression Models for Corrosion Current Density.

Aggregate Type	Regression models	R^2
H	$I_{corr} = -13.0 + 34.4R_{W/C} + 0.0244C_C + 3.83R_{F/T} + 0.0966C_L - 0.181C_V$	0.82
T	$I_{corr} = -18.4 + 43.8R_{W/C} + 0.027C_C + 4.77R_{F/T} + 0.115C_L - 0.203C_V$	0.94

5.3 UTILIZATION OF THE CORRELATION BETWEEN $I_{corr,g}$ AND $I_{corr,e}$ AND DEVELOPED MODELS

Correlation model developed between $I_{corr,g}$ and $I_{corr,e}$ and regression models obtained for corrosion current density are utilized in service-life prediction of existing RC structure and in carrying out durability based design of new RC structure. Use of the developed models is illustrated for typical case studies in the subsequent chapters.

CHAPTER 6

SERVICE LIFE PREDICTIONOF RC STRUCTURES

The service-life prediction of reinforced concrete structures was performed by utilizing the correlation between the corrosion current density determined using LPR method and gravimetric weight loss method developed in this study. The total service life is assumed to be the sum of time to corrosion initiation and time to corrosion cracking. The estimated time of corrosion initiation was determined using Fick's second law of diffusion, in which chloride ingress into concrete was assumed to be mainly through diffusion. The estimated time of corrosion cracking was determined using the empirical model developed by Morinaga [50].

6.1 METHODOLOGY FOR SERVICE LIFE PREDICTION

The following methodology was utilized to estimate the service life of a given RC structure:

i) Determine the diameter of steel bar (D), concrete cover (C_v), corrosion current density ($I_{corr,e}$), chloride concentration (C_L), threshold chloride concentration (C_{th}), surface chloride concentration (C_s), chloride diffusion coefficient (D_{app}) and the age of the structure (t).

ii) Convert the corrosion current density, $I_{corr,e}$ measured using electrochemical technique to equivalent corrosion current density, $I_{corr,g}$ using the relationship shown in Eq. 6.1.

$$I_{corr,g} = 0.86 I_{corr,e} \quad (6.1)$$

iii) Use Eq. 2.1 to determine the time to corrosion initiation, t_p using the values of concrete cover (C_v), threshold chloride concentration (C_{th}), surface chloride concentration (C_s) and chloride diffusion coefficient (D_{app}).

iv) Use Eqs. 2.4 through 2.6 to determine the time of corrosion cracking, t_{corr} using the values of concrete cover (C_v), diameter of tension bars (D) and corrosion current density ($I_{corr,g}$).

v) Determine the residual service life t_{RL} of the RC structure, by subtracting the given age of the structure (t) from the total service life as shown in eq. 6.2.

$$t_{RL} = t_p + t_{corr} - t \quad (6.2)$$

where: t_p = time to corrosion initiation and

t_{corr} = time to cover cracking

This five-step procedure for service life prediction is given in Figure 6.1. A case study is presented to illustrate this procedure.

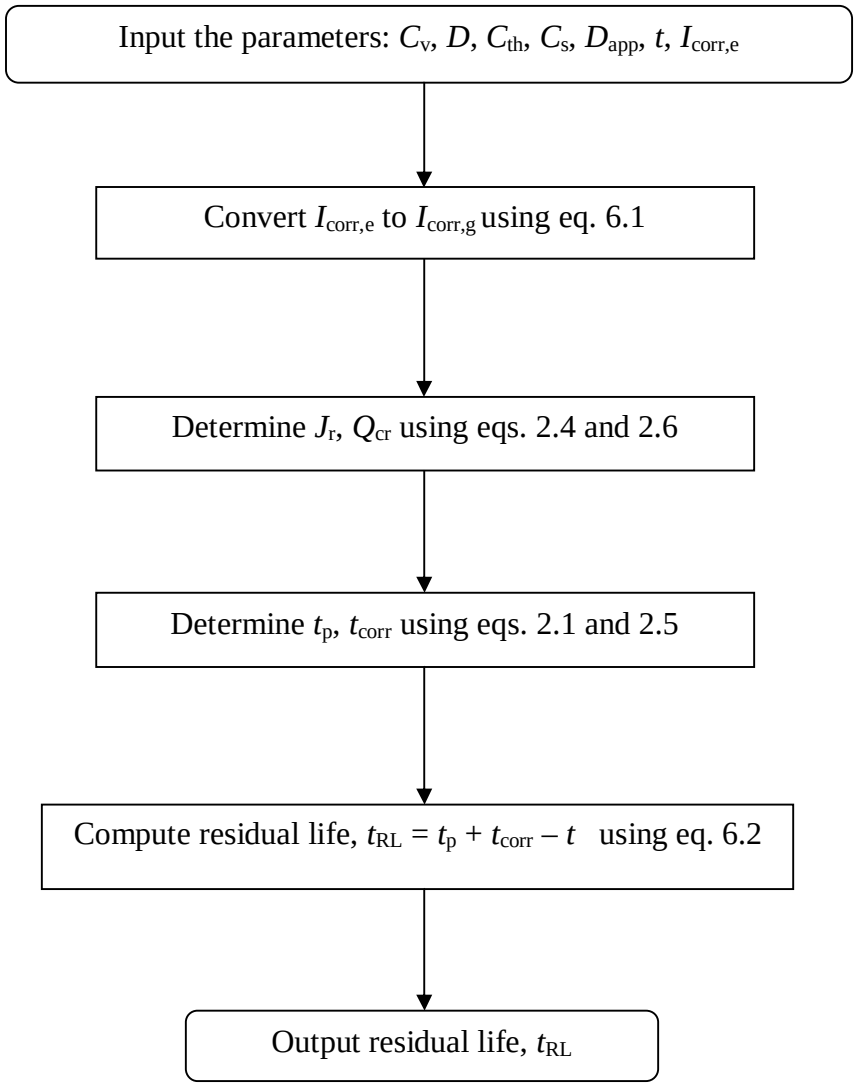

Figure 6.1: Flowchart for automated service life prediction of RC member

6.1.1 An example case-study of Service-life Prediction

For a given RC structure, the following information is to be used to determine the residual service life t_{RL} using the five-step procedure outlined above.

i) Diameter of tension bars, D = 16 mm

ii) Concrete cover, C_v = 50 mm

iii) Corrosion current density, $I_{corr,e}$(measured electrochemically) = 0.5 μA/cm^2

iv) Chloride concentration, C_L = 3%

v) Threshold chloride concentration, C_{th} = 0.1%

vi) Surface chloride concentration, C_s= 0.3%

vii) Chloride diffusion coefficient, D_{app} = 10^{-12} m^2/s

viii) Age of structure, t = 10 years

6.1.2 Solution Procedure

The corrosion current density is determined from the following relationship:

$I_{corr,g} = 0.86 I_{corr,e}$

$= 0.86 \times 0.5 = 0.43$ μA/cm^2

The values of C_v, C_{th}, C_s and D_{app} , the time of corrosion initiation t_p are determined as:

$$t_p = \frac{1}{12 D_{app}} \left[\frac{C_v}{1 - \left(C_{th} / C_s \right)^{0.5}} \right]^2$$

$$= \frac{1}{12 \times 10^{-12} \times 3600 \times 24 \times 365} \left[\frac{50 \times 0.001}{1 - \left(0.1 / 0.3 \right)^{0.5}} \right]^2$$

= 36.98 years

The time to corrosion cracking, t_{corr} is determined as follows:

$$t_{corr} = \frac{Q_{cr}}{J_r}$$

where:

$$Q_{cr} = 0.602 \times 10^{-4} \left(1 + \frac{2C_v}{D}\right)^{0.85} D$$

From which,

$$Q_{cr} = 0.602 \times 10^{-4} \left(1 + \frac{2 \times 50}{16}\right)^{0.85} \times 16 = 5.188 \times 10^{-3}\, g/cm^2$$

$$J_r = 9.126 \times 10^{-3} I_{corr}$$

$$= 9.126 \times 10^{-3} \times 0.43$$

$$= 3.924 \times 10^{-3} \text{ g/cm}^2\text{/year}$$

The time to cracking corrosion t_{corr} is computed as:

$$\therefore t_{corr} = \frac{5.188 \times 10^{-3}}{3.924 \times 10^{-3}} = 1.32 \text{ years}$$

The estimated residual service life is computed as:

$$t_{RL} = t_p + t_{corr} - t$$

$$= 36.98 + 1.32 - 10 = 28.3 \text{ years}$$

6.2 MICROSOFT EXCEL PROGRAM FOR SERVICE LIFE PREDICTION

The above five-step procedure (shown in the flowchart of Figure 6.1) was implemented in a Microsoft Excel program (SL_Predict) to provide a prediction for the service life of a RC structure in specified corrosive conditions. A sample printout of typical input and output data for service life prediction of RC members considered is presented in Table E

of Appendix E. The numerical example given in section 6.1 (above) is resolved using the program (SL_Predict) for other values of t, D, C_V, I_{corr} and C_L and the results obtained are listed in Table 6.1. It can be observed from the table that, as cover thickness (C_V) increased from 40 to 60 mm, residual service life increases (even at higher values of corrosion current density I_{corr} and chloride exposure C_L) from 15.68 to 31.08 years. This indicates that cover thickness have significant effect on service life of RC structures.

Table 6.1: Sample results of service-life prediction using the program **SL_Predict**

S/N	t (years)	D (mm)	C_V (mm)	I_{corr} ($\mu A/cm^2$)	C_L (%)	t_p (years)	t_{corr} (years)	Service life t_{RL} (years)
1	10	20	40	0.30	3	23.67	2.01	15.68
2	15	12	45	0.35	4	29.96	1.62	16.58
3	15	16	50	0.40	4	36.98	1.65	23.64
4	20	16	55	0.45	5	44.75	2.03	26.78
5	25	12	60	0.50	7	53.25	2.83	31.08

CHAPTER 7

DURABILITY-BASED DESIGN OF RC STRUCTURES

Durability-based design of reinforced concrete (RC) beams and columns can be performed by utilizing the regression models for prediction of corrosion current density developed in Chapter 5. The minimum value of corrosion current density (I_{corr}) can then be used to determine the loss of steel rebar due to corrosion which will be utilized for the durability-based design of a typical RC member. The procedure for durability-based structural design proposed by *Sarja and Vesikari* [61] was adopted in this work.

7.1 OPTIMIZATION OF CONCRETE MIXTURE PARAMETERS AND COVER THICKNESS

The developed regression models were utilized to determine optimum values of water/cementitious materials ratio ($R_{W/C}$), cementitious materials content (C_C), fine to total aggregate ratio ($R_{F/T}$) and concrete cover (C_V) for a given chloride concentration. A *Microsoft Excel Solver* was used to minimize the corrosion current density and obtained the corresponding optimum values of the concrete mixture parameters and cover thickness.

7.1.1 Objective function

The model for corrosion current density is set as an objective function for the optimization problem, given by Eqs. 7.1 and 7.2 for H-type aggregates and T-type aggregates, respectively.

For H-type aggregates

$$I_{corr} = -13.0 + 34.4R_{W/C} + 0.0244C_C + 3.83R_{F/T} + 0.0966C_L - 0.181C_V \quad (7.1)$$

For T-type aggregates

$$I_{corr} = -18.4 + 43.8R_{W/C} + 0.0270C_C + 4.77R_{F/T} + 0.115C_L - 0.203C_V \quad (7.2)$$

7.1.2 Decision variable

In optimization, a parameter is considered to be a decision variable if it significantly changes the value of the objective functions. In this problem, the concrete cover thickness (C_V) was found to be the decision variable.

7.1.3 Constraints

Constraints are the restrictions that must be satisfied for ensuring the acceptability of the optimal solutions obtained through objective functions. In this problem, the following are considered as constraints:

$$0.4 \leq R_{W/C} \leq 0.5 \quad (7.3)$$

$$350 \leq C_C \leq 400 \quad (7.4)$$

$$0.35 \leq R_{F/T} \leq 0.45 \quad (7.5)$$

$$25 \leq C_V \leq 50 \quad (7.6)$$

7.1.4 Optimization results

The minimum corrosion current density ($I_{corr,min}$)was set as 1μA/cm^2

H-type aggregates

For 3% NaCl concentration, the following optimum values are obtained as:

C_C = 350 Kg/m^3, $R_{W/C}$= 0.4, $R_{F/T}$ = 0.35, C_v = 50 mm, $I_{corr,min}$ = 1.88 μA/cm^2

By increasing the cover thickness (C_v) to 55 mm, $I_{corr,min}$ = 0.98 μA/cm^2

Hence, $I_{corr,min}$ = 0.98 μA/cm^2

T-type aggregates

For 3% NaCl concentration, the following optimum values are obtained:

C_c = 350 Kg/m^3, $R_{w/c}$ = 0.4, $R_{F/T}$ = 0.35, C_v = 50 mm, $I_{corr,min}$ = 0.43 μA/cm^2

Hence, $I_{corr,min}$ = 0.43 μA/cm^2

Print-outs of the *Microsoft Excel Solver* for H-aggregates and T-aggregates are shown in Figure F1 and F2, respectively in Appendix F.

The above optimization procedure was repeated using the models developed by Yusuf [6] as objective functions:

H-type aggregates

$$\begin{aligned} P_r = \; & 38.31 - 0.35C_C + 0.68Exp(-3.01R_{W/C}) + 54.68R_{F/T}^{3.6076} + 0.32C_V^{1.341} \\ & + 0.19Exp(-34.53C_L) + 0.78(C_C R_{W/C}) - 66.54(R_{W/C} R_{F/T}) \\ & - 4.01(R_{W/C} C_V) + 8.25Exp(13.20R_{W/C} C_L) - 0.97(C_V C_L) \end{aligned}$$

T-type aggregates

$$\begin{aligned} P_r = \; & -71.35 - 0.43C_C + 4.38Exp(2.011R_{W/C}) + 4.54R_{F/T}^{-0.0097} + 547.95C_V^{-1.046} \\ & + 13.81Exp(-60.83C_L) + 1.09C_C R_{W/C} + 0.0032C_C C_V \\ & + 57.65(R_{W/C} R_{F/T})^{0.703} - 0.037(R_{W/C} C_V)^{2.271} + 0.82(C_V C_L) \end{aligned}$$

It was found that, even at the maximum chloride exposure of 12%, the I_{corr} is negative for both types of aggregates as shown in Table F3 and F4 of Appendix F. This shows that, there will not be loss of rebar diameter.

7.2 METHODOLOGY FOR DURABILITY-BASED DESIGN

The following *five-step procedure* was utilized to design RC beams and columns considering durability as a design constraint:

i) *Microsoft Excel solver* is used to determine the optimum values of water to cementitious material ratio ($R_{W/C}$), cementitious material content (C_C), concrete cover (C_V), fine to total aggregate ratio ($R_{F/T}$) corresponding to minimum corrosion current density ($I_{corr,g}$) for a given chloride concentration, using the developed models for $I_{corr,g}$.

ii) The compressive strength $f_c^{'}$ and elastic modulus E_c of concrete are determined using the optimum values of $R_{W/C}$, C_C and $R_{F/T}$ in the following models developed by Yusuf [6].

$$f_c^{'} = -61.24 - 0.056C_c - 19.87Exp\left(2.083R_{w/c}\right) + 183.45R_{F/T}^{0.119} \quad (7.7)$$

$$E_c = -49.10 - 0.0048C_c - 13.23Exp\left(2.083R_{w/c}\right) + 145.68R_{F/T}^{0.106} \quad (7.8)$$

iii) The rate of loss of concrete cover and rebar diameter is determined using Eqs. 2.24 and 2.25 from the data obtained in steps (i) and (ii) given above. Then a preliminary section of the structural member is selected and the residual dimensions of the beam cross-section and the rebar diameter are determined.

iv) A structural durability-based design of reinforced concrete member is performed using the design information obtained in step (iii) given above.

v) The adequacy of the final cross-section and rebar diameter is checked against prescribed design requirements.

The executions of the design methodology for carrying out the structural durability-based design are outlined in the flowcharts shown in Figures 7.1 and 7.2 for the design of RC beams and columns, respectively. Case studies are presented to illustrate this procedure.

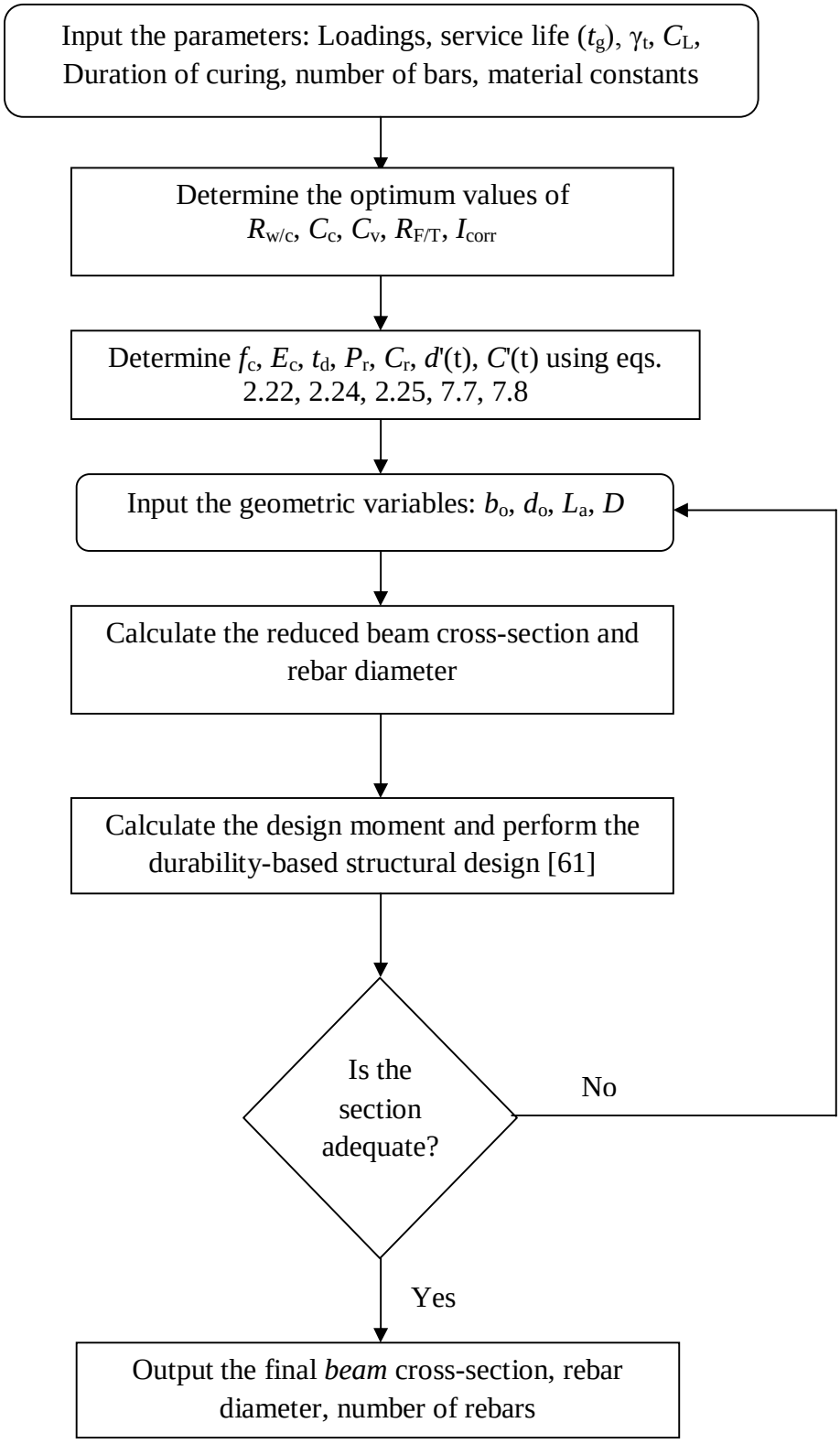

Figure 7.1: Flowchart for automated durability-based design of RC beam.

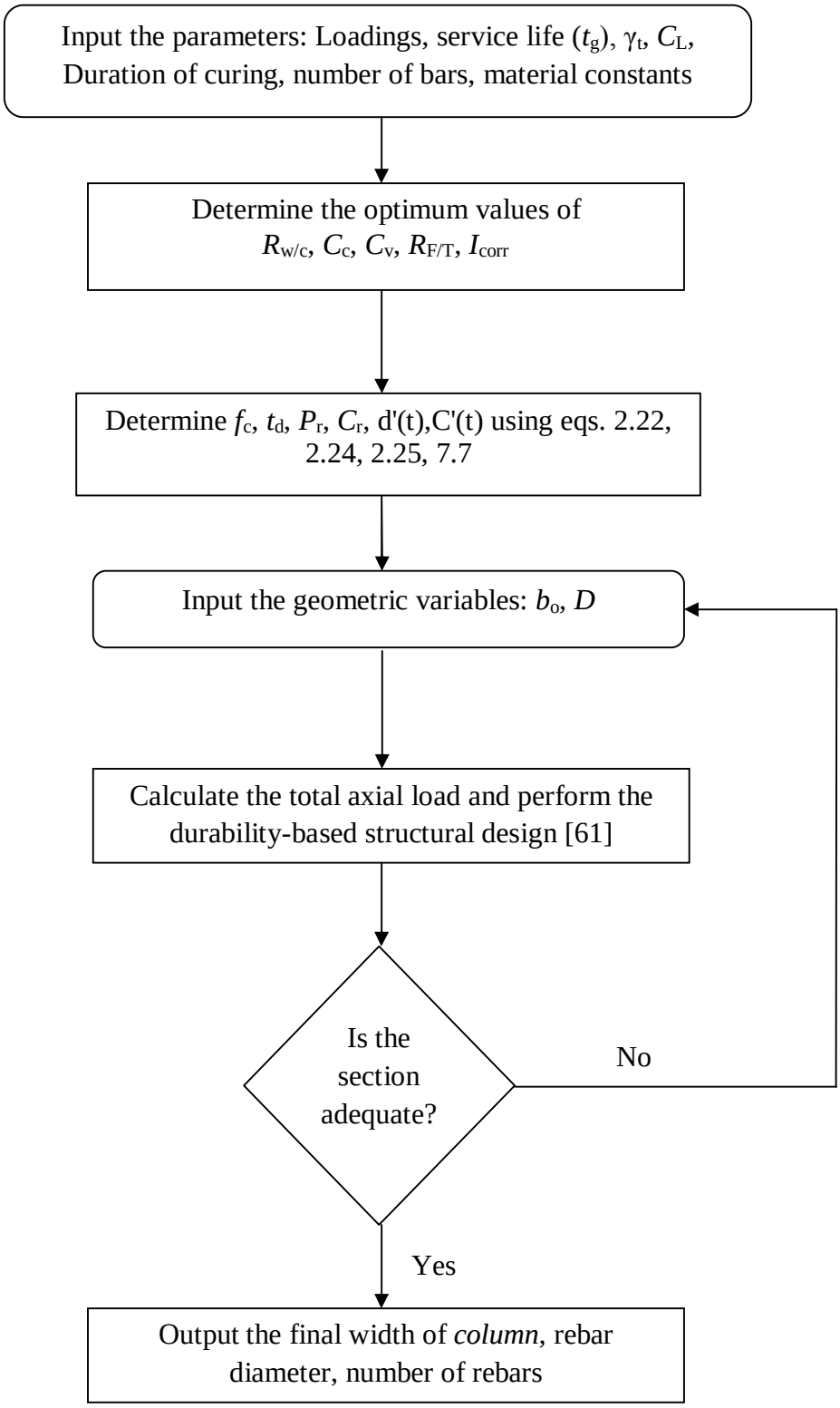

Figure 7.2: Flowchart for automated durability-based design of RC column.

7.3 EXAMPLE CASE-STUDIES ON DURABILITY-BASED DESIGN

7.3.1 Durability-based Design of RC Beam

Considering the durability requirement, a singly-reinforced concrete beam having a span of 6m and subjected to a dead load of 10kN/m and live load of15kN/m is to be designed according to ACI 318-08 [74] design specifications. Assume the following information:

i) Initial diameter of tension bars, D_o = 20 mm

ii) Number of tension rebars = 3

iii) Chloride concentration, C_L = 3%

iv) Target service-life, t_g = 50 years, and desired service-life factor, γ_t = 1.8

v) Yield strength of steel, f_y = 400 MPa

vi) Elastic modulus of steel, E_s = 200GPa

vii) Duration of curing = 28days

viii) Type of aggregate = H-type

Use the durability-based design methodology to determine a suitable cross section for the RC beam.

Solution steps

Given the values of loadings, and material constants etc, the durability-based design can be performed as follows:

i) Determination of optimum values of concrete mix and I_{corr}

For a specified chloride concentration, C_L of 3%, the optimum values of concrete mix, concrete cover and corrosion current density were determined using *Microsoft Excel Solver* by optimizing the model of corrosion current density for H-type aggregate shown in Table 5.1. The optimum values obtained are as follows:

$R_{W/C}$ = 0.4, C_V = 50 mm, C_C = 350 kg/m^3, $R_{F/T}$ = 0.35, I_{corr} = 1.88μA/cm^2

ii) Determination of compressive strength $f_c^{'}$ and elastic modulus E_c

The maximum values of compressive strength $f_c^{'}$ and elastic modulus E_c of the concrete are obtained as follows:

$$f_c^{'} = -61.24 - 0.056C_c - 19.87Exp(2.083R_{w/c}) + 183.45R_{F/T}^{0.119}$$

$$= -61.24 - 0.056 \times 350 - 19.87Exp(2.083 \times 0.4) + 183.45 \times 0.35^{0.119}$$

= 35.35 MPa

$$E_c = -49.10 - 0.0048C_c - 13.23Exp(2.083R_{w/c}) + 145.68R_{F/T}^{0.106}$$

$$= -49.10 - 0.0048 \times 350 - 13.23Exp(2.083 \times 0.4) + 145.68 \times 0.35^{0.106}$$

= 49.12 GPa

iii) Determination of rate of loss of concrete cover and rebar diameter

The design service life, t_d of the beam is obtained as:

$$t_d = \gamma_t t_g$$

$$= 1.8 \times 50 = 90 \text{ years}$$

The durability coefficients are determined as follows:

The curing coefficient C_{cur} is determined as:

$$C_{cur} = \frac{1}{0.85 + 0.17\log_{10}(d)}$$

$$= \frac{1}{0.85 + 0.17\log_{10}(28)}$$

= 0.912

Assuming an environmental coefficient C_{env} to be 10000, the rate of loss of concrete, C_r is determined as:

$$C_r = \frac{C_{env} C_{cur}}{f_c^{3.3}}$$

$$= \frac{1000 \times 0.912}{35.35^{3.3}} = 0.07085 \text{ mm/year}$$

The corrosion penetration rate is determined as:

$$P_r = 11.7 I_{\text{corr}}$$

$$= 11.7 \times 1.88 \times 10^{-3}$$

$$= 0.021996 \text{mm/year}$$

From the values of rate of loss of concrete and corrosion penetration rate, the loss of concrete cover and loss of rebar diameter are obtained as:

$$c'(t_d) = C_r t_d$$

$$= 0.07085 \times 90 = 6.38 \text{mm}$$

$$d'(t_d) = P_r t$$

$$= 0.021996 \times 90 = 1.98 \text{mm}$$

The residual dimensions of the beam cross-section and the rebar diameter are determined as:

$$b' = b_o - 2c'(t_d) = b_o - 2 \times 6.38 = (b_0 - 12.76) \text{mm}$$

$$d' = d_o - 2c'(t_d) = d_o - 6.38 = (d_0 - 6.38) \text{mm}$$

$$D' = D_o - 2d'(t_d) = 20 - 2 \times 1.98 = 16.04 \text{ mm}$$

Then with the initial width (b_o) and depth (d_o) of the beam given as 300 mm and 100 mm respectively, the reduced dimensions of the beam are obtained as follows:

$$b' = 300 - 12.76 = 287.24 \text{ mm}$$

$$d^{'} = 100 - 6.38 = 93.62\,\text{mm}$$

iv) Flexure-based design

Using the overload factors recommended in section 9-2 of ACI 308-08 for dead load (γ_d) and live load (γ_L) as 1.2 and 1.6 respectively, the total factored design load (w) and the design moment (M_d) are determined (for a simply supported beam) as:

$$w = \gamma_d D_d + \gamma_L D_L$$

$$= 1.2 \times 10 + 1.6 \times 15 = 36 \text{ kN/m}$$

$$M_d = \frac{wl^2}{8}$$

$$= \frac{36 \times 6^2}{8} = 162 \text{ kNm} = 1.62 \times 10^8 \text{ Nmm}$$

The factored load bearing capacity of the beam is determined as:

$$R_{ds} = \frac{A_s(t_d) Z(t_d) f_y}{\gamma_s}$$

$$R_{dc} = \frac{b(t_d).x.(t_d) f_c}{\gamma_c}$$

where: $A_s(t_d) =$ No. of bars $\times \frac{\pi}{4}\left[D_o - 2d^{'}(t_d)\right]^2$

$$= 3 \times \frac{\pi}{4}\left[20 - 2 \times 1.98\right]^2 = 606.34 \text{ mm}$$

$$x(t_d) = d^{'}.\mu(t_d).n.\left[-1 + \left(1 + \frac{2}{\mu.n}\right)^{1/2}\right]$$

$$\mu(t_d) = \frac{A_s(t_d)}{b'd'} = \frac{606.34}{287.24 \times 93.62} = 0.02255$$

$$n = \frac{E_s}{E_c} = \frac{200}{49.12} = 4.072$$

Then, $x(t_d) = 93.62 \times 0.02255 \times 4.072\left[-1+\left(1+\frac{2}{0.02255 \times 4.072}\right)^{1/2}\right] = 32.43$ mm

Internal force arm, $Z(t_d) = d' - 0.4(t_d) = 93.62 - 0.4 \times 32.43 = 80.65$ mm

$$\therefore R_{ds} = \frac{606.34 \times 80.65 \times 400}{1.15}$$

$$= 1.701 \times 10^7 \text{ Nmm}$$

$$R_{dc} = \frac{287.24 \times 32.43 \times 80.65 \times 35.35}{1.5}$$

$$= 8.85246874 \times 10^6 \text{ Nmm}$$

Error if steel stress is decisive, $e_s = (M_d - R_{ds})$

$$= 1.62 \times 10^8 - 1.701 \times 10^7$$

$$= 1.45 \times 10^8 \text{ Nmm}$$

Error if concrete stress is decisive, $e_c = (M_d - R_{dc})$

$$= 1.62 \times 10^8 - 8.85246874 \times 10^6$$

$$= 1.5315 \times 10^8 \text{ Nmm}$$

Microsoft Excel Solver is used to iteratively minimize the error. Then depth of the beam is found to be:

d = 818.46 mm (if the steel stress controls)

d = 572.04 mm (if the concrete stress controls)

By changing the initial diameter of the rebar being to 25mm, new depth of the beam is obtained as:

d = 495.37 mm (if the steel stress controls)

d = 497.74 mm (if the concrete stress controls)

Therefore, the depth of the beam (*d*) is taken as 500 mm.

v) Checking for adequacy of cross-section

To check the adequacy of the section;

$M_o = \gamma_d M_d + \gamma_L M_L$ (where $\gamma_d = \gamma_L = 1$)

$$= \frac{(1\times 10 + 1\times 15)\times 6^2}{8} = 112.5 \text{ kNm}$$

New area of steel, $A_s = 3\times\frac{\pi}{4}\times 25^2 = 1472.62 \text{ mm}^2$

New $d' = 497.74 - 6.38 = 491.36$ mm

Corrected internal force arm, z = $491.36 - 0.4\times 106.67 = 448.69$ mm

Initial state of load bearing capacity, $R_o = \frac{1472.62\times 448.69\times 400}{1}\times 10^{-6}$

= 264.30 kNm

Corrected area of steel, $A_s = 3\times\frac{\pi}{4}\times(25 - 2\times 1.98)^2 = 1043.04 \text{ mm}^2$

Final state of load bearing capacity, $R_m = \frac{1043.04\times 448.69\times 400}{1}\times 10^{-6}$

= 187.20 kNm

Safety margin at the initial state of the structure, $\theta_o = R_o - M_o$

= 264.30 – 112.5 = 151.80 kNm

Safety margin at the initial state of the structure, $\theta_m = R_m - M_o$

= 187.20 – 112.5 = 74.70 kNm

Relative reduction of the safety margin during design service life,

$$m = \frac{\theta_o - \theta_m}{\theta_o} = \frac{151.8 - 74.7}{151.8} = 0.508 < 0.7, \text{ hence the design is OK}$$

Final section of the beam would be as follows:

Steel bar diameter, D_o = 25 mm

Cross-sectional dimension b_o = 300 mm and d_o = 500 mm

7.3.2 Durability-based Design of RC Column

Considering durability-based requirement, an RC column is subjected to dead load of 1000 kN and live load of 2000 kN and is to be designed with the following information:

i) Initial diameter of tension bars, D_o= 12 mm

ii) Number of tension rebars = 4

iii) Chloride concentration, C_L = 3%

iv) Target service-life, t_g = 50 years, and desired service-life factor, γ_t = 2

v) Yield strength of steel, f_y = 400 MPa

vi) Duration of curing = 28 days

vii) Type of aggregate = H-type

Design this RC column according to ACI 318-08 design specification.

Solution steps

Given the values of loadings, and material constants etc, the durability-based design can be performed as follows:

i) Determination of optimum values of concrete mix and I_{corr}

For specified chloride concentration, C_L of 3%, optimum values of concrete mix, concrete cover and corrosion current density were determined using *Microsoft Excel*

Solver by optimizing the model of corrosion current density for H-type aggregate shown in Table 4.9.

The optimum values obtained are:

$R_{W/C} = 0.4$, $C_V = 50$ mm, $C_C = 350$ kg/m^3, $R_{F/T} = 0.35$, $I_{corr} = 1.88$ μA/cm^2

ii) Determination of compressive strength $f_c^{'}$

The maximum value of compressive strength $f_c^{'}$ is:

$$f_c^{'} = -61.24 - 0.056C_c - 19.87Exp(2.083R_{w/c}) + 183.45R_{F/T}^{0.119}$$

$$= -61.24 - 0.056 \times 350 - 19.87Exp(2.083 \times 0.4) + 183.45 \times 0.35^{0.119} = 35.35 \text{ MPa}$$

iii) Determination of rate of loss of concrete cover and rebar diameter

The design service life, t_d of the column is obtained as:

$$t_d = \gamma_t t_g$$

$$= 2 \times 50 = 100 \text{ years}$$

The durability coefficients are determined as follows:

The curing coefficient C_{cur} is determined using eq. 2.23 as:

$$C_{cur} = \frac{1}{0.85 + 0.17\log_{10}(d)}$$

$$= \frac{1}{0.85 + 0.17\log_{10}(28)} = 0.912$$

Assuming an environmental coefficient C_{env} to be 10000, the rate of loss of concrete, C_r is determined using eq. 2.22 as:

$$C_r = \frac{C_{env}C_{cur}}{f_c^{3.3}}$$

$$= \frac{1000 \times 0.912}{35.35^{3.3}} = 0.07085 \text{ mm/year}$$

The corrosion penetration rate is determined using eq. 3.5 as:

$P_r = 11.7 I_{corr}$

$= 11.7 \times 1.88 \times 10^{-3} = 0.021996$ mm/year

From the values of rate of loss of concrete and corrosion penetration rate, the loss of concrete cover and loss of rebar diameter are obtained as:

$$c^{'}(t) = C_r t_d$$

$$= 0.07085 \times 100 = 7.09 \text{ mm}$$

$$d^{'}(t) = P_r\, t$$

$$= 0.021996 \times 100 = 2.199 \text{ mm}$$

iv) Design for axial load

Based on overload factors for dead load (γ_d) and live load (γ_L) taken as 1.2 and 1.6 respectively, the total factored design axial load (M_d) is determined [ACI 308-08 section 9-2] as :

$$M_d = \gamma_d D_d + \gamma_L D_L$$

$$= 1.2 \times 1000 + 1.6 \times 2000 = 4400 \text{ KN} = 4.4 \times 10^6 \text{ N}$$

The factored load bearing capacity of the column at the end of the service life is determined as;

$$R_d(t_d) = \frac{A_c(t_d) f_c}{\gamma_c} + \frac{A_s(t_d) f_y}{\gamma_s}$$

where: $A_s(t_d) = \text{Area of steel} = \text{No. of bars} \times \frac{\pi}{4}\left[D_o - 2d^{'}(t_d)\right]^2$

$$= 4 \times \frac{\pi}{4}[12 - 2 \times 2.199]^2 = 181.49\,\text{mm}^2$$

$A_c(t_d) =$ Area of concrete $= [b_o - 2c'(t_d)]^2$

By letting the initial trial width (b_o) value of the column to be 100 mm, it implies that:

$$A_c(t_d) = [100 - 2 \times 7.09]^2 = 7366.19 \text{ mm}^2$$

Hence, $R_d(t_d) = \frac{7366.19 \times 35.35}{1.5} + \frac{181.49 \times 400}{1.2}$

$$= 2.341 \times 10^5 \text{ N}$$

Error = ($M_d - R_d$) = $4.4 \times 10^6 - 2.341 \times 10^5 = 4.17 \times 10^6$ N

By using an automated *Microsoft Excel Solver*, the error has been iteratively reduced to zero and width of the column cross section is found to be:

b = 443.28 mm

Therefore, the width of the column (b) is taken as 445 mm.

v) Checking for adequacy of cross-section

To check the adequacy of the section;

$M_o = \gamma_d M_d + \gamma_L M_L$ (where $\gamma_d = \gamma_L = 1$)

$$= 1 \times 1000 + 1 \times 2000 = 3000\,\text{kN}$$

Initial state of load bearing capacity,

$$R_o = \frac{443.28^2 \times 35.35 + 3.142 \times 12^2 \times 400}{1} \times 10^{-3} = 7127.34 \text{ kN}$$

Final state of load bearing capacity,

$$R_m = \frac{(443.28 - 2 \times 7.09)^2 \times 35.35 + 181.49 \times 400}{1} \times 10^{-3} = 6581.85 \text{ kN}$$

Safety margin at the initial state of the structure, $\theta_o = R_o - M_o$

$= 7127.34 - 3000 = 4127.34$ kN

Safety margin at the final state of the structure, $\theta_m = R_m - M_o$

$= 6581.85 - 3000 = 3581.85$ kN

Relative reduction of the safety margin during design service life,

$$m = \frac{\theta_o - \theta_m}{\theta_m} = \frac{4071.86 - 3579.69}{4071.86} = 0.1322 < 0.7,$$ hence the design is OK

Final cross section of the column would be as follows:

Steel bar diameter $D_o = 12$ mm and $b_o = 443$ mm (square cross section)

7.4 AUTOMATED DURABILITY-BASED DESIGN OF RC MEMBERS

The above five-step procedure (shown in the flowcharts of Figures 7.1 and 7.2) was implemented in *Microsoft Excel* programs developed to perform durability-based structural design of RC beams and columns. The programs (named: RC_B_DDesign and RC_C_DDesign) are designed to make use of *Solver* command and automatically give the section of the member and the diameter of steel reinforcing bars, for specified input data. Sample print-outs of typical input design-data and output-design values for durability design of RC beam and column considered in section 7.3 are provided in Tables G1 and G2, respectively in Appendix G.

The two programs (*namely*: RC_B_DDesign and RC_C_DDesign) are used to re-solve the examples described in sections 7.3.1 and 7.3.2. The durability-based designs for two typical design case-studies for a beam-case and a column-case with other values of t_g, and loadings, etc. are listed in Tables 7.1 and 7.2. The numerical results (summarized below)

also include values obtained for two comparative-design case studies that highlight the utilization of the proposed design procedures.

a) Design Case-study for a RC-Beam

The sample results from using the RC_B_DDesign program for durability-based design of RC beam are presented in Table 7.1. For the case-study A (corresponding to rows 1 to 3) the chloride concentration C_L is constrained to vary between 3% to 12% and target service-life is specified as 40 years with other input design variables kept constant. For 3% chloride concentration, the optimum beam width and depth were found as 200 and 528 mm, respectively, while optimum bar diameter was found as 18 mm. Also, for 7% chloride concentration, the optimum beam width and depth were found as 200 and 403 mm, respectively, while optimum bar diameter was found as 20 mm. The optimum beam width and depth were found as 200 and 310 mm, respectively, while optimum bar diameter was found as 23 mm for 12% chloride concentration. Similarly, for the second case-study B (corresponding to rows 4 to 6); chloride concentration C_L is varied between 3% to 12% and target service-life is specified as 50 years with other input design variables kept constant. For 3% chloride concentration, the optimum beam width and depth were found as 225 and 436 mm, respectively, while optimum bar diameter was found as 20 mm. Also, for 7% chloride concentration, the optimum beam width and depth were found as 225 and 331 mm, respectively, while optimum bar diameter was found as 22 mm. The optimum beam width and depth were found as 225 and 300 mm, respectively, while optimum bar diameter was found as 24 mm for 12% chloride concentration. Also, for the third case-study C (corresponding to rows 7 to 9); chloride concentration C_L is varied between 3% to 12% and target service-life is specified as 70

years with other input design variables kept constant. For 3% chloride concentration, the optimum beam width and depth were found as 225 and 345 mm, respectively, while optimum bar diameter was found as 22 mm. For 7% chloride concentration, the optimum beam width and depth were found as 225 and 300 mm, respectively, while optimum bar diameter was found as 24 mm. The optimum beam width and depth were found as 225 and 300 mm, respectively, while optimum bar diameter was found as 24 mm for 12% chloride concentration. For *comparative study purposes*, it is observed that in case A, the optimum values of design variables of the beam were found to correspond to the least specified 3% value of chloride concentration C_L. And the optimal values of reinforcing steel bar diameter D_{optim} of 18.11 mm, 19.60 mm, 22.04 mm correspond to the target design life t_g of 40, 50, and 70 years, respectively.

b) Design Case-study for a RC-Column

The sample results from using the RC_C_DDesign program for durability-based design of RC column are presented in Table 7.2. For the case-study A (corresponding to rows 1 to 3) the chloride concentration C_L is constrained to vary between 3% to 12% and target service-life is specified as 40 years with other input-design variables kept constant. The optimum cross-section dimension of the *square* column was found as 150 mm, while optimum bar diameter was found as 16 mm for all the three chloride concentrations. For the second case-study B (corresponding to rows 4 to 6), chloride concentration C_L is varied between 3% to 12% and target service-life is specified as 50 years with other input design variables kept constant. The optimum section of the column was found as 150 mm, while optimum bar diameter was found as 16 mm, for both 3% and 7% chloride concentrations. For 12% chloride concentration, the optimum section of the column was

found as 170 mm, while optimum bar diameter was found as 16 mm. Also, for the third case-study C (corresponding to rows 7 to 9), chloride concentration C_L is varied between 3% to 12% and target service-life was specified as 70 years with other input design variables kept constant. For 3% chloride concentration, the optimum section of the column was found as 150 mm, while optimum bar diameter was found as 16 mm. For 7% chloride concentration, the optimum section of the column was found as 268 mm, while optimum bar diameter was found as 16 mm. For 12% chloride concentration, the optimum section of the column was found as 650 mm, while optimum bar diameter was found as 16 mm. And for *comparative purposes*, it is *interesting* to note that for the column case-studies with the given specified design conditions (*with axial load that are unlikely to cause concrete cracking*), and *unlike* the beam-case studies, the optimal-design values of column cross-section and steel bar diameter D are *not* influenced by the variation of the chloride-concentration.

Table 7.1: Sample results from using the **program RC_B_DDesign** for durability-based design of RC beam.

S/N	Input design values						Optimal design values		
	Span of beam, L_a (mm)	Dead load (kN/m)	Live load (kN/m)	Target life, t_g (years)	No. of bars, N	C_L (%)	Beam-width b_{optim} (mm)	Beam-depth, d_{optim} (mm)	Bar diameter, D_{optim} = D+ΔD (mm)
1	3.0	10	12	40	4	3	200	528	18.11
2	3.0	10	12	40	4	7	200	403	20.71
3	3.0	10	12	40	4	12	200	310	23.59
4	3.0	10	12	50	4	3	225	436	19.60
5	3.0	10	12	50	4	7	225	331	22.49
6	3.0	10	12	50	4	12	225	300	23.63
7	3.0	10	12	70	4	3	225	345	22.04
8	3.0	10	12	70	4	7	225	300	23.63
9	3.0	10	12	70	4	12	225	300	23.63
Comparative Studies:							Optimum values:		
A	Case-study A (corresponding to rows 1 to 3) chloride concentration C_L is constrained to vary between 3% to 12%.						D_{optim} = 18.11 mm		
B	Case-study B (corresponding to rows 4 to 6) chloride concentration C_L is constrained to vary between 3% to 12%.						D_{optim} = 19.60 mm		
C	Case-study C (corresponding to rows 7 to 9) chloride concentration C_L is constrained to vary between 3% to 12%.						D_{optim} = 22.04 mm		

Note: ΔD = Additional increment to steel bar diameter to off-set corrosion effect

Table 7.2: Sample results from using the **program RC_C_DDesign** for durability-based design of RC column.

S/N	Input design values					Optimal design values	
	Dead load (kN)	Live load (kN)	Target life, t_g (years)	No. of bars, N	C_L (%)	Column width, b_{optim} (mm)	Bar diameter, $D_{optim=}$ D+ΔD (mm)
1	100	120	40	4	3	150	15.76
2	100	120	40	4	7	150	15.76
3	100	120	40	4	12	150	15.76
4	100	120	50	4	3	150	15.76
5	100	120	50	4	7	150	15.76
6	100	120	50	4	12	170	15.76
7	100	120	70	4	3	150	15.76
8	100	120	70	4	7	268	15.76
9	100	120	70	4	12	650	15.76

CHAPTER 8

CONCLUSIONS AND RECOMMENDATIONS

8.1 CONCLUSIONS

In this research study, 486 concrete specimens with centrally placed reinforcing steel bar were subjected to experimental conditions for chloride-induced corrosion. The study was conducted to develop a correlation between the corrosion current density determined based on the data from linear polarization resistance method (LPRM) and gravimetric weight loss method (GWLM). Reliable models for prediction of reinforcement corrosion rate were also developed. The key design parameters considered were aggregate type, water to cementitious materials ratio $R_{W/C}$, cementitious materials content C_C, fine to total aggregate ratio $R_{F/T}$, concrete cover thickness C_V, and chloride concentration C_L. The models developed were utilized to minimize the corrosion current density I_{corr} by selecting optimal values of concrete mix parameters and cover thickness for a given chloride concentration. The developed correlation and models were utilized in developing an approach for service life prediction of existing RC structure and outlining a methodology for durability-based design of a new RC structure. Based on the results obtained the following conclusions are made:

1. Values of corrosion current density I_{corr} determined using both linear polarization resistance method (LPRM) and gravimetric weight loss method (GWLM) for both types of aggregates (namely: H-type aggregate and T-type aggregate) generally increased with an increase in the water to cementitious materials ratio.
2. This study affirms that service life of a RC structure increases with a decrease in water to cementitious materials ratio. This affirmation is due to the fact that corrosion current density (being a significant factor for service life prediction of RC structures) is found to increase with an increase in the water to cementitious materials ratio.
3. Corrosion current density I_{corr} decreases with concrete cover thickness increase from 25 to 50 mm. As the cover thickness influences the corrosion of the reinforcing steel, and its quality influences the diffusion rate of oxygen through concrete matrix, the findings of this study are in agreement with the findings of other researchers, that there is a significant increase in the time required for chloride ions to reach the steel reinforcing bars with increasing cover thickness, which in turn extends the service life of RC structure.
4. There is a significant decrease in the corrosion current density I_{corr} when concrete cover thickness was increased from 25 to 37.5 mm while the decrease in corrosion current density was not proportionally appreciable with cover thickness increase from 37.5 to 50 mm.
5. Corrosion current density I_{corr}-value increased with an increase in chloride concentration. This finding re-affirms similar findings in relevant literature as regards effects of chloride concentration on corrosion current density.

6. There is no clear trend in the values of corrosion current density I_{corr} when cementitious materials content increased from 350 to 400 kg/m^3. This finding may be attributed to the fact that increase in cementitious materials content from 350 to 400 kg/m^3 has been proven not to significantly improve quality of concrete matrix.
7. Fine to total aggregate ratio does not have a significant effect on the corrosion current density I_{corr}-value, since there is no definite trend in the values of corrosion current density with an increase of fine to total aggregate ratio. This finding may be attributed to the fact that the increase in fine to total aggregate ratio from 0.35 to 0.45 has been proven not to significantly improve quality of concrete matrix.
8. At lower *w/c ratio*, the corrosion current density I_{corr}-values in the concrete specimens prepared with H-type aggregates were generally more than that in the concrete specimens prepared with T-type aggregates. But, at higher *w/c ratio*, the corrosion current density values for H-type aggregate were either lower or nearly the same with that of T-type aggregate. This finding may be attributed to the particular properties of the tested H-type aggregates showing higher value of water absorption and this implicitly means that concrete specimens with T-type aggregates performed better than those with H-type aggregates at lower *w/c ratio*.
9. Results from analysis of variance of compiled data indicate that $R_{W/C}$ and C_V have significant effect on the corrosion current density I_{corr}. However, the results also show that $R_{F/T}$, C_C and C_L have minor effect in predicting corrosion current density I_{corr}.

10. Correlation analysis of corrosion current density values determined by LPRM and GWLM for both H-type aggregates and T-type aggregates shows a close agreement of results obtained from the two methods as evident from the values of regression coefficient of 0.80 and 0.88, determined respectively for the two methods. Moreover, the relationship of the corrosion current density from the two methods for H-type aggregates and T-type aggregates are respectively 0.84 and 0.86, which are close to the average value of 0.85. This finding indicates that the effect of aggregate type on the relationship between the values of corrosion current density (i.e. $I_{corr,e}$ and $I_{corr,g}$ obtained using LPRM and GWLM) is insignificant.
11. Correlation between corrosion current density values $I_{corr,e}$ and $I_{corr,g}$ determined by LPRM and GWLM for concrete specimens with 25, 37.5 and 50 mm concrete cover thickness indicates a close agreement of results obtained from the two methods as evident from the values of regression coefficient of 0.82, 0.84 and 0.86, respectively. Moreover, the relationship of the corrosion current density determined by the two methods for 25, 37.5 and 50 mm, respectively, are 0.84, 0.91 and 0.87. Then the values are also close to the average value of 0.87. This indicates that the effect of concrete cover thickness on the relationship between corrosion current density obtained using LPRM and GWLM is also insignificant.
12. The relationship of the corrosion current density from the LPRM and GWLM for chloride concentration of 3%, 7% and 12%, respectively, are 0.88, 0.84 and 0.83. These values are close to the average value of 0.85, and show that effect of

chloride concentration on the relationship between corrosion current density values obtained using LPRM and GWLM is also insignificant.

13. The results obtained in this research study are expressed in terms of corrosion current density values $I_{corr,g}$ and $I_{corr,e}$. It is also found that $I_{corr,g}$ values are consistently lower than $I_{corr,e}$ values. Considering the multi-dimensional nature of design variables considered in a typical concrete mix design and/or the experimental testing set-up, it may be concluded that the GWLM yield results that are less conservative for design purposes compared to results by the LPRM. But, with realizing limitations imposed on the experimental modeling due to the neglect of real random spatial variations of materials, structural properties (i.e. due to in homogeneities) and environmental variations that all combine to affect the LPR measurements set-up, it is concluded that $I_{corr,g}$ model would be more accurate and reliable to use for durability-based design.

8.2 RECOMMENDATIONS

Based on the results obtained from this research work and the analysis provided, the following recommendations are made:

1. The experimental investigation described herein should be extended to evaluate the performance of different types of reinforcing steel bars and concrete quality against chloride induced reinforcement corrosion.
2. A more refined research study should be carried out to examine the combined effect of chloride and carbonation on reinforcement corrosion.
3. This work can be extended to consider more refined studies for multi-objective functions for beam and beam-columns with other loading and support conditions.
4. A future work on the subject of durability-based design of RC structures should be extended to consider the influence of non systematic (random) spatial variations of material, structural and environmental conditions.

REFERENCES

1. Bentur A., Diamond S. and Berke N. S., "*Steel Corrosion in Concrete: Fundamentals and Civil Engineering Practice*", E&FN Spon, London, UK, 1997.

2. Saricimen H., "*Concrete Durability Problems in the Arabian Gulf Region- A review*", Proceedings Fourth international conference deterioration and repair of R.C. in the Arabian Gulf, Bahrain, 1993.

3. Shameem M., Maslehuddin M., Saricimen H., and Al-Mana A. I., "*Extending the Life of Reinforced Concrete Structures in the Arabian Gulf Environment", Proceedings, S*tructural Faults and Repairs conference, London, July 1995, pp. 115-126.

4. Ali S. I., "*Effects of aggregate quality on reinforcement corrosion*", MSc thesis submitted to the Deanship of Graduate Studies, King Fahd University of Petroleum and Minerals, Dhahran, 2003.

5. ACI 222R-01, "*Protection of Metals in Concrete Against Corrosion*," American Concrete Institute, 2001, pp. 2-4

6. Yusuf M. O. *"Towards Optimal Design of Reinforced Concrete Structures for Corrosive Environments in Saudi Arabia*", MSc thesis submitted to the Deanship of Graduate Studies, King Fahd University of Petroleum and Minerals, Dhahran, 2009.

7. Page C.L. "*Corrosion of reinforcement in concrete construction*", The Royal Society of Chemistry, Cambridge, 1996, p. 55.

8. Pradhan, B. and Bhattacharjee, B. "*Performance evaluation of rebar in chloride contaminated concrete by corrosion rate*", Journal of Construction and Building Materials, Vol. 23, 2009, pp. 2346-2356.

9. Sathiyanarayanan, S., Natarajan, P., Saravanan, K., Srinivasan, S. and Venkatachari G., "*Corrosion monitoring of steel in concrete by galvanostatic pulse technique*", Journal of Cement and Concrete Composites, Vol. 28, 2006, pp. 630-637

10. Ganesan, K., Rajagopal, K. and Thangavel, K. "*Evaluation of bagasse ash as corrosion resisting admixture for carbon steel in concrete*" Journal of Anti-corrosion Methods and Materials, Vol. 54, 2007, pp. 230-236.

11. Oh B. H., Jang S. Y. and Shin Y. S. "*Experimental investigation of the threshold chloride concentration for corrosion initiation in reinforced concrete structures"*, Journal of Magazine of Concrete Research, Vol. 55 No. 2, 2003, pp 117-124.

12. Pedefferi, P., "*Cathodic Protection and Cathodic Prevention*," Construction and Building Materials, Vol. 10, 1996, pp. 391-402.

13. Alonso, C., Castellote, M., and Andrade, C., "*Dependence of Chloride Threshold with the Electrical Potential of Reinforcement*," Proc., 2nd International RILEM Workshop on Testing and Modelling the Chloride Ingress into Concrete, C. Andrade and J. Kropp (Eds.), PRO 19, RILEM Publication, 2000, pp. 415-425.

14. COST 521, "*Determination of Chloride Threshold in Concrete*," in: Corrosion of Steel in RC Structures, Final Report, R. Cigna, C. Andrade, U. Nurnberger, R. Polder, R. Weydert, and E. Seitz (Eds.), European Community *EUR 20599*, Luxembourg, 2003, pp. 100-108.

15. Glass, G.K. and Buenfield, N.R., "*The Inhibitive Effects of Electrochemical Treatment Applied to Steel in Concrete*," Corrosion Science, Vol. 42, 2000, pp. 923-927.

16. Neville, A. M. "*Properties of Concrete*" Fourth Edition, Pearson Prentice hall, England, 2010

17. Glass, G.K. and Buenfield, N.R., "*The Presentation of Chloride Threshold Level for Corrosion of Steel in Concrete*," Corrosion Science, Vol. 39, 1997, pp. 1001-1013.

18. Page, C.L., "*Advances in Understanding and Techniques for Controlling Reinforcement Corrosion*," 15th International Corrosion Congress, Granada, 22-27 September, 2002.

19. Hausmann, D.A., "*Steel Corrosion in Concrete, How Does It Occur*?," Material Protection, Vol. 11, 1967, pp. 19-23.

20. Yang, L. "*Techniques for corrosion monitoring*", First Edition, Woodhead Publishing Limited, UK, 2008.

21. Bertolini, L., Bernhard E., Pedeferri, P., and Polder, R., *Corrosion of Steel in Concrete*, Wiley-VCH Verlag GmbH & Co., KGA, Germany, 2004.

22. Pradhan, B. and Bhattacharjee, B. "*Performance evaluation of rebar in chloride contaminated concrete by corrosion rate*", Journal of Construction and Building Materials, Vol. 23, 2009, pp. 2346-2356.

23. Sathiyanarayanan, S., Natarajan, P., Saravanan, K., Srinivasan, S. and Venkatachari G., "*Corrosion monitoring of steel in concrete by galvanostatic pulse technique*", Journal of Cement and Concrete Composites, Vol. 28, 2006, pp. 630-637.

24. Vedalakshmi, R., Rajagopal, K. and Palaniswamy, N. "*Longterm corrosion performance of rebar embedded in blended cement concrete under macro cell corrosion condition*". Journal of Construction and Building Materials, Vol. 22, 2008, pp. 186-199.

25. Ganesan, K., Rajagopal, K. and Thangavel, K. "*Evaluation of bagasse ash as corrosion resisting admixture for carbon steel in concrete*" Journal of Anti-corrosion Methods and Materials, Vol. 54, 2007, pp. 230-236.

26. Hsieh, M., Dzombak, D.A. and Vidic, R.D. "*Bridging Gravimetric and Electrochemical Approaches to determine the Corrosion rate of Metals and Metals alloys in cooling systems: Bench Scale Evaluation method*", Journal of Ind. Eng. Chem. Res., Vol. 49, 2010, pp. 9117-9123.

27. Zou, Y., Wang, J. and Zheng Y.Y. "*Electrochemical techniques for determining corrosion rate of rusted in seawater*", Journal of Corrosion Science, Vol. 53, 2011, pp. 208-216.

28. Bertolini, L., Elsener, B., Pedeferri, P. and Polder, R. "*Corrosion of steel in concrete –preventation, diagnosis, repair*", First Edition, Wiley-VCH Verlag, Weinheim, 2004.

29. Saetta, A.V., "*Deterioration of RC Structures Due to Chemical-Physical Phenomena: Model-Based Simulation*," Journal of Materials in Civil Engineering, ASCE, Vol. 17, No. 3, June 2005, pp. 313-319.

30. Federal Highway Administration, "*Material and Method for Corrosion Control of Reinforced and Prestressed Concrete Structures in New Construction*," US Department of Transportation Pub. No. 00-081, 6300 Georgetown Pike, Mclean VA 22101-2296, 2001, pp. 1-29.

31. Park, J. I., Bae, S. H., Yu, K. G. Lee, K. M. and Choi, S. "*Factors influencing the service life of concrete structures exposed to coastal environment*", The 3rd ACF International Conference-ACF/VCA , 2008, pp 1090-1095.

32. Chalee, W., Teekavanit, M., Kiattikomol, K., Siripanichgorn, A., and Jaturapitakkul, C. "*Effect of W/C ratio on covering depth of fly ash concrete in marine environment*" Journal of Construction and Building materials, Vol. 21, 2007, pp. 965-971.

33. Oh, B. H., Jang, B. S. and Lee, S. C. "*Chloride diffusion and corrosion initiation time of reinforced concrete structures*", Proceedings of the International Workshop on Microstructure and Durability to Predict Service Life of Concrete Structures Sapporo, Japan, Feb. 2004.

34. Ahmad, S. and Bhattacharjee, B., "*A Simple Arrangement and Procedure for In-situ No. 5, Measurement of Corrosion Rate of Rebar Embedded in Concrete*," Corrosion Science, Vol. 37, 1995, pp. 781-791.

35. Al-Tayyib, A.J. and Khan, M.S., "*Corrosion Rate Measurement of Reinforcing Steel in Concrete by Electrochemical Techniques*," ACI Materials J., May-June I988, pp. 172-177.

36. Mehta, P.K., "*Effect of Cement Composition on Corrosion of Reinforcing Steel in Concrete*," Chloride Corrosion of Steel in Concrete, ASTM STP 629, West Conshohocken, Pa., 1977, pp. 12-19.

37. Mehta, P.K., "Durability of Concrete in Marine Environment: A Review," *Performance of Concrete in Marine Environment*, ACI Publication, SP-65, 1986.

38. Page, C.L., Short, N.R., and El-Tarras, A., "*Diffusion of Chloride Ions in Hardened Cement Pastes,"* Cement and Concrete Research, Vol. 11, No. 3, 1981, pp. 295-406.

39. Page, C.L., Short, N.R., and Holden, W.R., "*The Influence of Different Cements on Chloride-Induced Corrosion of Reinforcing Steel*," Cement and Concrete Research, Vol. 16,No. 1, 1986, pp. 79-86.

40. Al-Amoudi, O.S.B, Abduljauwad, S.N., Rasheeduzaffar, and Maslehuddin, M., "*Effect of Chloride and Sulfate Contamination in Soils on Corrosion of Steel and Concrete*, Transportation Research Record No. 1345, 1992, pp. 67-73.

41. Bhattacharjee, B. "*Risk of rebar corrosion in cracked RC flexural member, incorporated with fly ash"*, The Indian Concrete Journal, March 2006.

42. Amleh, L.; Lounis, Z.; Mirza, M.S. "*Assessment of corrosion-damaged concrete bridgedecks - a case study investigation*", National Research Council, Canada, 2002.

43. Shekarchi, M. and Moradi, F. "*Concrete durability issues in the Persian gulf*", CBM - CI International Workshop, Karachi, Pakistan, 2006.

44. Chalee, W., Ausapanit, P. and Jaturapitakkul, C. "*Utilization of fly ash concrete in marine environment for long term design life analysis"*, Journal of Materials and Design, Vol. 31, 2010, pp. 1242–1249.

45. ACI Committee 201, "*Guide to Durable Concrete*," (ACI 201.2R-77), (Reapproved 1982),American Concrete Institute, Farmington Hills, Mich., 1977, pp. 1-37.

46. Beeby, A.W., "*Corrosion of Reinforcing Steel in Concrete and Its Relation to Cracking*," The Structural Engineer, Vol. 56A, No. 3, 1978, pp. 77-81.

47. David, T. and Kenneth, R. "*Justifying Materials Selection for Reinforced Concrete Structures. I: Sensitivity Analysis"*,Journal of Bridge Engineering, Vol. 12, No. 1, 2007, pp. 31-37.

48. Bazant, Z.P., "*Physical Model for Steel Corrosion in Concrete Sea Structures-Application*", ASCE Journal of Structural Division, Vol. 105, 1979, pp. 1155-1166.

49. Ahmad, S., Bhattacharjee, B., "*Assessment of service lives of reinforced concrete structures subjected to chloride-induced rebar corrosion"*. Journal of Struct Eng., 1997; 23(4):177-82.

50. Morinaga, S. "*Prediction of service lives of reinforced concrete buildings based on the corrosion rate of reinforcing steel*", Proceedings of Building Materials and Components, Brighton, *UK*, 7–9 November 1990:5–16.

51. Wang, X.M.; Zhao, H.Y. "*The residual service life prediction of R.C. structures*", In: 1993. Nagataki S et al., editors. Durability of building materials and components, 6. E & FN Spon; pp. 1107–14.

52. Dagher, H.J.; Kulendran, S. "*Finite element model of corrosion damage in concrete structures*", ACI Struct Journal 1992;89(6): pp. 699–708.

53 Oslakovic, I. S., Bjegovic, D. and Mikulic D. "*Evaluation of service life design models on* 43,*concrete structures exposed to marine environment*", Journal of Materials and Structures, Vol. 43, 2010, pp. 1397-1412.

54. Vu, K. A. T. and Steward, M. G. "*Service Life Prediction of Reinforced ConcreteStructures Exposed to Aggressive Environments*" 9DBMC-2002, paper 119, pp 1-10.

55. Azad, A.K. and Ahmad, S., "*A study of the size-effect of corroded reinforced concrete beams in prediction of residual strength*, Final Report of the SABIC Project (# SABIC 2005/03) funded by KFUPM, 2008.

56. Jin, W.L., and Zhao, Y.X. "*Effect of corrosion on bond behavior and bending strength of reinforced concrete beams*," Journal of Zhejiang University (Science), Vol. 2,No. 3, July-September 2001, pp. 298-308.

57. Castel, A.; Francois, R.; Arliguie, G. "*Mechanical behavior of corroded reinforced concrete beams* - Part 1: bond and notch effects," Materials and Structures/Materiauxet Constructions, Vol. 33, No. 233, 2000, pp. 539-544.

58. Aziz, A.R. "*Reduction in bond and the strength of slabs due to corrosion of reinforcement"*, M.S. Thesis, King Fahd University of Petroleum and Minerals, June, 1994.

59. Mangat, P.S., and Elgarf, M.S. "*Flexural strength of concrete beams with corroding reinforcement*," ACI Structural Journal, Vol. 96, No. 1, January-February 1999, pp. 149-158.

60. Uomoto, T., and Misra, S. "*Behaviour of concrete beams and columns in marine, environment when corrosion of reinforcing bars takes place*," ACI Special Publication SP-10, 1988, pp. 127-145.

61. Sarja, A. and Vesikari, E., "*Durability design of concrete structures*", Report of RILEM Technical Committee, E & FN Spon, 1996.

62. Anoop, M.B., Rao, K.B., and AppaRao, T.V.S.R., "*A Methodology for Durability-Based Service Life Design of Reinforced Concrete Flexural Members*", Magazine of Concrete Research, Vol. 55, No. 3, June 2003, pp. 289-303.

63. Pihlajavaara, S.E., "*Contributions for the Development of the Estimation of Long-term Performance and Service-life of Concrete," Report 3, Articles 49, Helsinki University* of Technology, Faculty of Civil Engineering and Surveying, Espoo, 1994, pp. 1-26.

64. Vesikari, E., "*Service-life Design of Concrete Structures," RIL 183-4.9, Association of Finnish Civil Engineers*, RIL, Helsinki, 1995, 120 pp.

65. ASTM C 128-07a, "*Standard Test Method for Density, Relative Density (Specific Gravity) and Absorption of Fine Aggregate*," ASTM, West Conshohocken, Pa.

66. Alghamdi, S.A. and Ahmad S., "*Multi-criteria Optimal Designs of R/C Beams and Columns – Experimental and Analytical Studies*," Final Report, KACST Project AT-23-21, 2010.

67. PowerCORR *User's Manual*, Corrosion Measurement Software, Princeton Applied Research, USA, 2001.

68. ASTM G 1-03. *Standard practice for preparing, cleaning, and evaluating corrosion test specimens.*West Conshohocken, PA; 2003.

69. Goyal, M. "*Computer-based numerical and statistical techniques*", Infinity Science Press, 2007.

70. JOEL SEM JSM-5800 LV *Operating Manual* Hi-Tech and Scientific Equipment, Southfield, USA, 1994.

71. McClave, J.T. and Sincich T. "*A first course in statistics*", Prentice hall, New Jersy, 6th Edition, 1997.

72. MINITAB statistical package release 13. Minitab Inc., 2000. www.minitab.com

73. Aitcin, P.C. and Neville, A. "*High performance concrete*" Demystified Concrete International, ACI Journal, Vol. 15, No. 1, January 1993, pp. 21-26.

74. ACI 318-08, "*Building Code Requirement for Structural Concrete*," American Concrete Institute, 38800 Country Club Drive, Farmington Hills, MI 48331, USA, 2008.

75. Bockris J.O., Reddy A.K.N. and Gamboa A. M., "*Modern Electrochemistry*", 2nd Edition, Kluwer Academic/Plenum Publishers, 2000.

APPENDIX A

Butler-Volmer Equation

The Butler–Volmer equation is one of the most fundamental relationships in electrochemistry. It describes how the electrical current on an electrode depends on the electrode potential, considering that both a *cathodic* and an *anodic* reaction occur on the same electrode. The equation is valid when the electrode reaction is controlled by electrical charge transfer at the electrode (and not by the mass transfer to or from the electrode surface from or to the bulk electrolyte). Nevertheless, the utility of the Butler–Volmer equation in electrochemistry is wide, and it is often considered central in the phenomenological electrode kinetics [6, 75].

When a net current flows, there is a shift in the potential of the electrodes from E_{corr} to E. If, $E>E_{corr}$, then the anodic process is favored ($i_a>|i_c|$), whereas, if $E<E_{corr}$, the cathodic process predominates ($i_a<|i_c|$). The difference between the polarized potential (E) and the unpolarized potential is called overvoltage or overpotential (ε). The anodic and cathodic overpotential are given as:

$$\varepsilon_a = E - E_{corr} \quad \text{(A-1)}$$

$$\varepsilon_c = E_{corr} - E \quad \text{(A-2)}$$

The relationship between over potential (ε) and current density (i) is known as the Tafel equation as given by:

$$\varepsilon_a = \beta_a \log\left(\frac{i_a}{i_o}\right) \quad \text{(A-3)}$$

$$\varepsilon_c = \beta_c \log\left(\frac{i_c}{i_o}\right) \tag{A-4}$$

where: β_a and β_c are called anodic and cathodic Tafel constants.

The relationship between the polarizing current (i) and resulting over potential (ε) is given as:

$$i = i_{corr}\left[\exp\left(\frac{2.303\varepsilon_a}{\beta_a}\right) - \exp\left(\frac{-2.303\varepsilon_c}{\beta_c}\right)\right] \tag{A-5}$$

Assuming $\varepsilon_a = \Delta E = (E - E_{corr}) > 0$ and $\varepsilon_c = \Delta E = (E - E_{corr}) < 0$

$$i = i_{corr}\left[\exp\left(\frac{2.303(E - E_{corr})}{\beta_a}\right) - \exp\left(\frac{-2.303(E - E_{corr})}{\beta_c}\right)\right] \tag{A-6}$$

The inverse polarization resistance R_p is obtained by differentiating eq. A-6 with respect to electrical potential E,

$$\frac{1}{R_p} = \frac{d}{dE} i = 2.303 i_{corr}\left\{\beta^{-1}\exp\left[\frac{2.303(E - E_{corr})}{\beta_a}\right] - \beta^{-1}\exp\left[\frac{2.303(E - E_{corr})}{\beta_c}\right]\right\} \tag{A-7}$$

The second derivative of equation is:

$$\frac{d^2 i}{dE^2} = 5.3038\, i_{corr}\left\{\beta^{-2}\exp\left[\frac{2.303(E - E_{corr})}{\beta_a}\right] - \beta^{-2}\exp\left[\frac{2.303(E - E_{corr})}{\beta_c}\right]\right\} \tag{A-8}$$

And evaluation of eq. A-8 may lead to one of the following three possibilities:

$$\frac{d^2 i}{dE^2} = \begin{cases} < 0 \ \ for\ E = E_{\max} > E_{corr} \\ = 0 \ \ for \ \text{ point of inflection} : E = E_{corr} \\ > 0 \ for\ E < E_{corr} \end{cases}$$

At point of inflection, eq. A-8 is evaluated as:

$$\left(\frac{d^2 i}{dE^2}\right)_{E=E_{corr}} = 5.3038\ i_{corr}\left\{\beta_a{}^{-2} - \beta_c{}^{-2}\right\} \qquad \text{(A-9)}$$

For $\beta_a = \beta_c$ and $E = E_{\text{corr}}$, eq. A-8 is evaluated as:

$$\left(\frac{di}{dE}\right)_{E=E_{corr}} = \frac{1}{R_p} = 2.303 i_{corr}\left(\frac{\beta_a + \beta_c}{\beta_a \beta_c}\right) \qquad \text{(A-10)}$$

$$R_p = \left(\frac{di}{dE}\right)^{-1}_{E=E_{corr}} = \left(\frac{\beta_a \beta_c}{2.303(\beta_a + \beta_c) i_{corr}}\right) \qquad \text{(A-11)}$$

This relationship is often re-written in the following short form.

$$R_p = \frac{B}{i_{corr}} \qquad \text{(A-12)}$$

where B is called Stern-Geary constants

E is polarized potential (mV)

E_{corr} is corrosion potential (mV)

i is polarized current density ($\mu A/cm^2$)

i_{corr} is corrosion current density ($\mu A/cm^2$)

i_{a} is anodic current density ($\mu A/cm^2$)

i_c is cathodic current density ($\mu A/cm^2$)

ε is overvoltage or overpotential (mV)

ε_a is anodic overpotential (mV)

ε_c is cathodic overpotential (mV)

β_a is anodic Tafel coefficient

β_c is cathodic Tafel coefficient

$$B = \frac{\beta_a \beta_c}{2.303(\beta_a + \beta_c)} \quad \text{(mV)}$$

Appendix B

Plots of I_{corr} versus Time

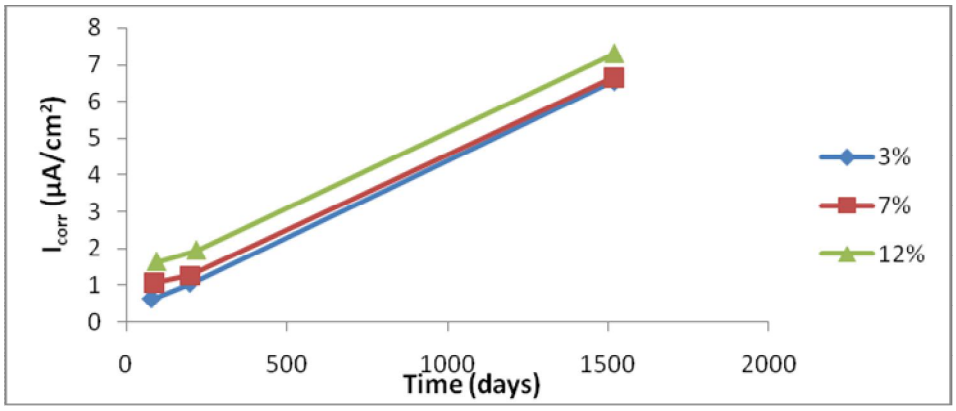

a) $R_{W/C}$ = 0.4, C_C = 350 kg/m^3, C_V = 25 mm

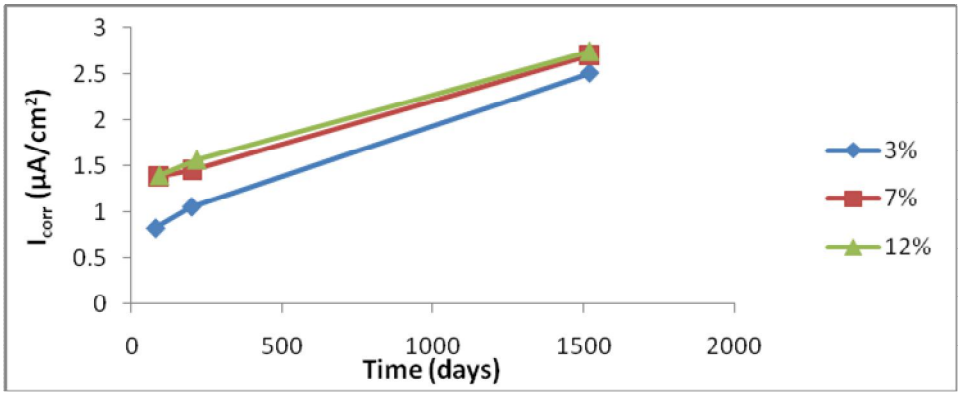

b) $R_{W/C}$ = 0.4, C_C = 350 kg/m^3, C_V = 37.5 mm

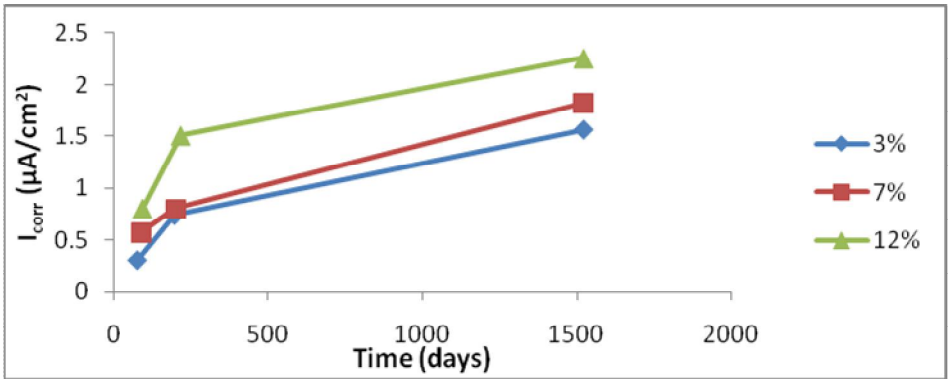

c) $R_{W/C}$ = 0.4, C_C = 350 kg/m^3, C_V = 50 mm

Figure B1: Variation of I_{corr} with time for $R_{W/C}$ = 0.4, C_C = 350 kg/m^3 of H-type aggregates

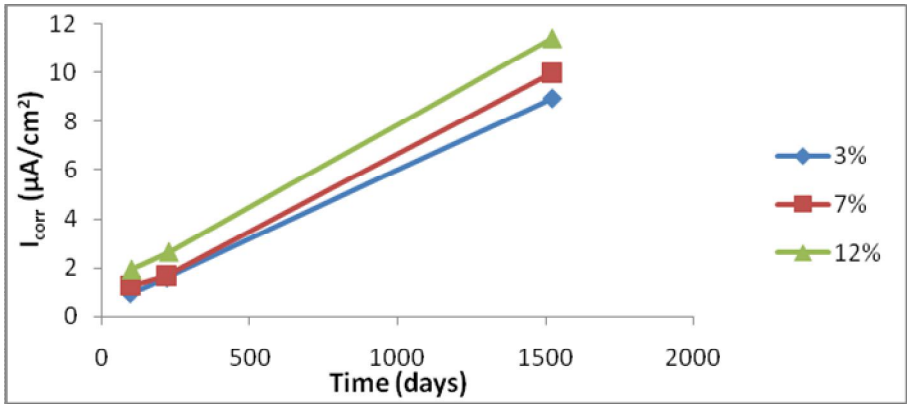

a) w/c = 0.4, C_C = 375 kg/m^3, C_V = 25 mm

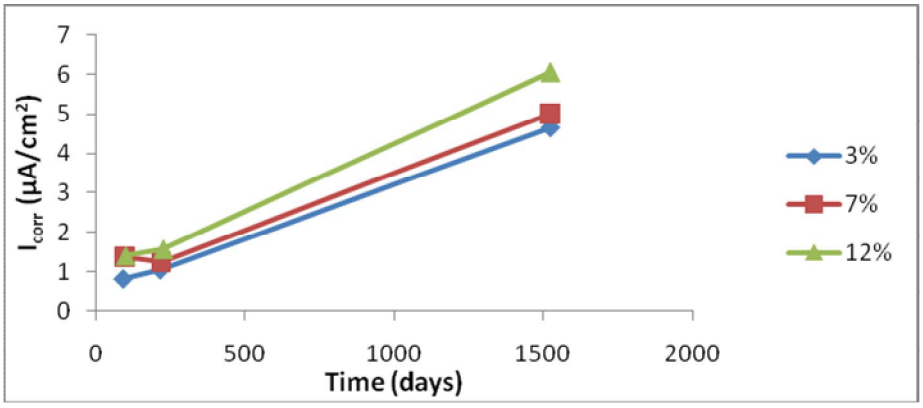

b) w/c = 0.4, C_C = 375 kg/m^3, C_V = 37.5 mm

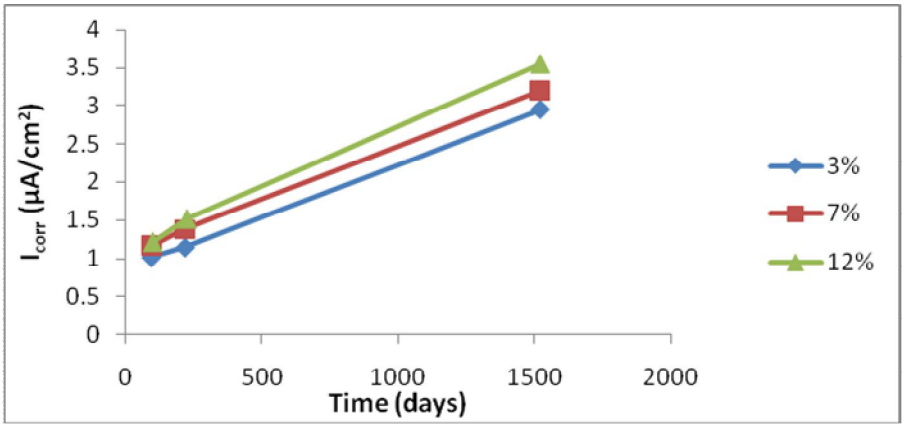

c) w/c = 0.4, C_C = 375 kg/m^3, C_V = 50 mm

Figure B2: Variation of I_{corr} with time for w/c = 0.4, C_C = 375 kg/m^3 of H-type aggregates

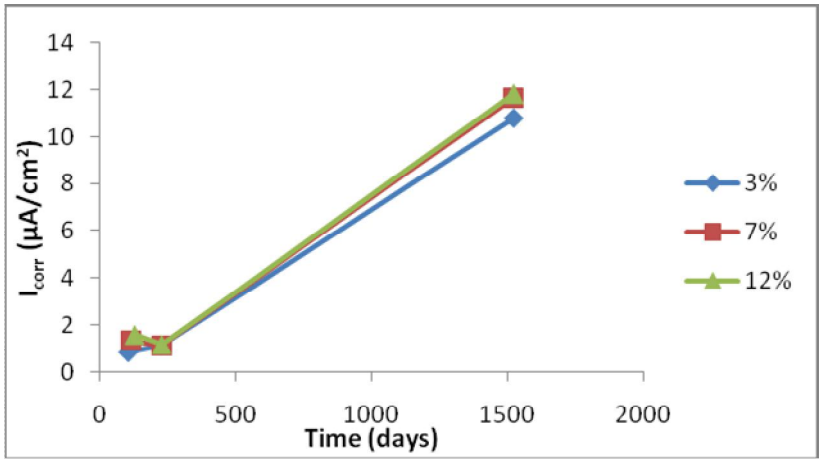

a) w/c = 0.4, C_C = 400 kg/m^3, C_V = 25 mm

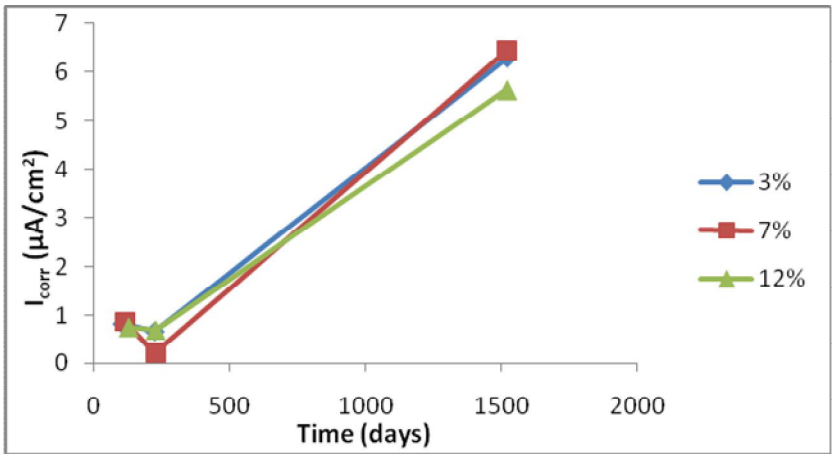

b) w/c = 0.4, C_C = 400 kg/m^3, C_V = 37.5 mm

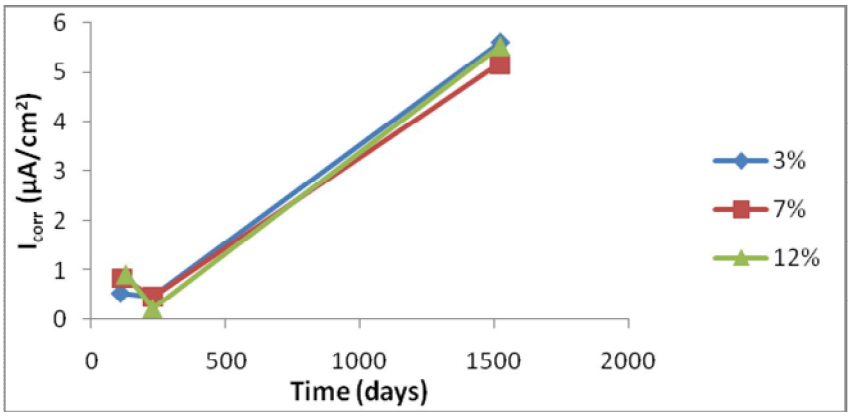

c) w/c = 0.4, C_C = 400 kg/m^3, C_V = 50 mm

Figure B3: Variation of I_{corr} with time for w/c = 0.4, C_C = 400 kg/m^3 of H-type aggregates

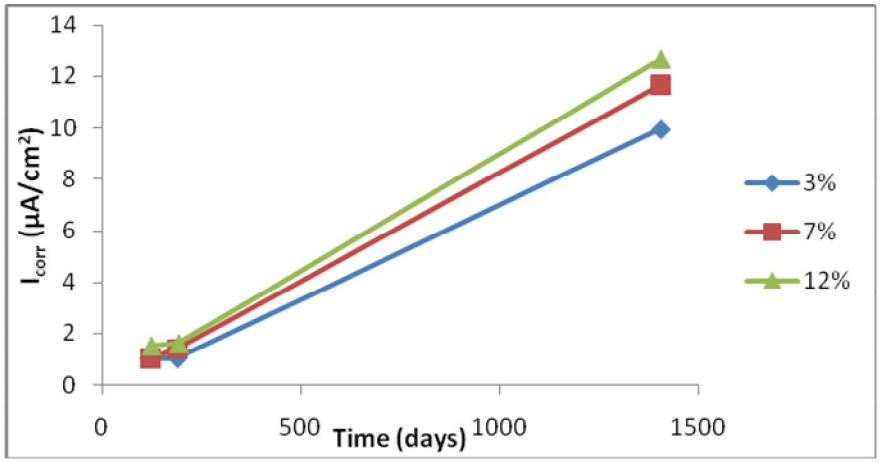

a) w/c = 0.45, C_C = 350 kg/m^3, C_V = 25 mm

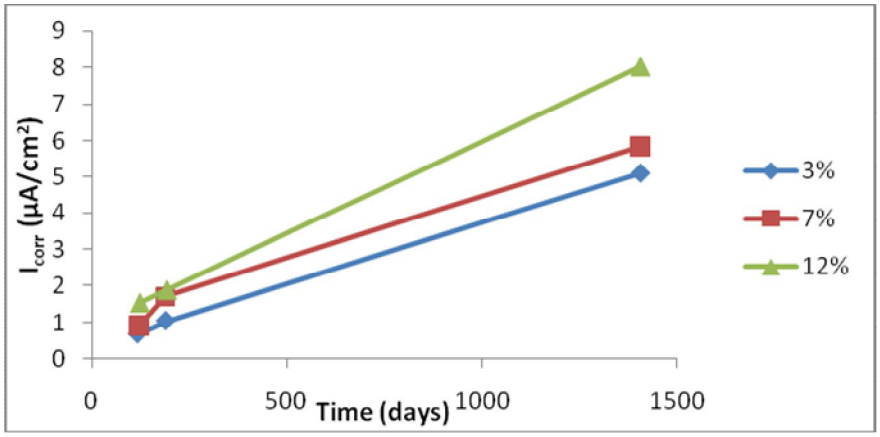

b) w/c = 0.45, C_C = 350 kg/m^3, C_V = 37.5 mm

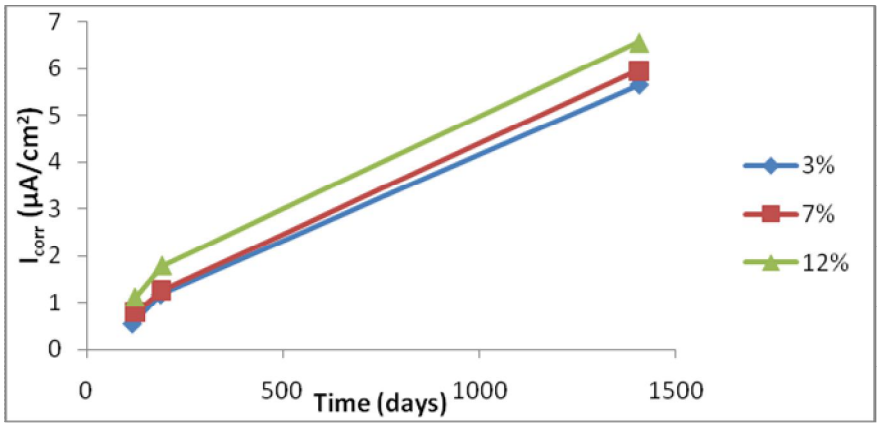

c) w/c = 0.45, C_C = 350 kg/m^3, C_V = 50 mm

Figure B4: Variation of I_{corr} with time for w/c = 0.45, C_C = 350 kg/m^3 of H-type aggregates

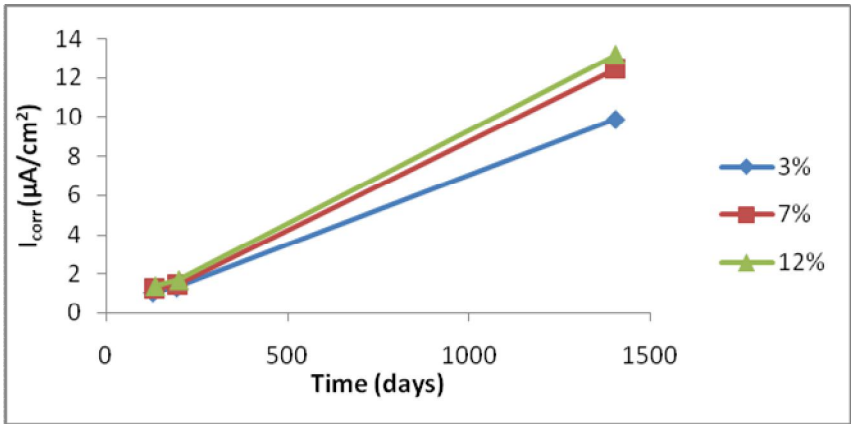

a) w/c = 0.45, C_C = 375 kg/m^3, C_V = 25 mm

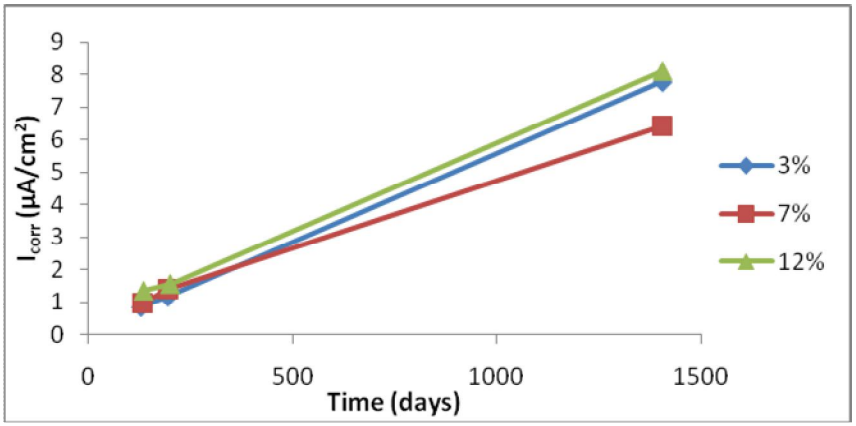

b) w/c = 0.45, C_C = 375 kg/m^3, C_V = 37.5 mm

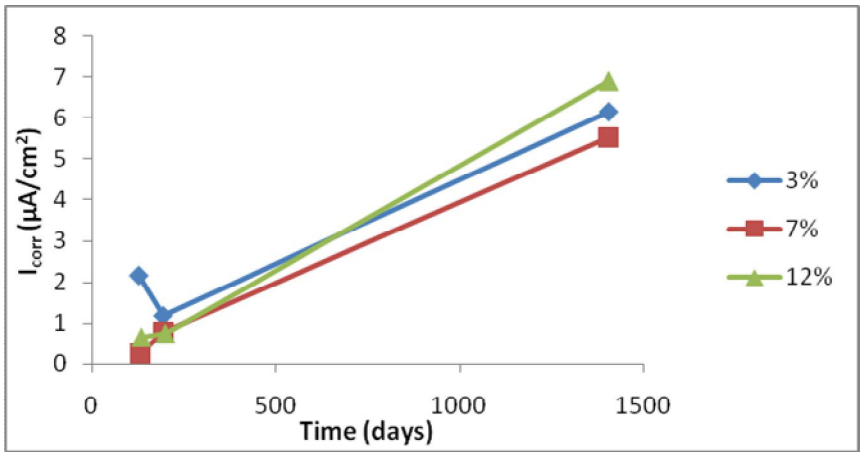

c) w/c = 0.45, C_C = 375 kg/m^3, C_V = 50 mm

Figure B5: Variation of I_{corr} with time for w/c = 0.45, C_C = 375 kg/m^3 of H-type aggregates

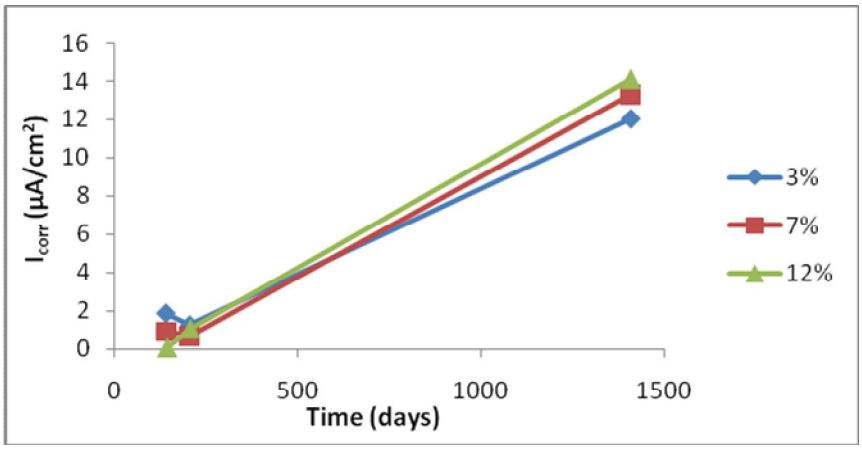

a) w/c = 0.45, C_C = 400 kg/m^3, C_V = 25 mm

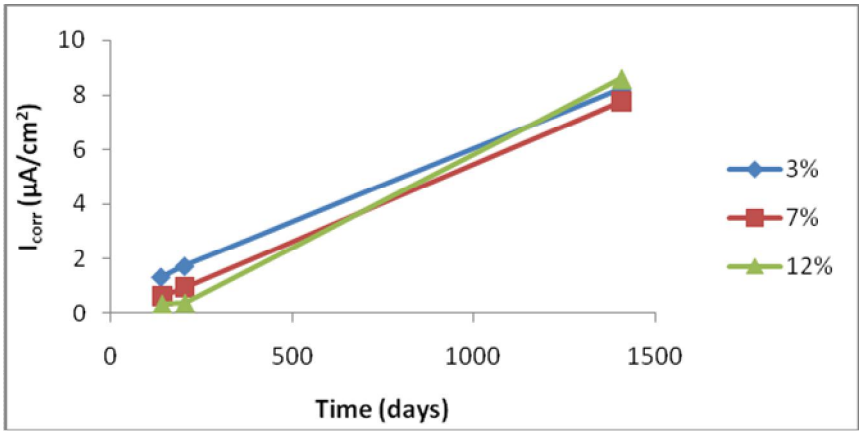

b) w/c = 0.45, C_C = 400 kg/m^3, C_V = 37.5 mm

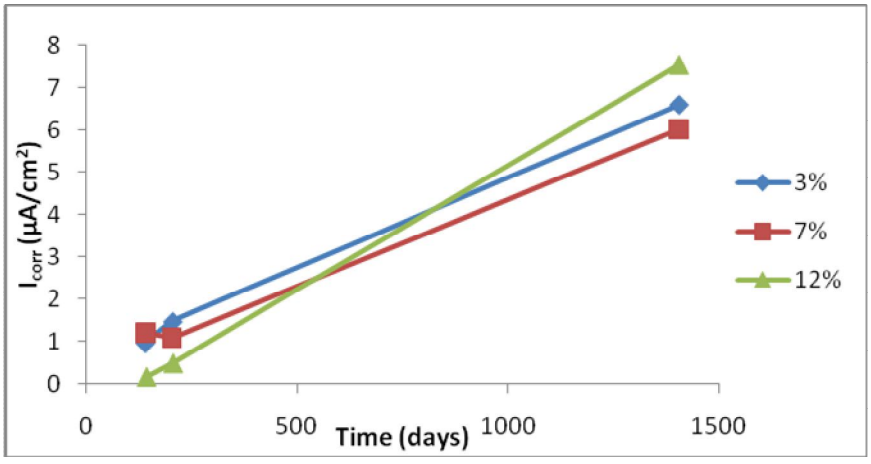

c) w/c = 0.45, C_C = 400 kg/m^3, C_V = 50 mm

Figure B6: Variation of I_{corr} with time for w/c = 0.45, C_C = 400 kg/m^3 of H-type aggregates

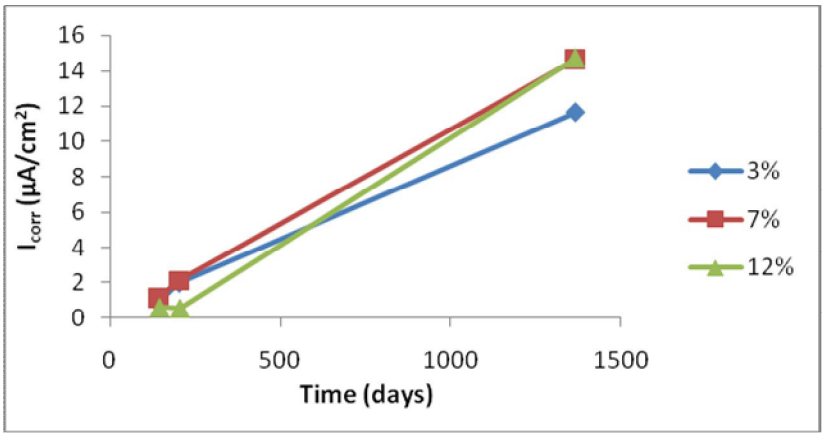

a) w/c = 0.5, C_C = 350 kg/m^3, C_V = 25 mm

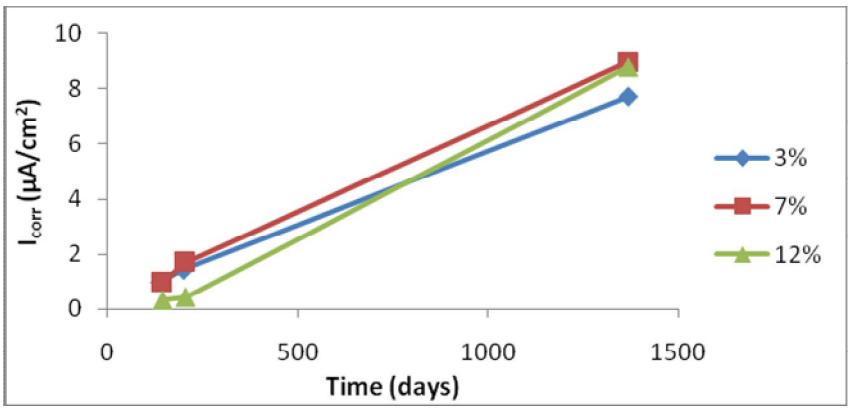

b) w/c = 0.5, C_C = 350 kg/m^3, C_V = 37.5 mm

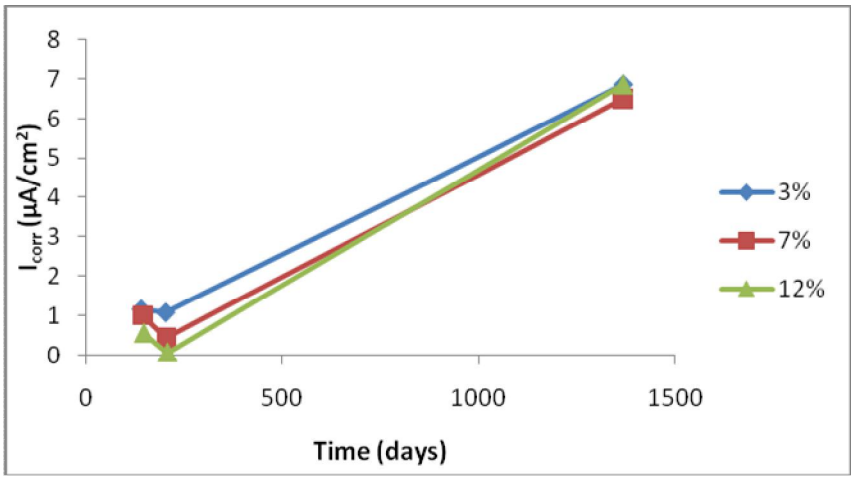

c) w/c = 0.5, C_C = 350 kg/m^3, C_V = 50 mm

Figure B7: Variation of I_{corr} with time for w/c = 0.5, C_C = 350 kg/m^3 of H-type aggregates

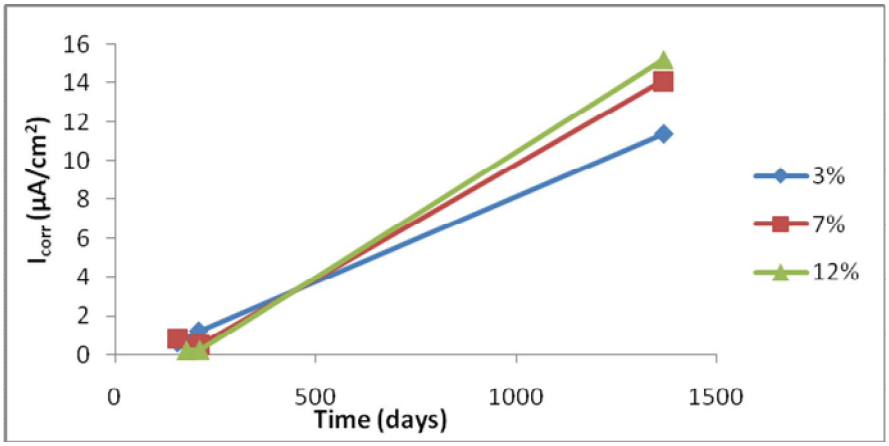

a) w/c = 0.5, C_C = 375 kg/m^3, C_V = 25 mm

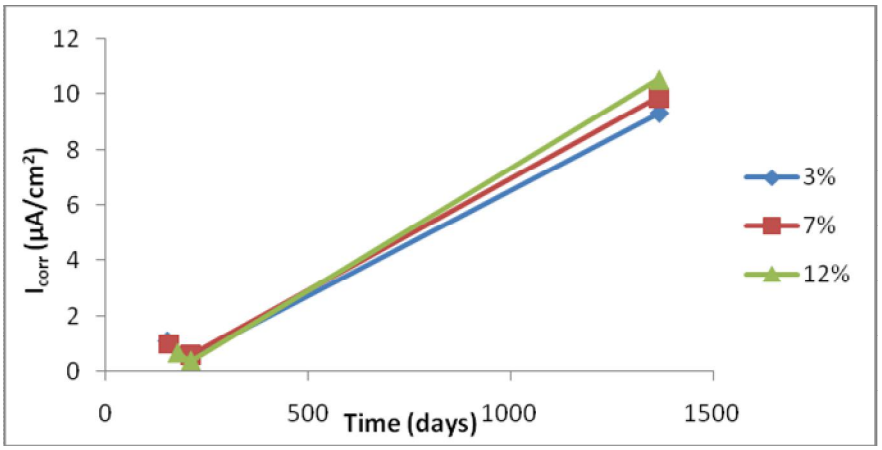

b) w/c = 0.5, C_C = 375 kg/m^3, C_V = 37.5 mm

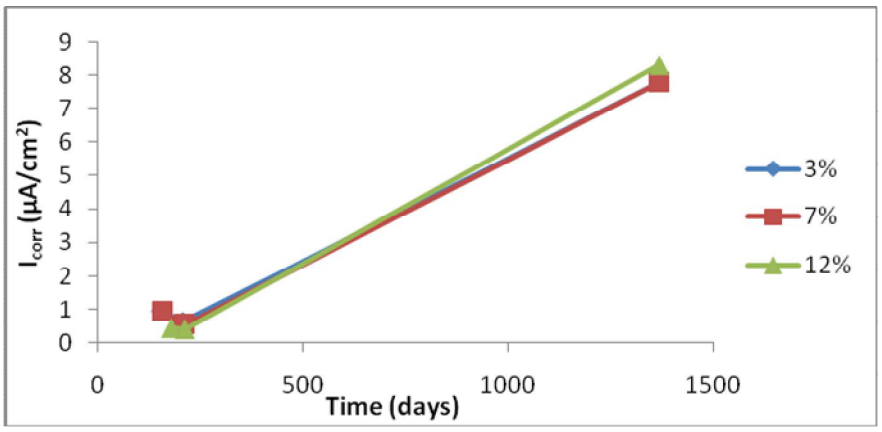

c) w/c = 0.5, C_C = 375 kg/m^3, C_V = 50 mm

Figure B8: Variation of I_{corr} with time for w/c = 0.5, C_C = 375 kg/m^3 of H-type aggregates

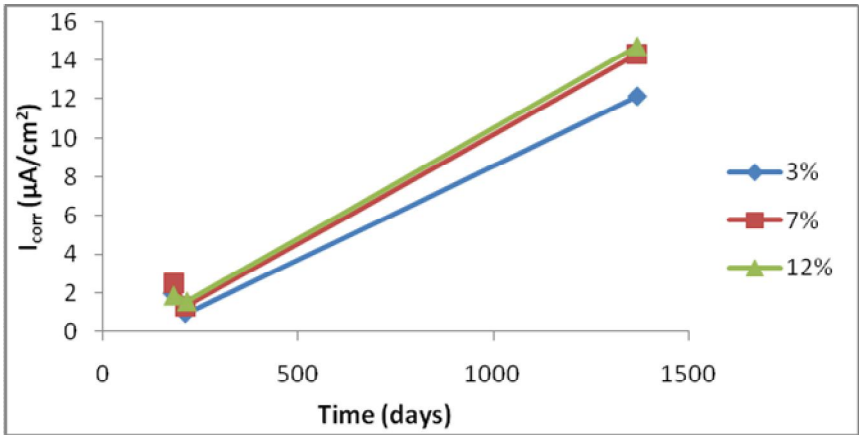

a) w/c = 0.5, C_C = 400 kg/m^3, C_V = 25 mm

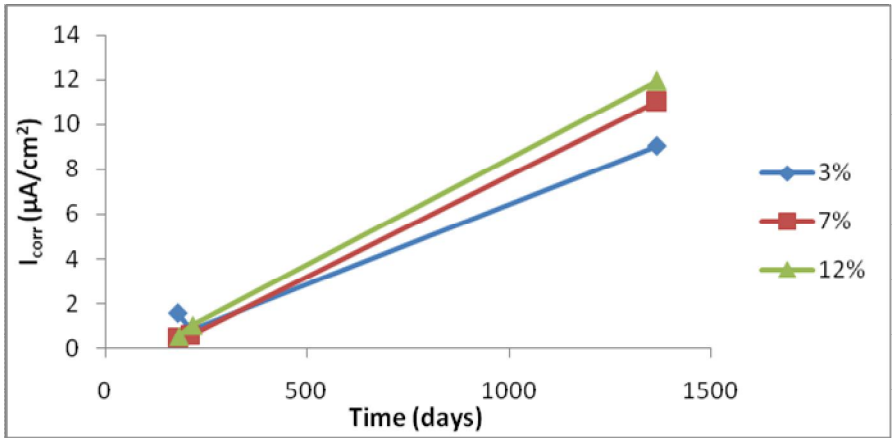

b) w/c = 0.5, C_C = 400 kg/m^3, C_V = 37.5 mm

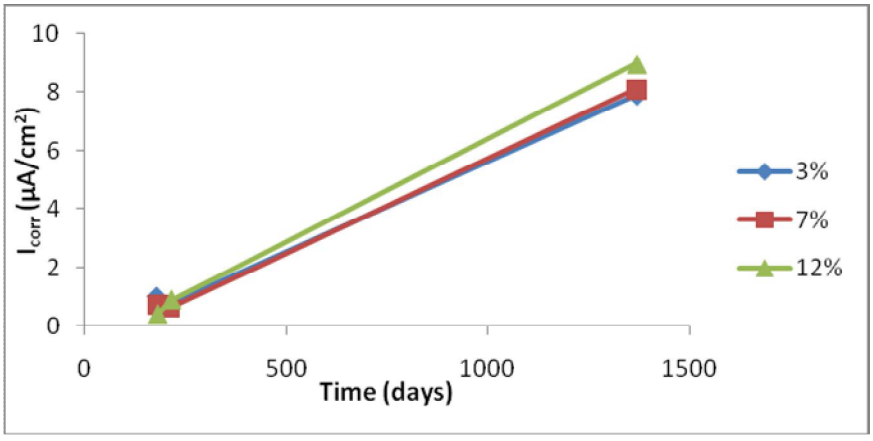

c) w/c = 0.5, C_C = 400 kg/m^3, C_V = 50 mm

Figure B9: Variation of I_{corr} with time for w/c = 0.5, C_C = 400 kg/m^3 of H-type aggregates

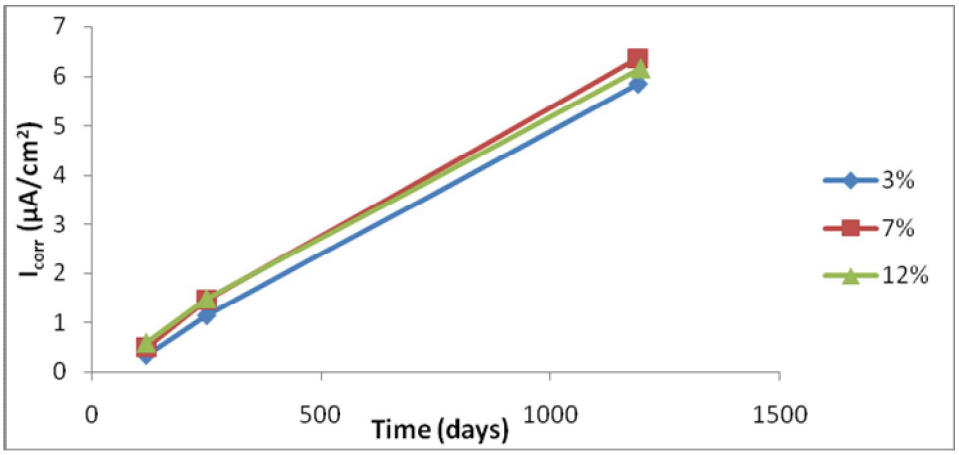

a) w/c = 0.4, C_C = 350 kg/m^3, C_V = 25 mm

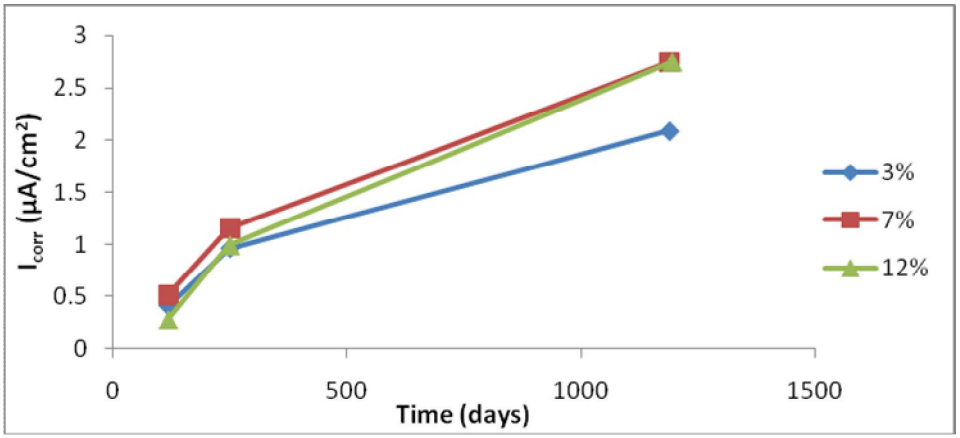

b) w/c = 0.4, C_C = 350 kg/m^3, C_V = 37.5 mm

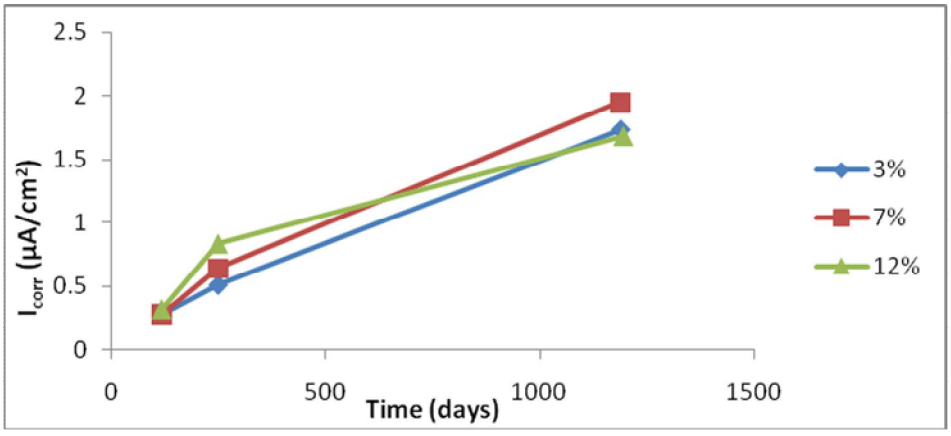

c) w/c = 0.4, C_C = 350 kg/m^3, C_V = 50 mm

Figure B10: Variation of I_{corr} with time for w/c = 0.4, C_C = 350 kg/m^3 of T-type aggregates

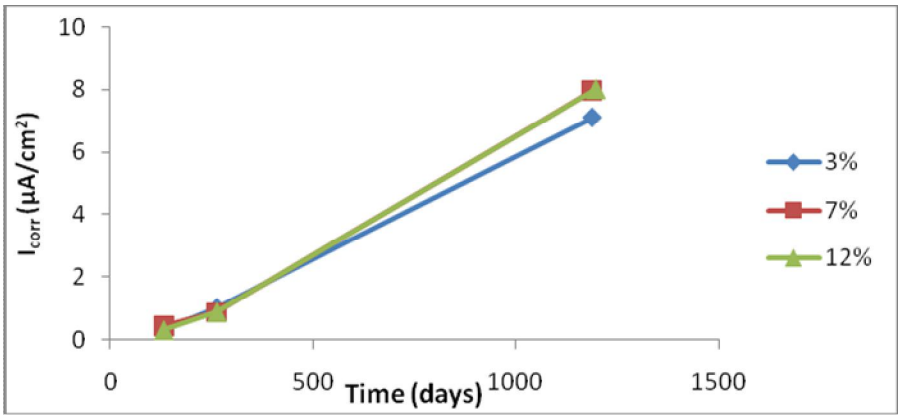

a) w/c = 0.4, C_C = 375 kg/m^3, C_V = 25 mm

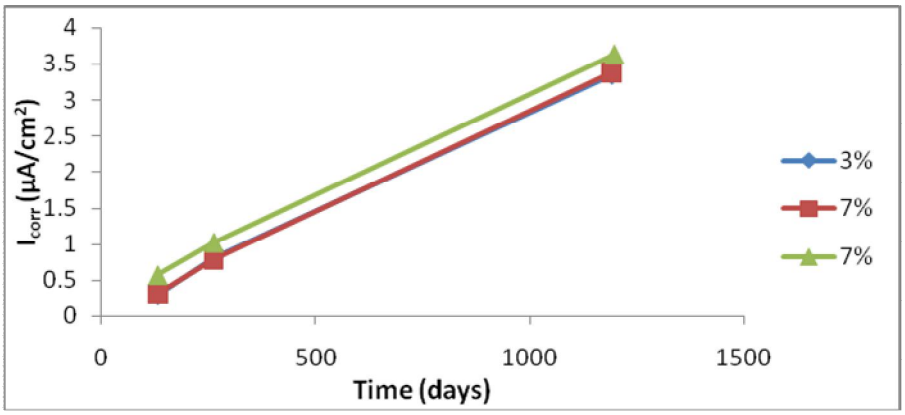

b) w/c = 0.4, C_C = 375 kg/m^3, C_V = 37.5 mm

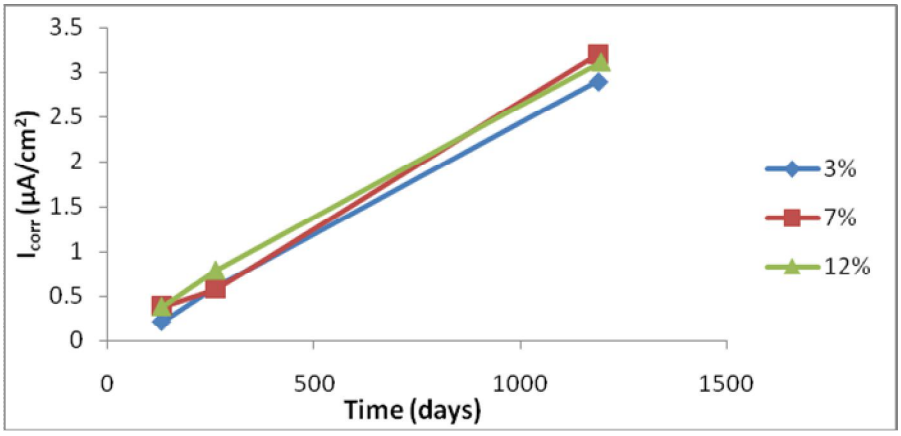

c) w/c = 0.4, C_C = 375 kg/m^3, C_V = 50 mm

Figure B11: Variation of I_{corr} with time for w/c = 0.4, C_C = 375 kg/m^3 of T-type aggregates

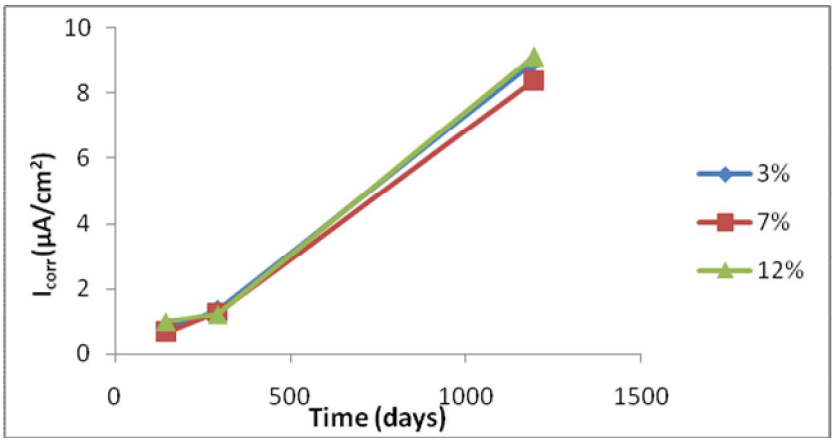

a) w/c = 0.4, C_C = 400 kg/m^3, C_V = 25 mm

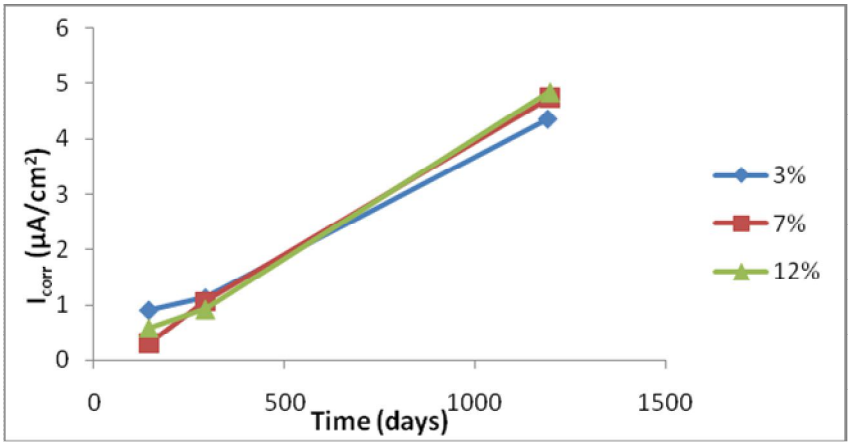

b) w/c = 0.4, C_C = 400 kg/m^3, C_V = 37.5 mm

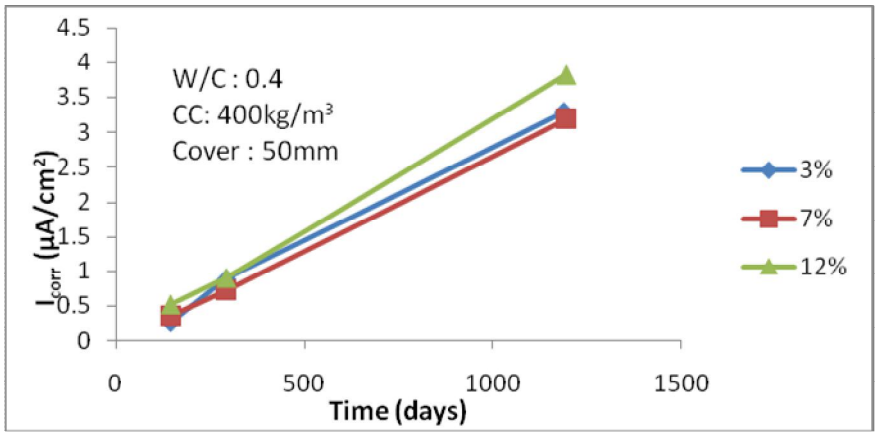

c) w/c = 0.4, C_C = 400 kg/m^3, C_V = 50 mm

Figure B12: Variation of I_{corr} with time for w/c = 0.4, C_C = 400 kg/m^3 of T-type aggregates

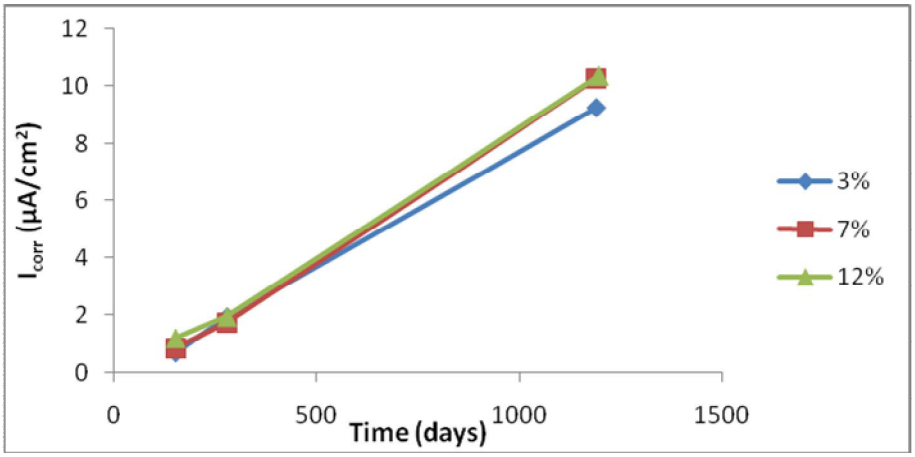

a) w/c = 0.45, C_C = 350 kg/m^3, C_V = 25 mm

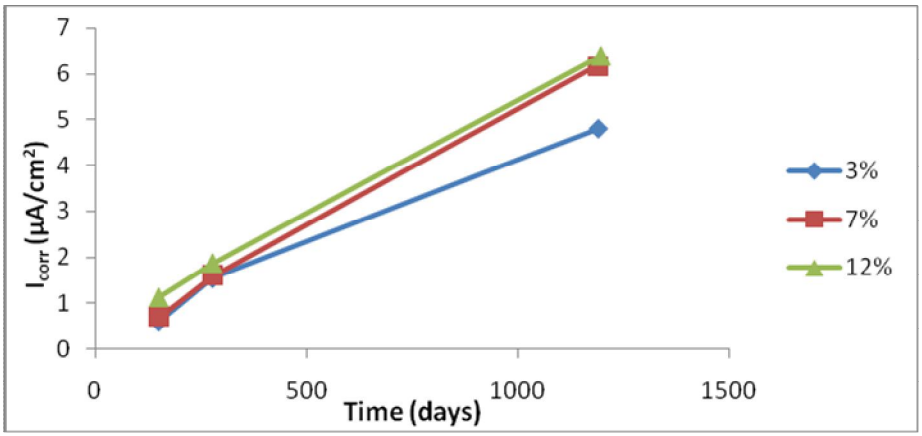

b) w/c = 0.45, C_C = 350 kg/m^3, C_V = 37.5 mm

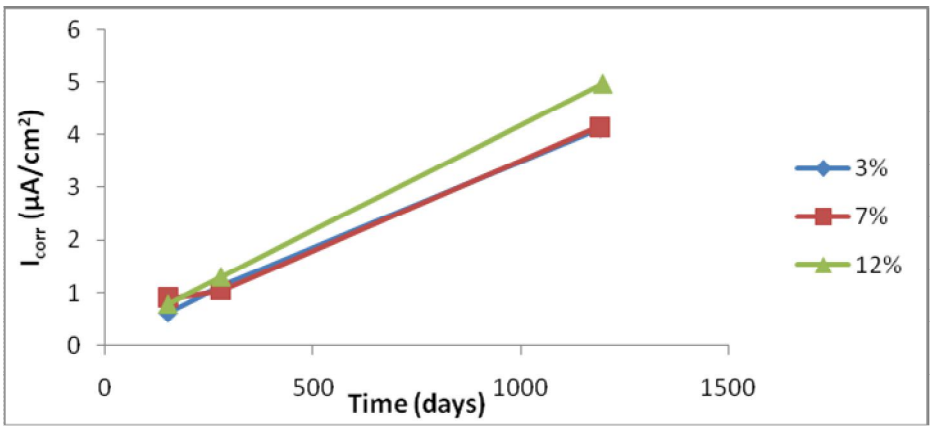

c) w/c = 0.45, C_C = 350 kg/m^3, C_V = 50 mm.

Figure B13: Variation of I_{corr} with time for w/c = 0.45, C_C = 350 kg/m^3 of T-type aggregates

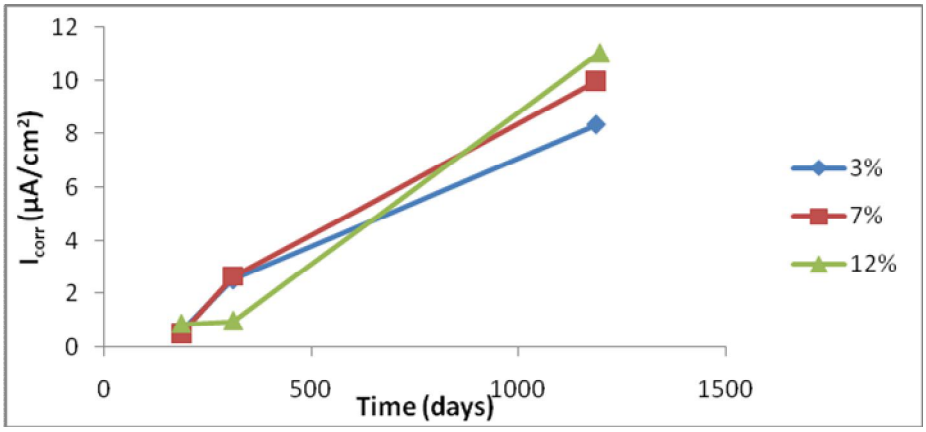

a) w/c = 0.45, C_C = 375 kg/m^3, C_V = 25 mm.

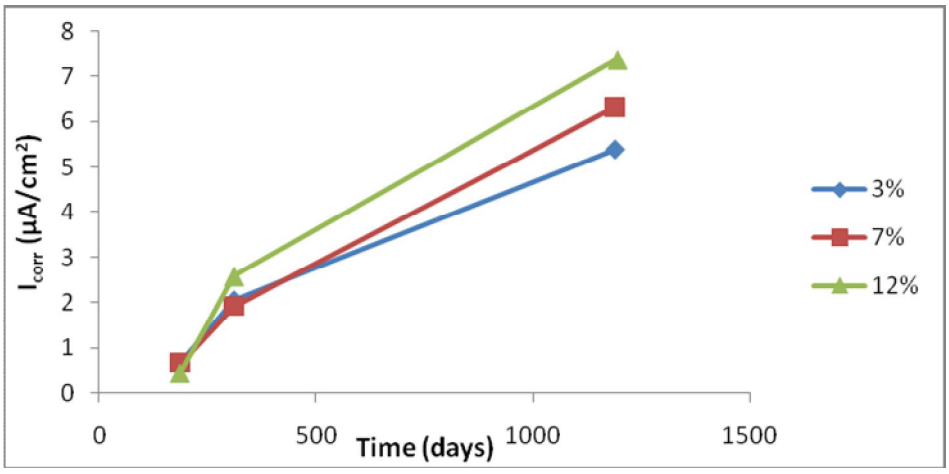

b) w/c = 0.45, C_C = 375 kg/m^3, C_V = 37.5 mm.

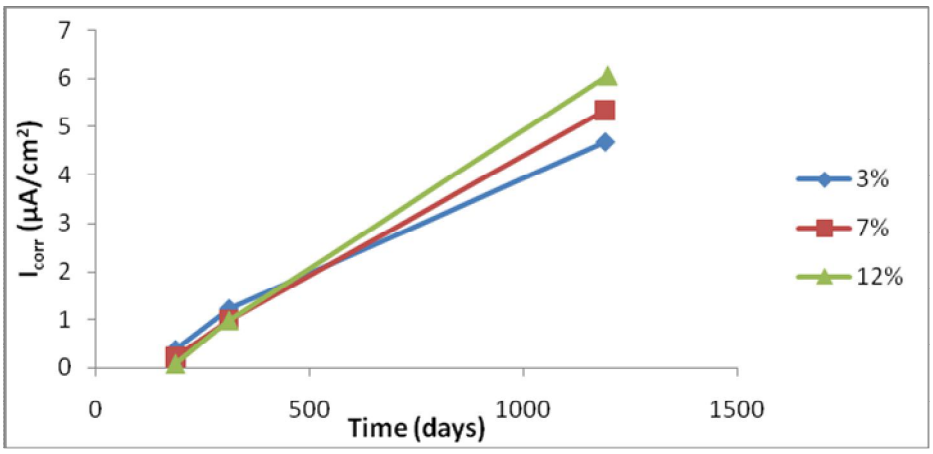

c) w/c = 0.45, C_C = 375 kg/m^3, C_V = 50 mm.

Figure B14: Variation of I_{corr} with time for w/c = 0.45, C_C = 375 kg/m^3 of T-type aggregates

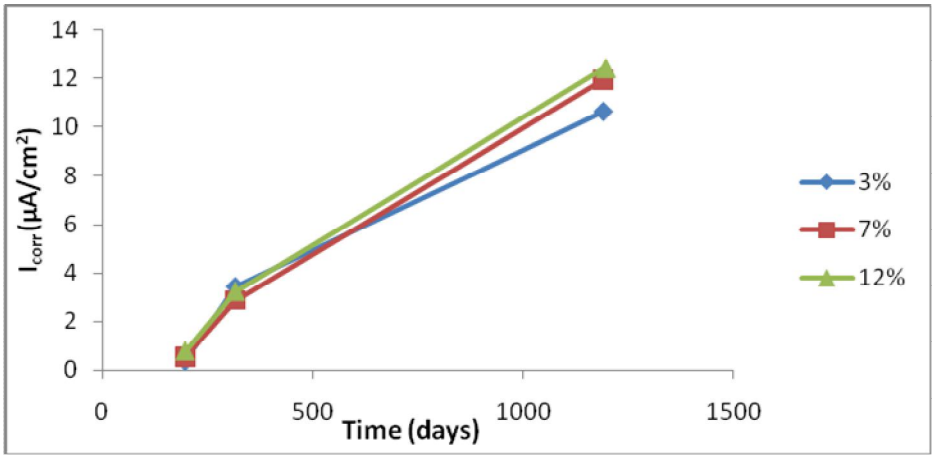

a) w/c = 0.45, C_C = 400 kg/m^3, C_V = 25 mm.

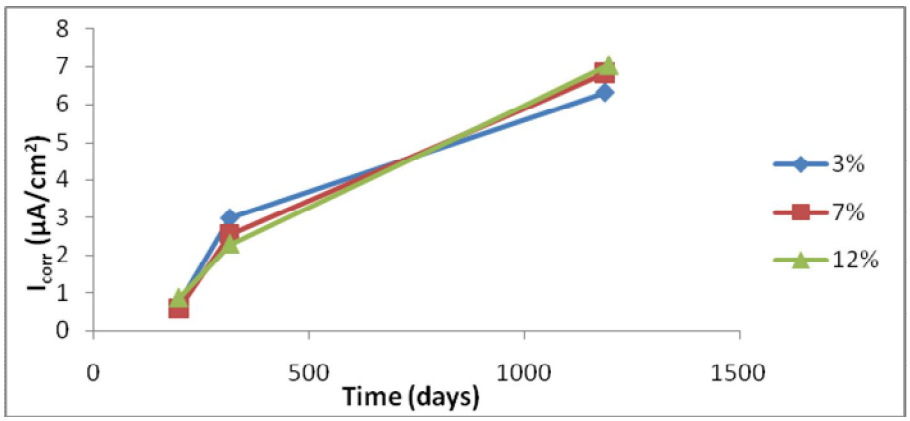

b) w/c = 0.45, C_C = 400 kg/m^3, C_V = 37.5 mm.

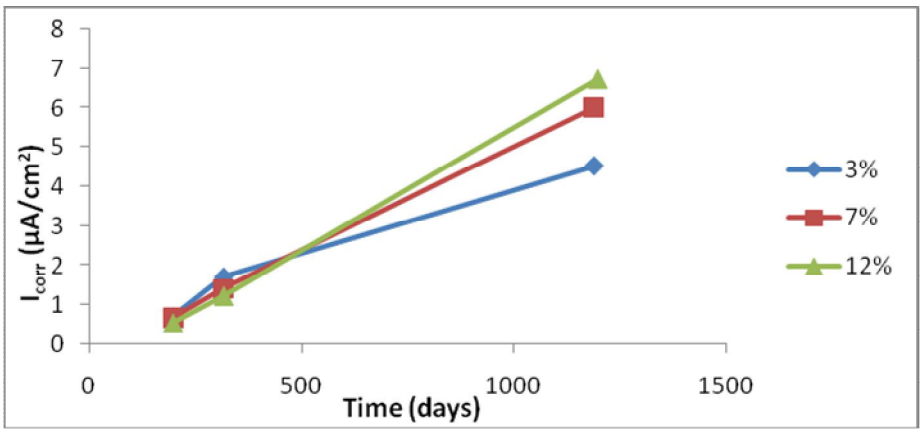

c) w/c = 0.45, C_C = 400 kg/m^3, C_V = 50 mm.

Figure B15: Variation of I_{corr} with time for w/c = 0.45, C_C = 400 kg/m^3 of T-type aggregates

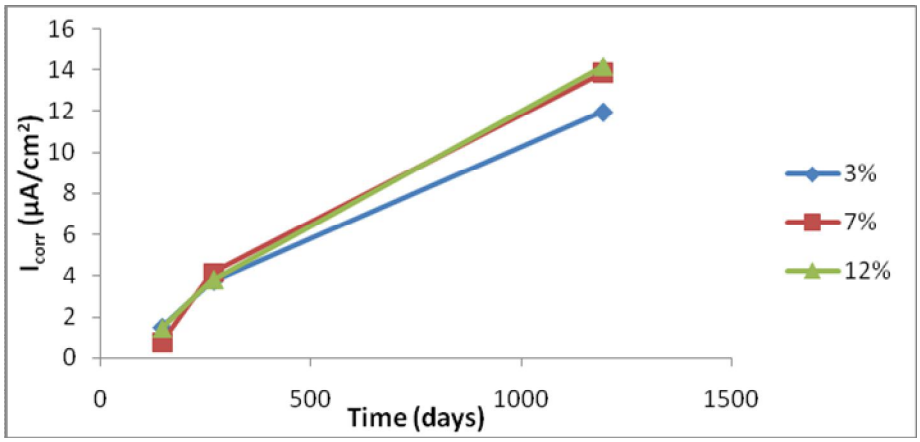

a) w/c = 0.5, C_C = 350 kg/m^3, C_V = 25 mm.

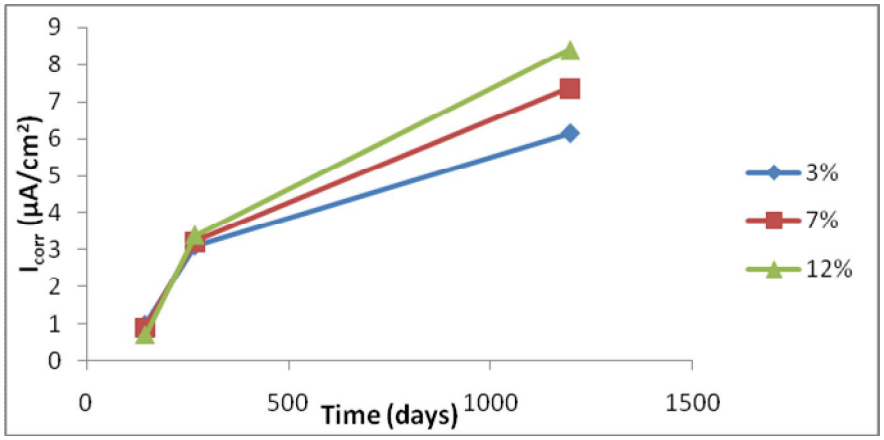

b) w/c = 0.5, C_C = 350 kg/m^3, C_V = 37.5 mm

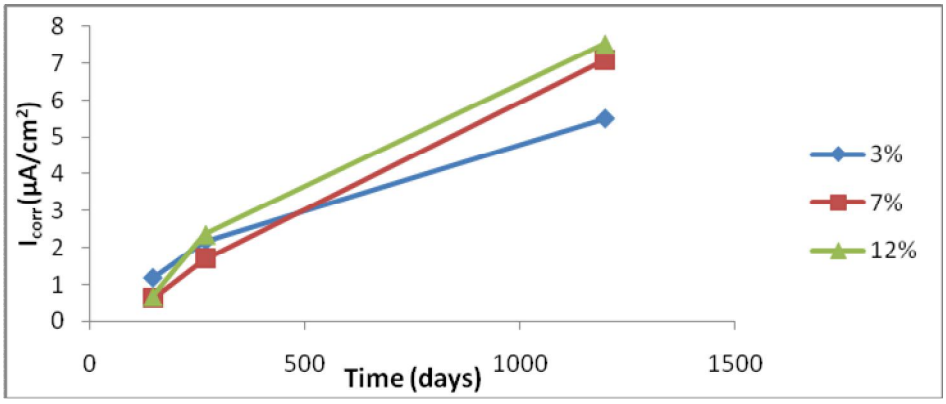

c) w/c = 0.5, C_C = 350 kg/m^3, C_V = 50 mm

Figure B16: Variation of I_{corr} with time for w/c = 0.5, C_C = 350 kg/m^3 of T-type aggregates

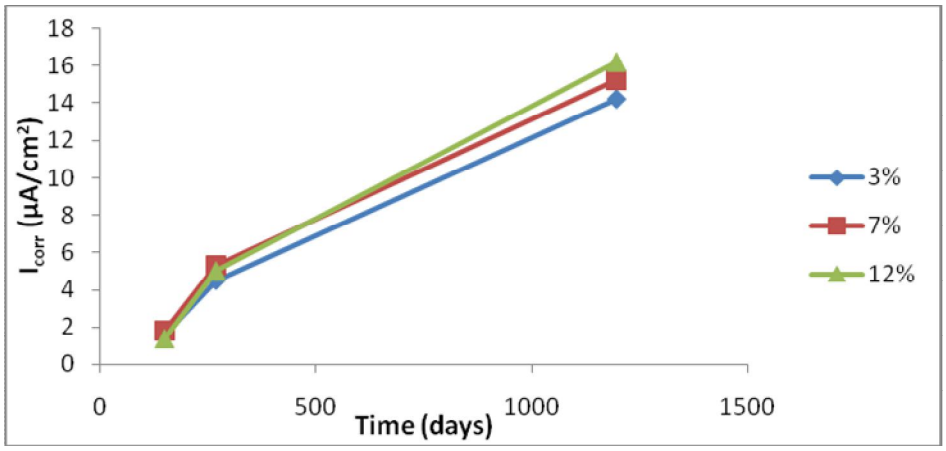

a) w/c = 0.5, C_C = 375 kg/m^3, C_V = 25 mm

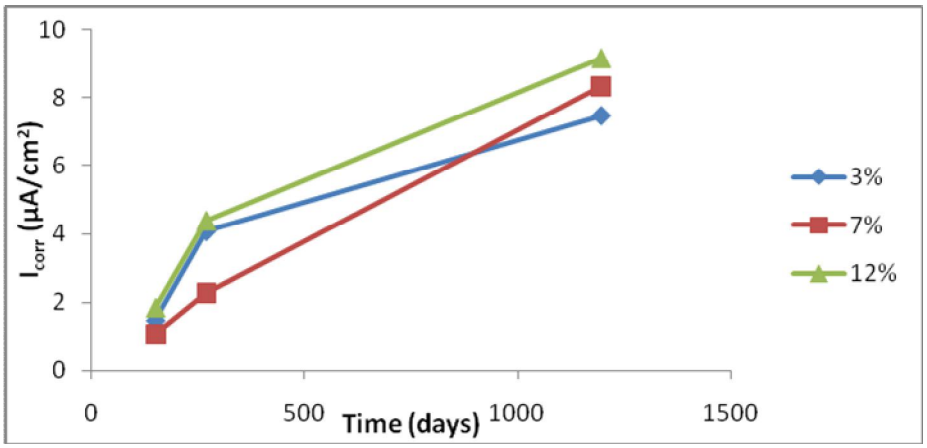

b) w/c = 0.5, C_C = 375 kg/m^3, C_V = 37.5 mm

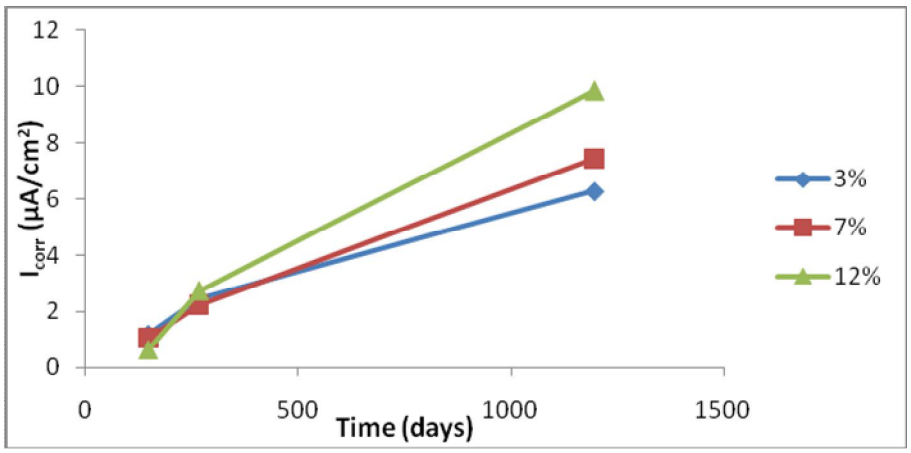

c) w/c = 0.5, C_C = 375 kg/m^3, C_V = 50 mm

Figure B17: Variation of I_{corr} with time for w/c = 0.5, C_C = 375 kg/m^3 of T-type aggregates

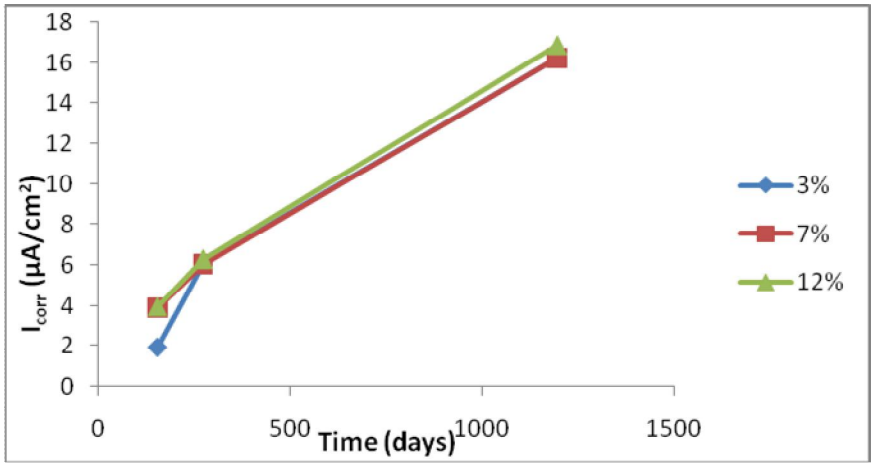

a) w/c = 0.5, C_C = 400 kg/m^3, C_V = 25 mm

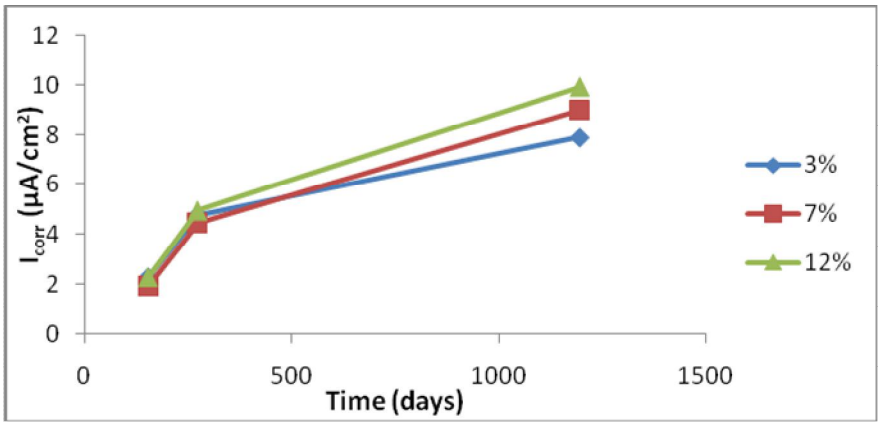

b) w/c = 0.5, C_C = 400 kg/m^3, C_V = 37.5 mm

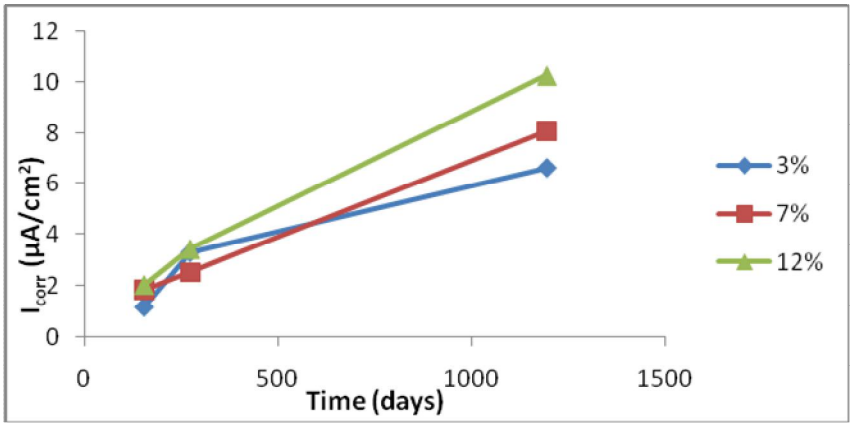

c) w/c = 0.5, C_C = 400 kg/m^3, C_V = 50 mm

Figure B18: Variation of I_{corr} with time for w/c = 0.5, C_C = 400 kg/m^3 of T-type aggregates

Appendix C

Plots of $I_{corr,g}$ versus $R_{W/C}$

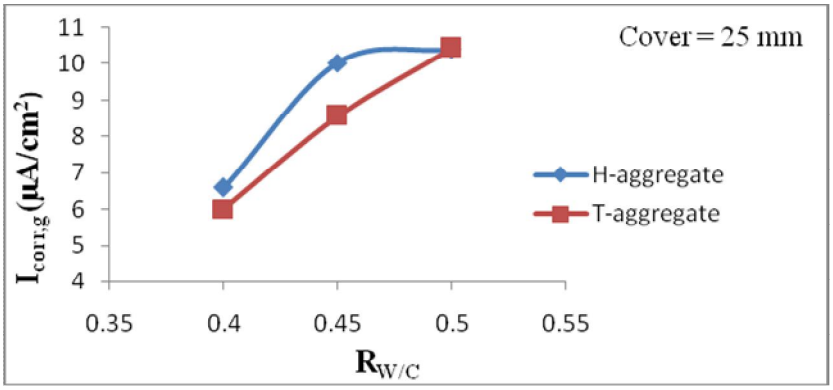

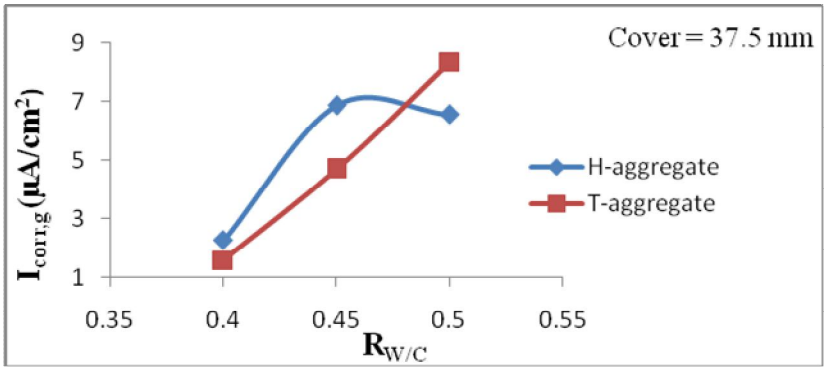

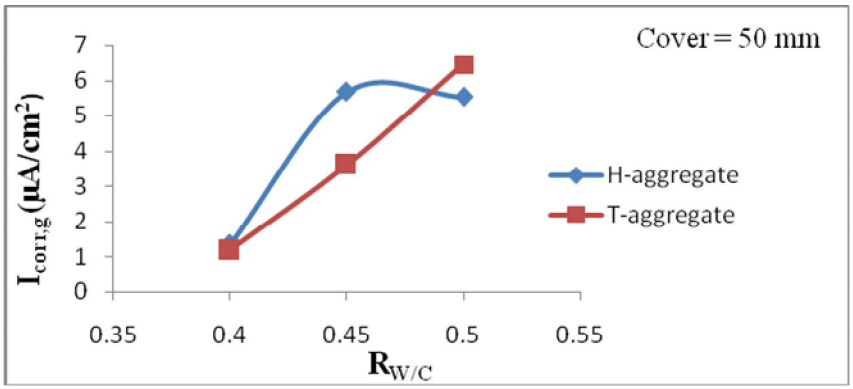

Figure C1: Variation of $I_{corr,g}$ with $R_{W/C}$ for C_C = 350 Kg/m^3, $R_{FA/TA}$ = 0.35.

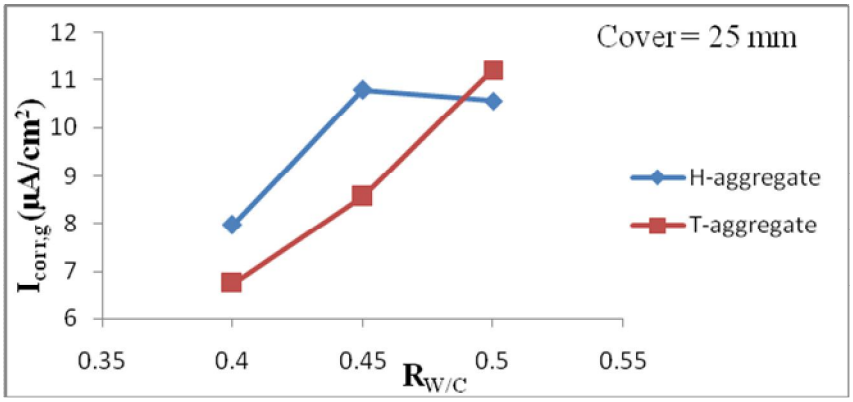

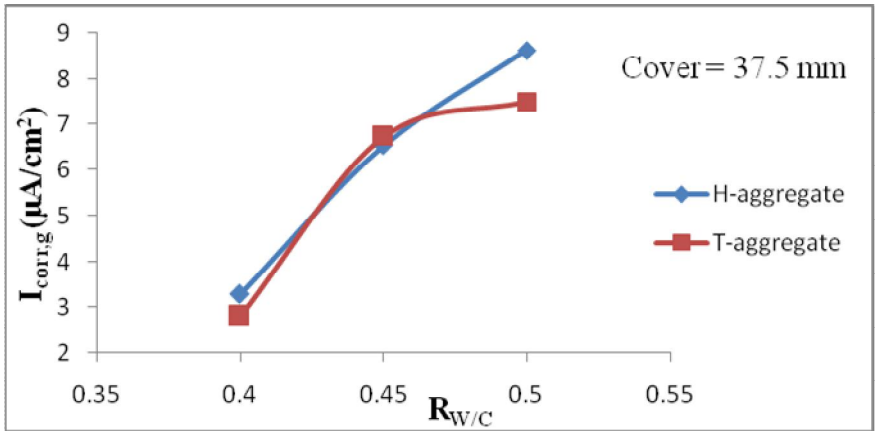

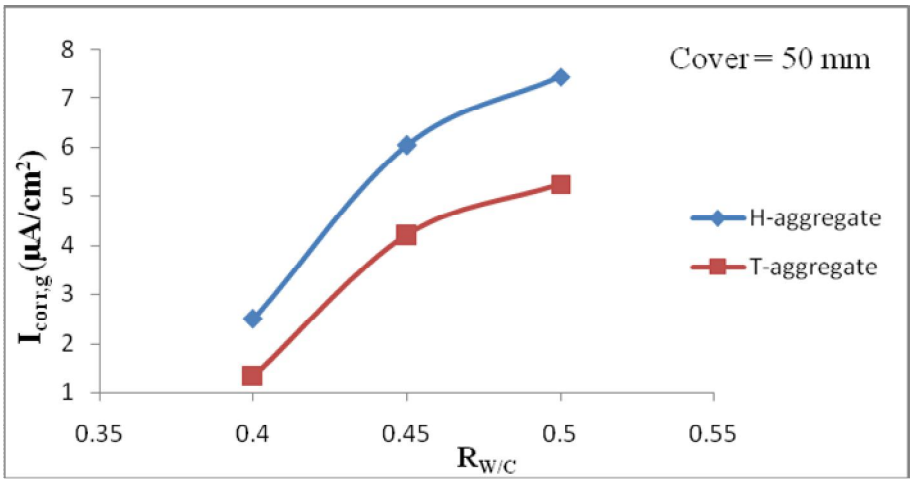

Figure C2: Variation of $I_{corr,g}$ with $R_{W/C}$ for C_C = 375 Kg/m^3, $R_{FA/TA}$ = 0.35.

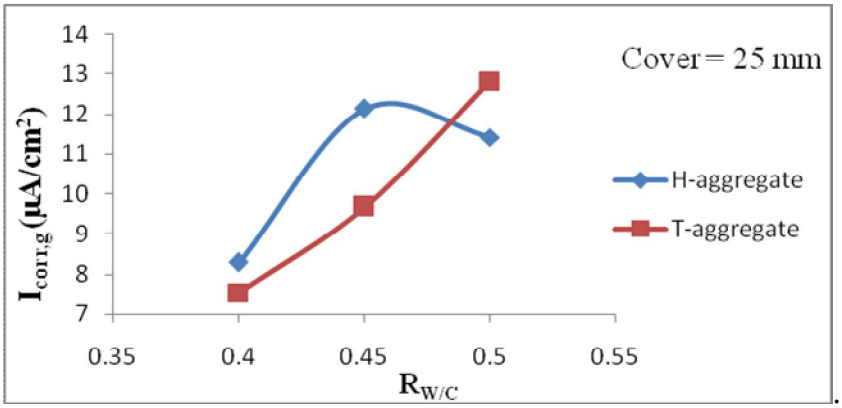

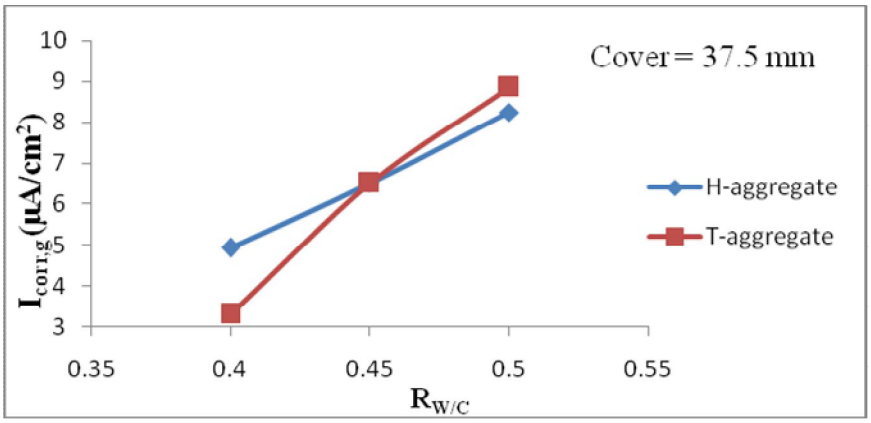

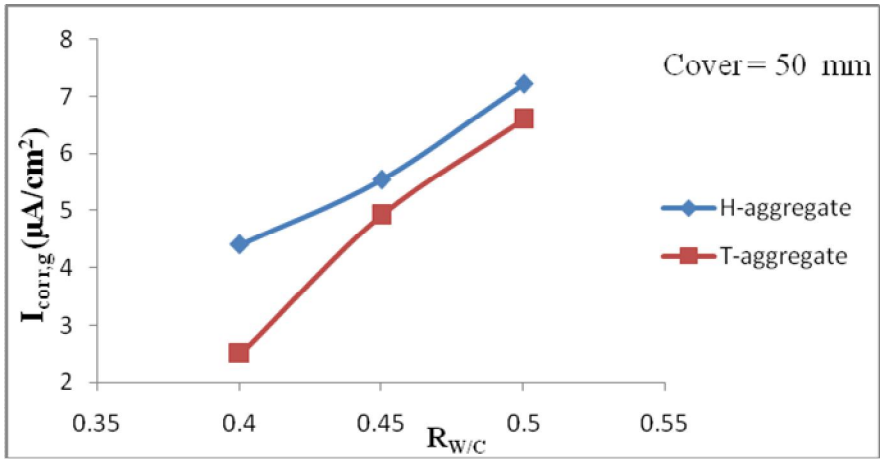

Figure C3: Variation of $I_{corr,g}$ with $R_{W/C}$ for C_C = 400 Kg/m^3, $R_{FA/TA}$ = 0.35.

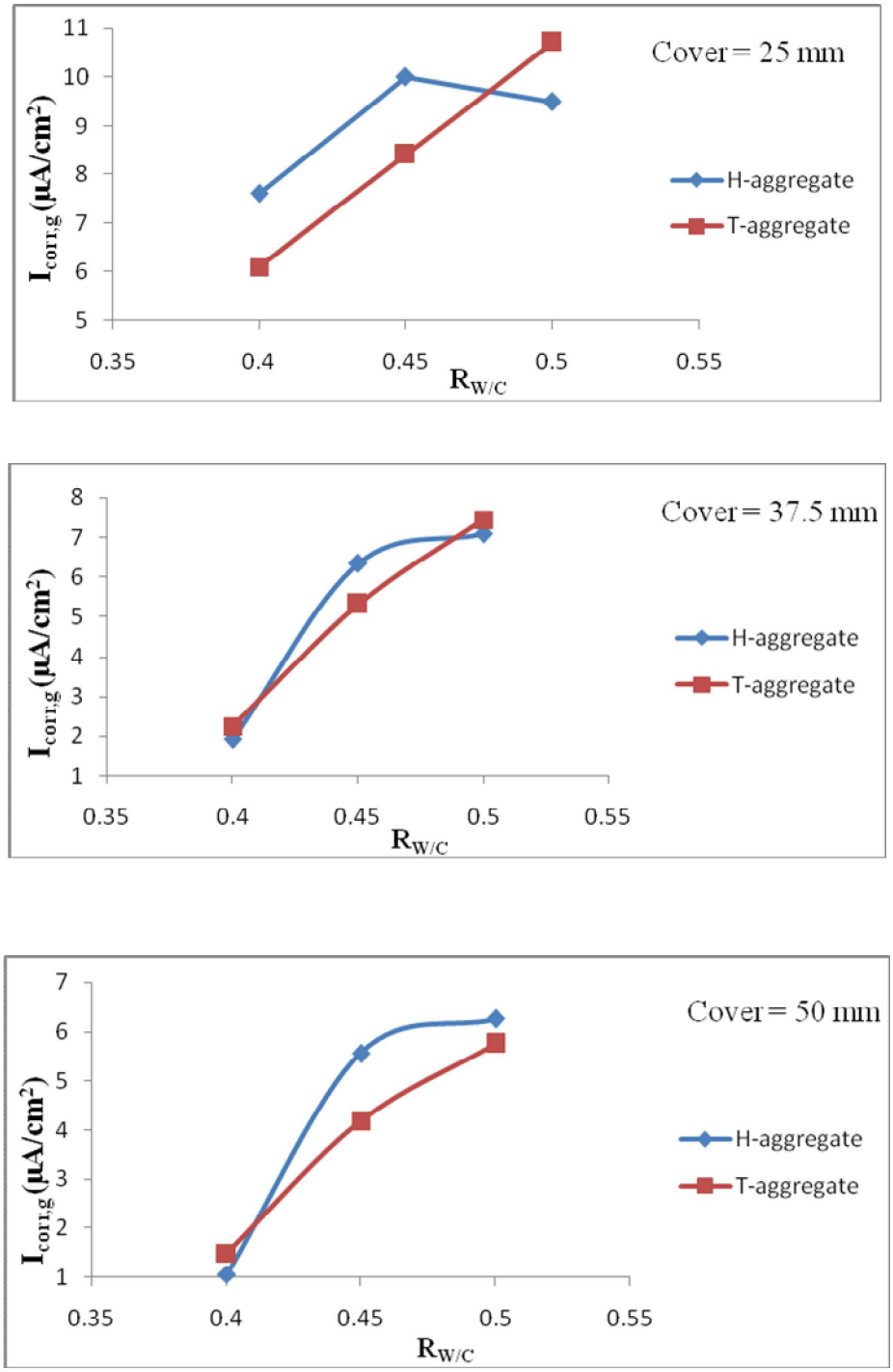

Figure C4: Variation of $I_{corr,g}$ with $R_{W/C}$ for C_C = 350 Kg/m^3, $R_{FA/TA}$ = 0.4.

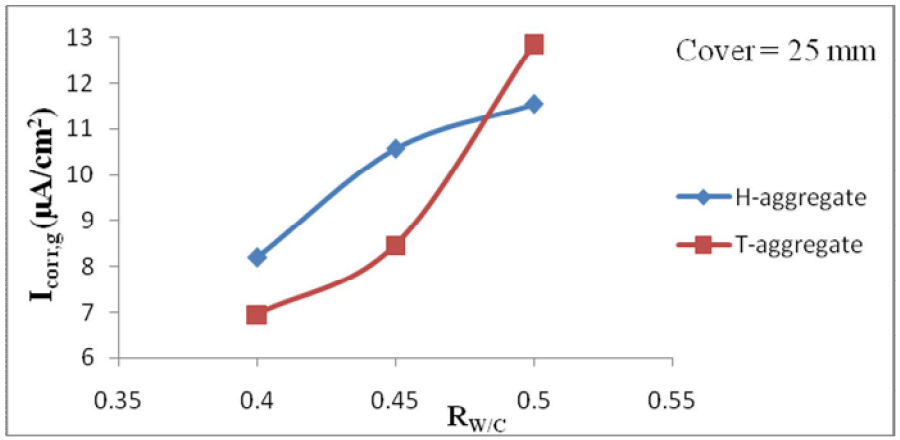

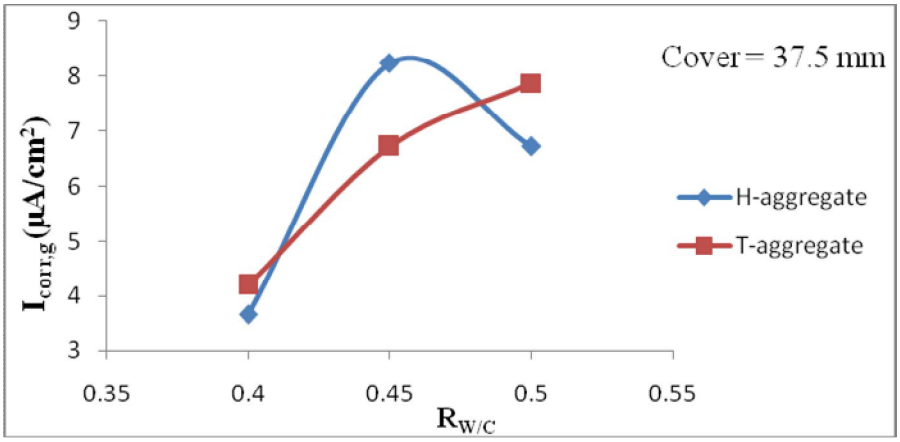

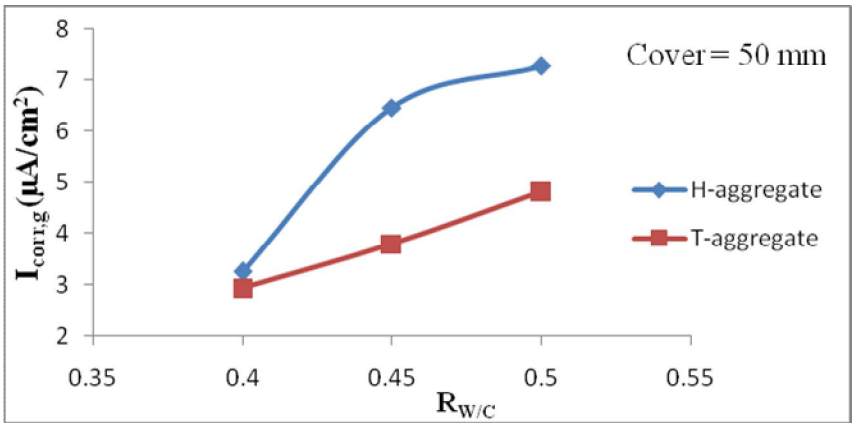

Figure C5: Variation of $I_{corr,g}$ with $R_{W/C}$ for C_C = 375 Kg/m^3, $R_{FA/TA}$ = 0.4.

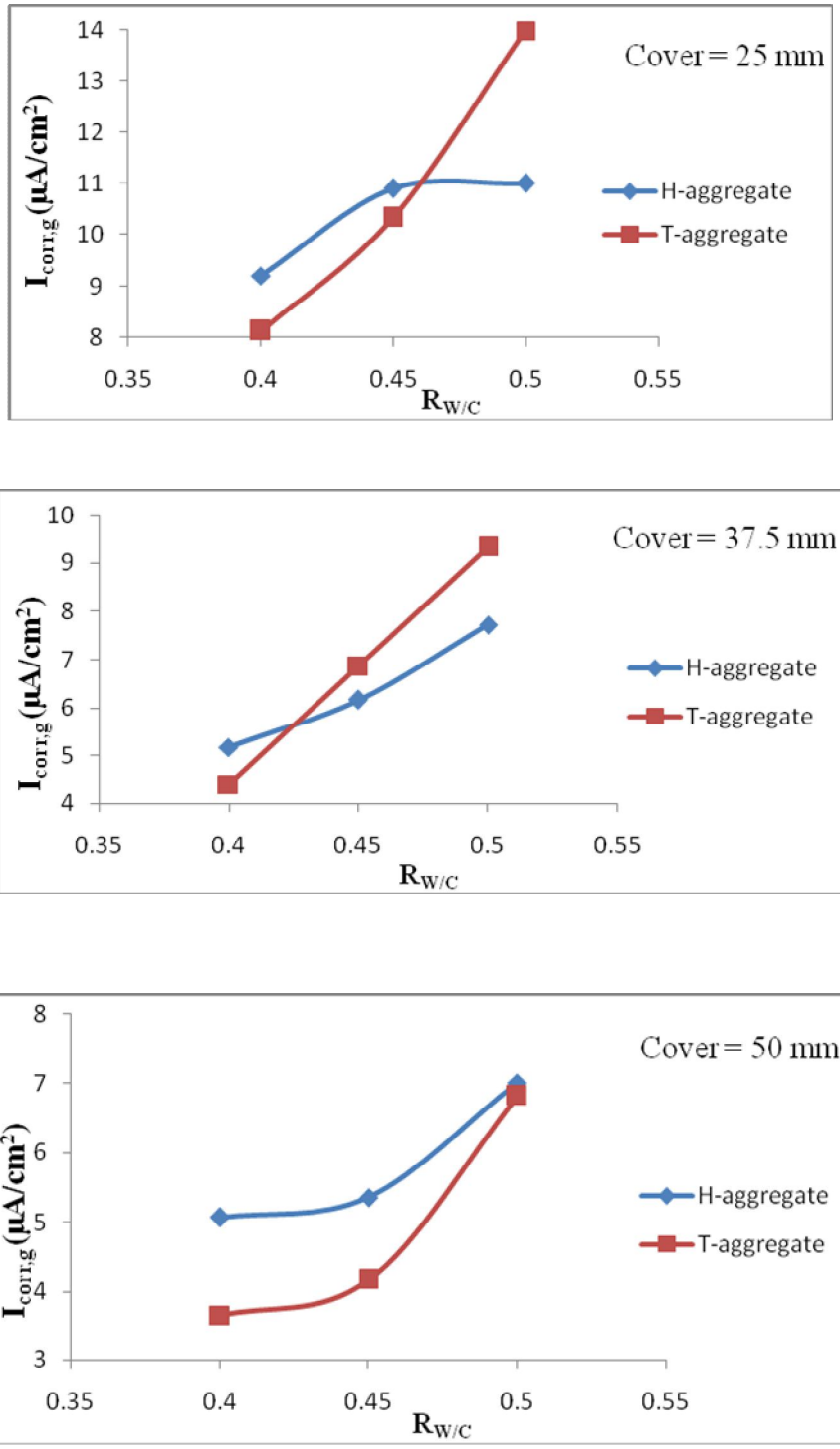

Figure C6: Variation of $I_{corr,g}$ with $R_{W/C}$ for C_C= 400 Kg/m^3, $R_{FA/TA}$ = 0.4.

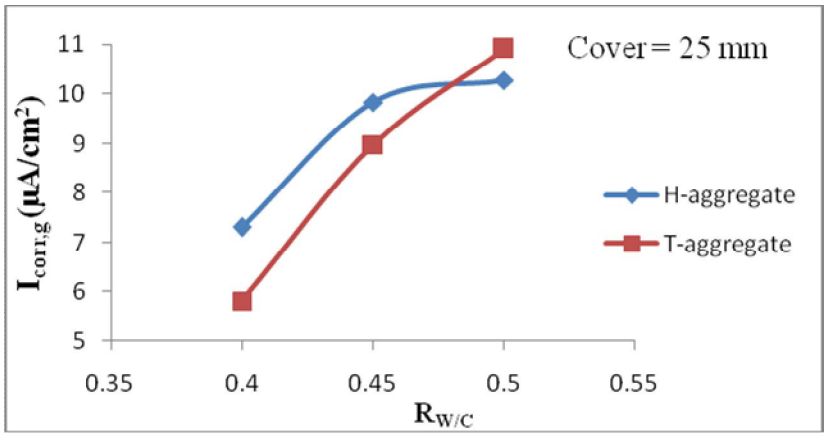

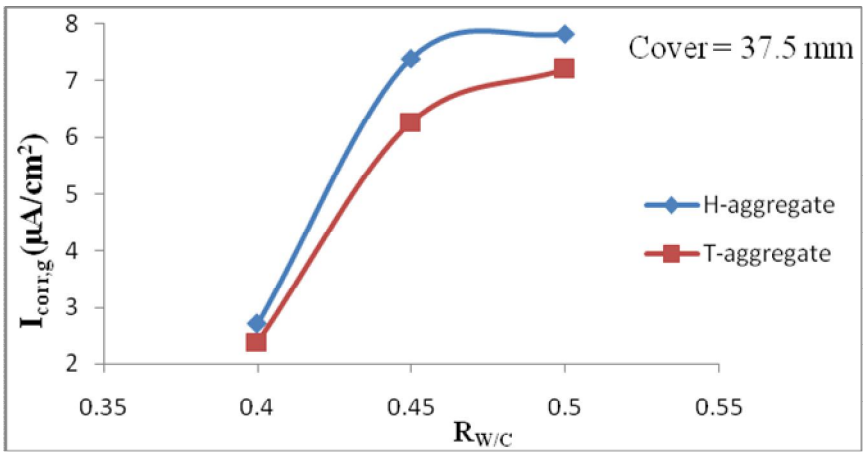

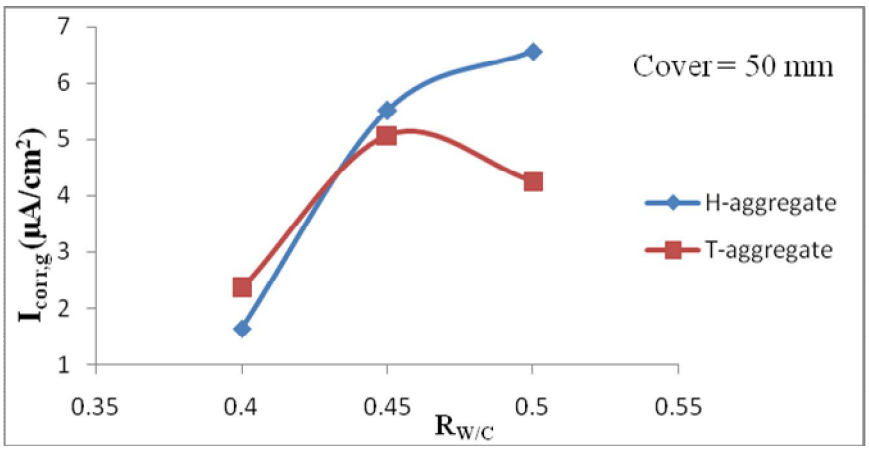

Figure C7: Variation of $I_{corr,g}$ with $R_{W/C}$ for C_C = 350 Kg/m^3, $R_{FA/TA}$ = 0.45.

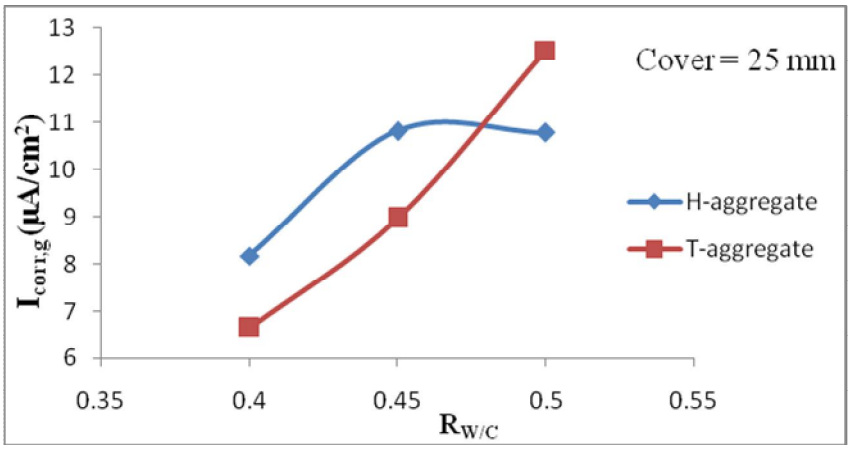

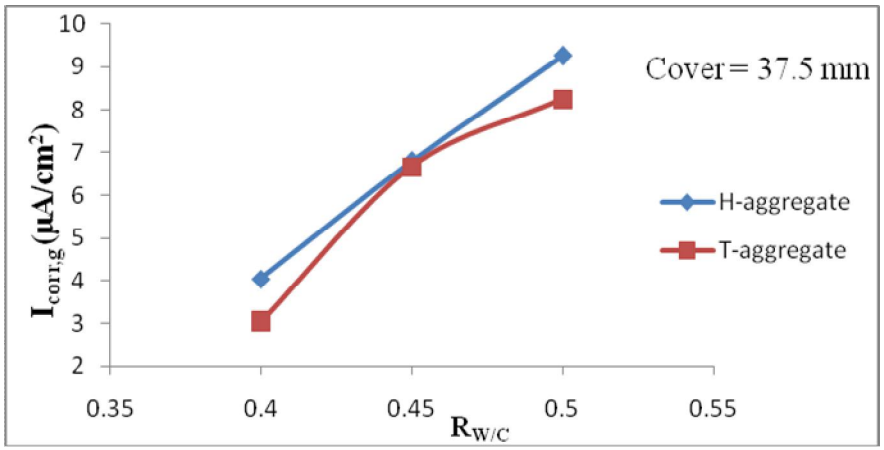

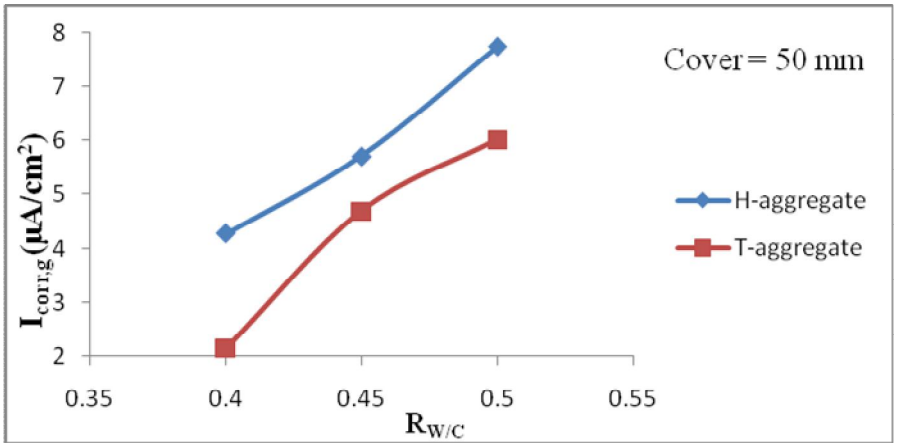

Figure C8: Variation of $I_{corr,g}$ with $R_{W/C}$ for C_C = 375 Kg/m^3, $R_{FA/TA}$ = 0.45.

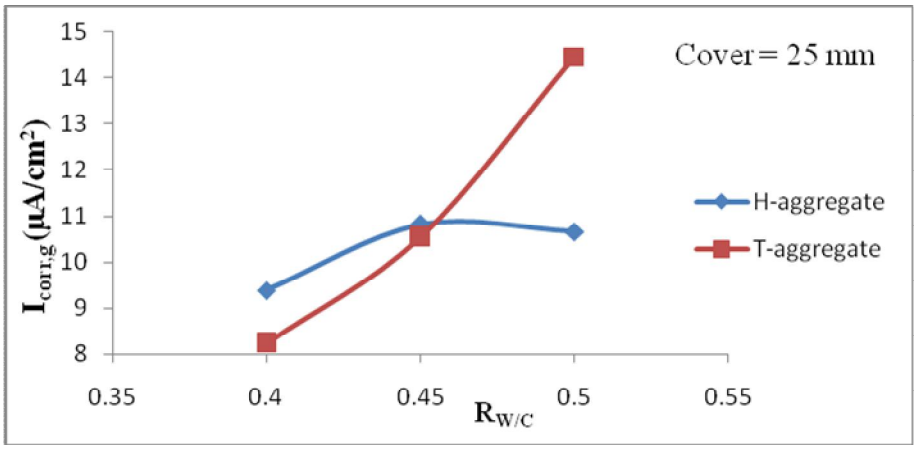

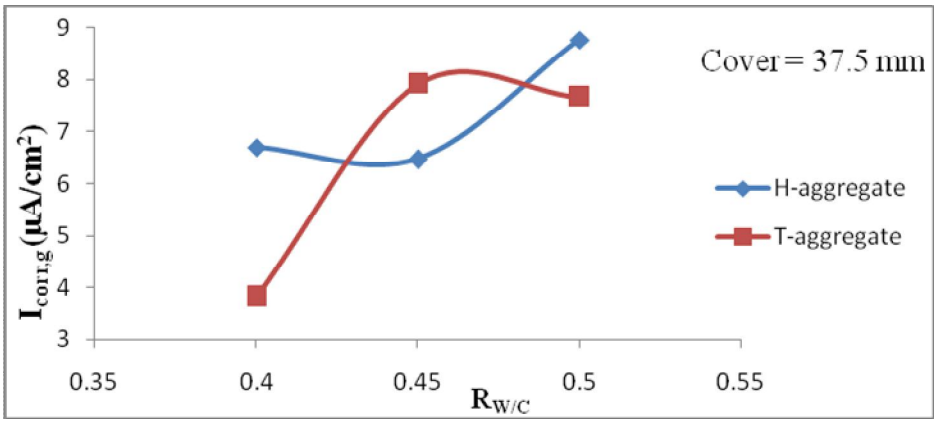

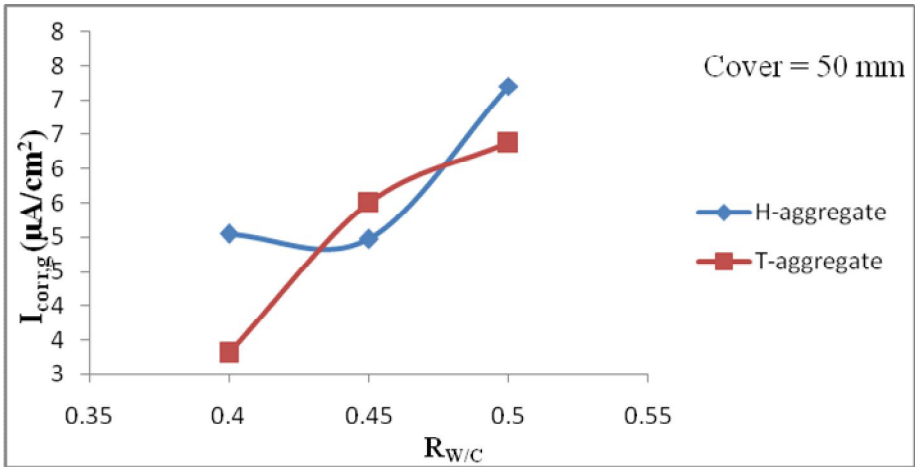

Figure C9: Variation of $I_{corr,g}$ with $R_{W/C}$ for C_C = 400 Kg/m^3, $R_{FA/TA}$ = 0.45.

APPENDIX D

Overview of Analysis of variance (ANOVA)

Analysis of Variance (ANOVA) [70] is a parametric procedure that yields values that can be used to determine whether a statistically significant relation exists between *dependent variable* (*X*) and *independent variables* (*Y*). By parametric, it is meant that the data are *normally* distributed in a *normal* or *bell-shaped* curve. The dependent variable may be referred to as the "*response*" or "*outcome variable*". Independent variables are sometimes called "factors" or "predictors". The ANOVA model is a univariate model, in that interest is in how the predictors affect a single dependent variable. A one-way ANOVA compares the means of a variable that is classified by only one variable, which is called the *factor*. The possible *values* of the factor are called the *levels* of the factor. In ANOVA, the following statistical terminologies are used:

Data points

Data points are the replicate observations of the dependent variable (X_1, X_2, X_i, X_n) measured at each level of the independent variable.

Sample mean $\left(\overline{X}\right)$

$\overline{X}$ = total sum of data points/total number of data points

Correction factor (*CF*)

CF = (total sum of all data points)^2/total number of data points

Degree of freedom (df)

Degree of freedom is the number of values in the final calculation of a statistic that are free to vary.

$\text{df} = n - 1$

where *n* represents the number of groups

Error (residual)

It is the amount by which an observed variate differs from the value predicted by the assumed statistical model. Errors or residuals are the segments of scores not accounted for by the analysis. In ANOVA, the errors are assumed to be independent of each other, and are assumed *normally* distributed about the sample means. They are also assumed to be identically distributed for each sample (since the analysis is seeking only a significant difference between sample means), which is known as the assumption of homogeneity of variances.

Sum of squares (SS)

The sum of square is the squared distance between each data point (X_i) and the sample mean**(** $\overline{X}$ **)**, summed for all *N* data points.

$$\text{SS} = \sum_{i=1}^{n} \left(X_i - \overline{X} \right)^2$$

where X_i represents the *i* observations and $\overline{X}$ represents the sample mean.

Mean square (MS)

Mean square is a measure of the variability of *group mean* around the *grand mean*. It is the average sum of squares. In other words MS is the sum of squared deviations from the mean divided by the appropriate degrees of freedom.

MS = SS/df

Null hypothesis

The hypothesis used in statistics to propose that no statistical significance exists in a set of given observations is called a *Null* hypothesis, H_o. The *null* hypothesis is presumed to be true until statistical evidence (through testing of a hypothesis) *nullifies* it for an *alternative* hypothesis, H_a.

F-ratio

The ratio is a statistical measure calculated by procedure of variance analysis, and reveals the significance of a hypothesis that *dependent* variable depends on *independent* variable. It comprises the ratio of two mean- squares. The F-ratio tells us precisely how much more of the variation in *Y* is explained by *X*. A large proportion indicates a significant effect of *Y.* The observed F-ratio is connected by an equation to the exact probability of a true null hypothesis, (i.e. that the ratio equals unity), but the standard tables can be used to find out whether the observed F-ratio indicates a significant relationship.

F-ratio = MS of the source effect/ MS of the residual error.

P-value

P-value is a measure of *acceptance* or *rejection* of a statistical significance based on a standard that no more than 5 % (0.05 level) of the difference is due to chance or sampling error.

Appendix E

Microsoft Excel program for service life prediction

Table E: Automated Microsoft Excel program (SL_Predict) for service life prediction

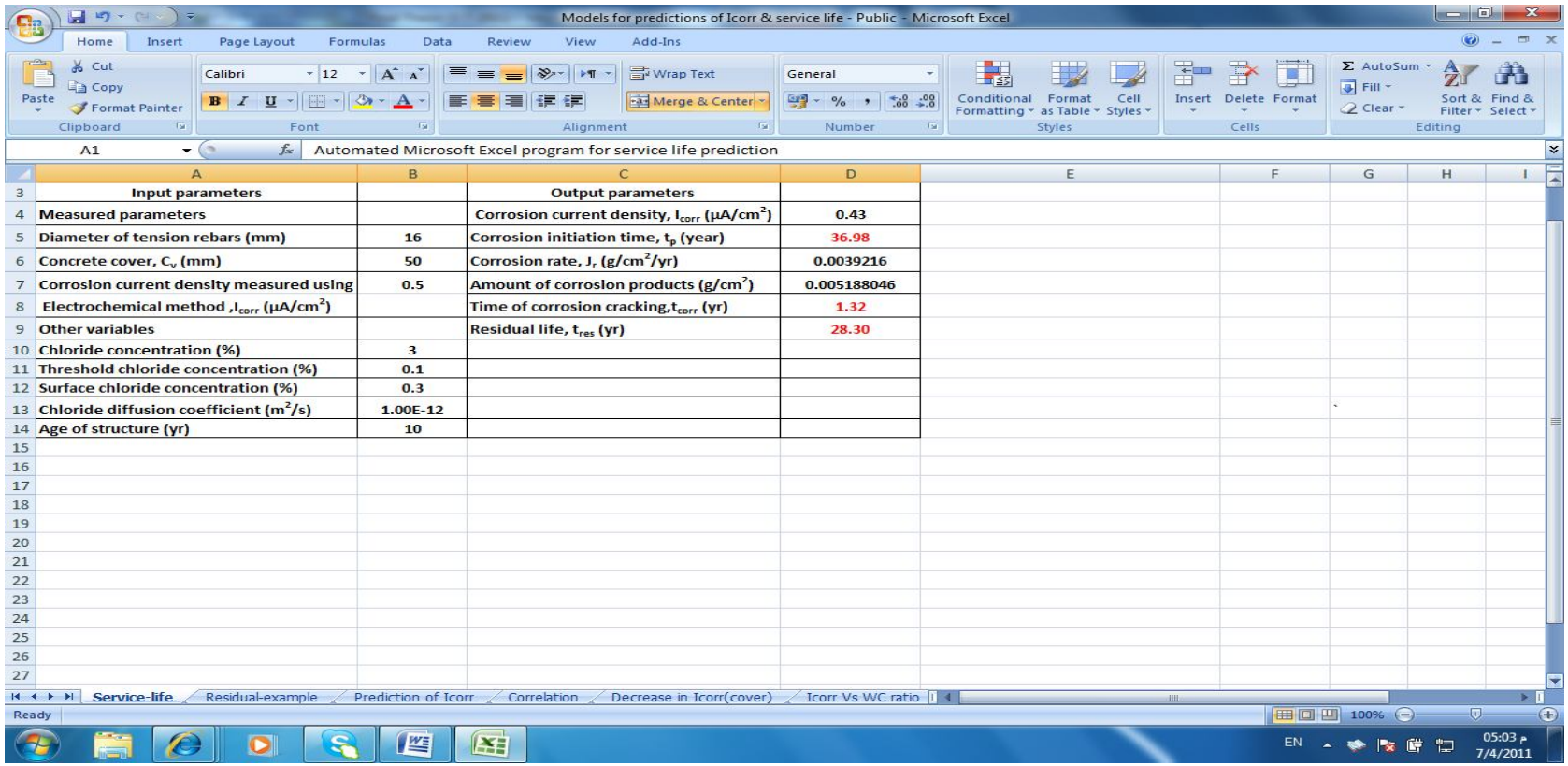

	A	B	C	D
3	**Input parameters**		**Output parameters**	
4	**Measured parameters**		**Corrosion current density, I_{corr} (μA/cm^2)**	**0.43**
5	**Diameter of tension rebars (mm)**	**16**	**Corrosion initiation time, t_p (year)**	**36.98**
6	**Concrete cover, C_v (mm)**	**50**	**Corrosion rate, J_r (g/cm^2/yr)**	**0.0039216**
7	**Corrosion current density measured using**	**0.5**	**Amount of corrosion products (g/cm^2)**	**0.005188046**
8	**Electrochemical method ,I_{corr} (μA/cm^2)**		**Time of corrosion cracking,t_{corr} (yr)**	**1.32**
9	**Other variables**		**Residual life, t_{res} (yr)**	**28.30**
10	**Chloride concentration (%)**	**3**		
11	**Threshold chloride concentration (%)**	**0.1**		
12	**Surface chloride concentration (%)**	**0.3**		
13	**Chloride diffusion coefficient (m^2/s)**	**1.00E-12**		
14	**Age of structure (yr)**	**10**		

Appendix F

Microsoft Excel Solver for optimization of I_{corr}

Table F1: Microsoft Excel Solver for H-type aggregates

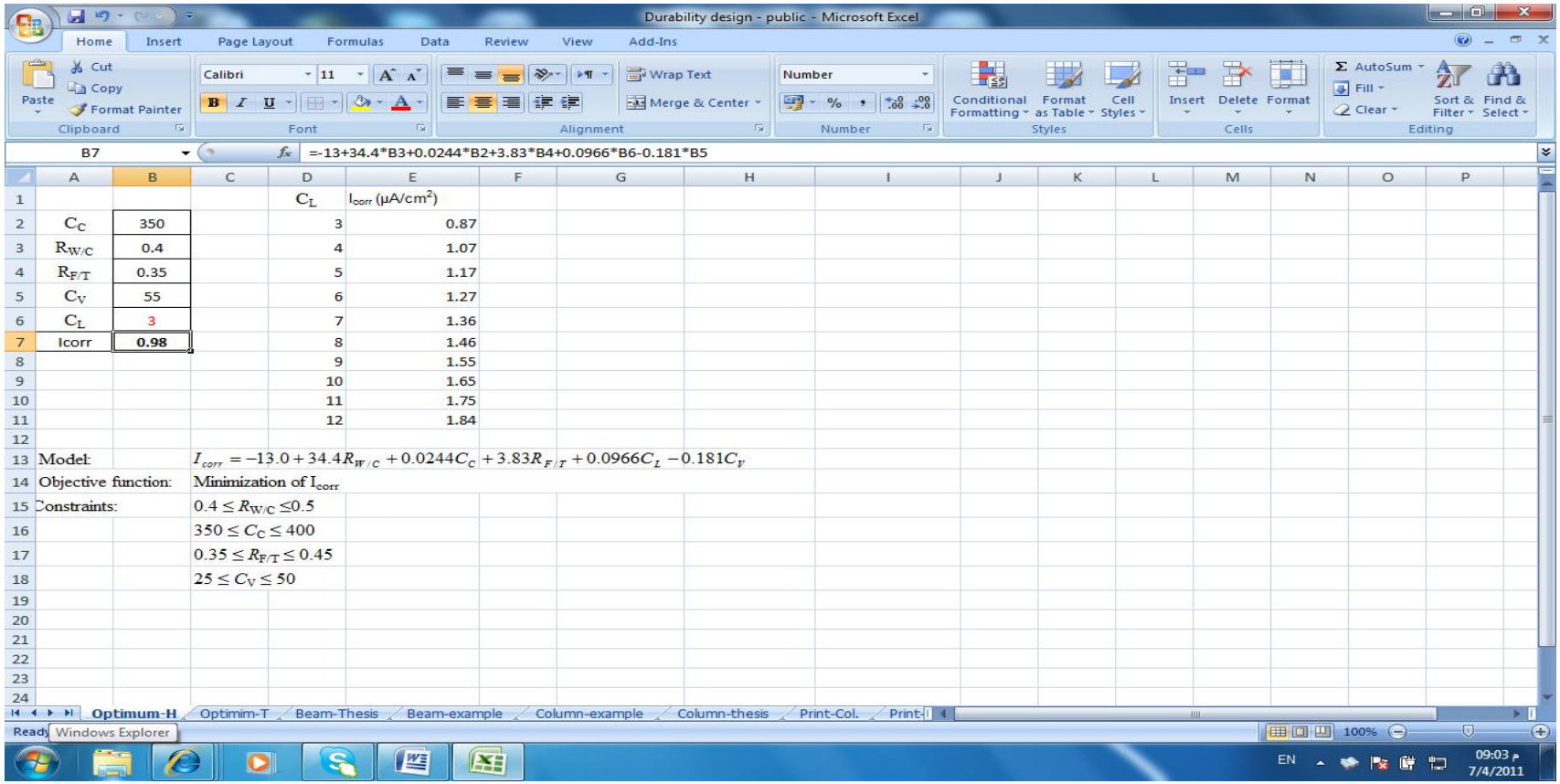

	A	B	C	D	E
1				C_L	I_{corr} (μA/cm²)
2	C_C	350		3	0.87
3	$R_{W/C}$	0.4		4	1.07
4	$R_{F/T}$	0.35		5	1.17
5	C_V	55		6	1.27
6	C_L	3		7	1.36
7	Icorr	0.98		8	1.46
8				9	1.55
9				10	1.65
10				11	1.75
11				12	1.84
12					
13	Model:		$I_{corr} = -13.0 + 34.4R_{W/C} + 0.0244C_C + 3.83R_{F/T} + 0.0966C_L - 0.181C_V$		
14	Objective function:		Minimization of I_{corr}		
15	Constraints:		$0.4 \le R_{W/C} \le 0.5$		
16			$350 \le C_C \le 400$		
17			$0.35 \le R_{F/T} \le 0.45$		
18			$25 \le C_V \le 50$		
19					
20					
21					
22					
23					
24					

Table F2: Microsoft Excel Solver for T-type aggregates

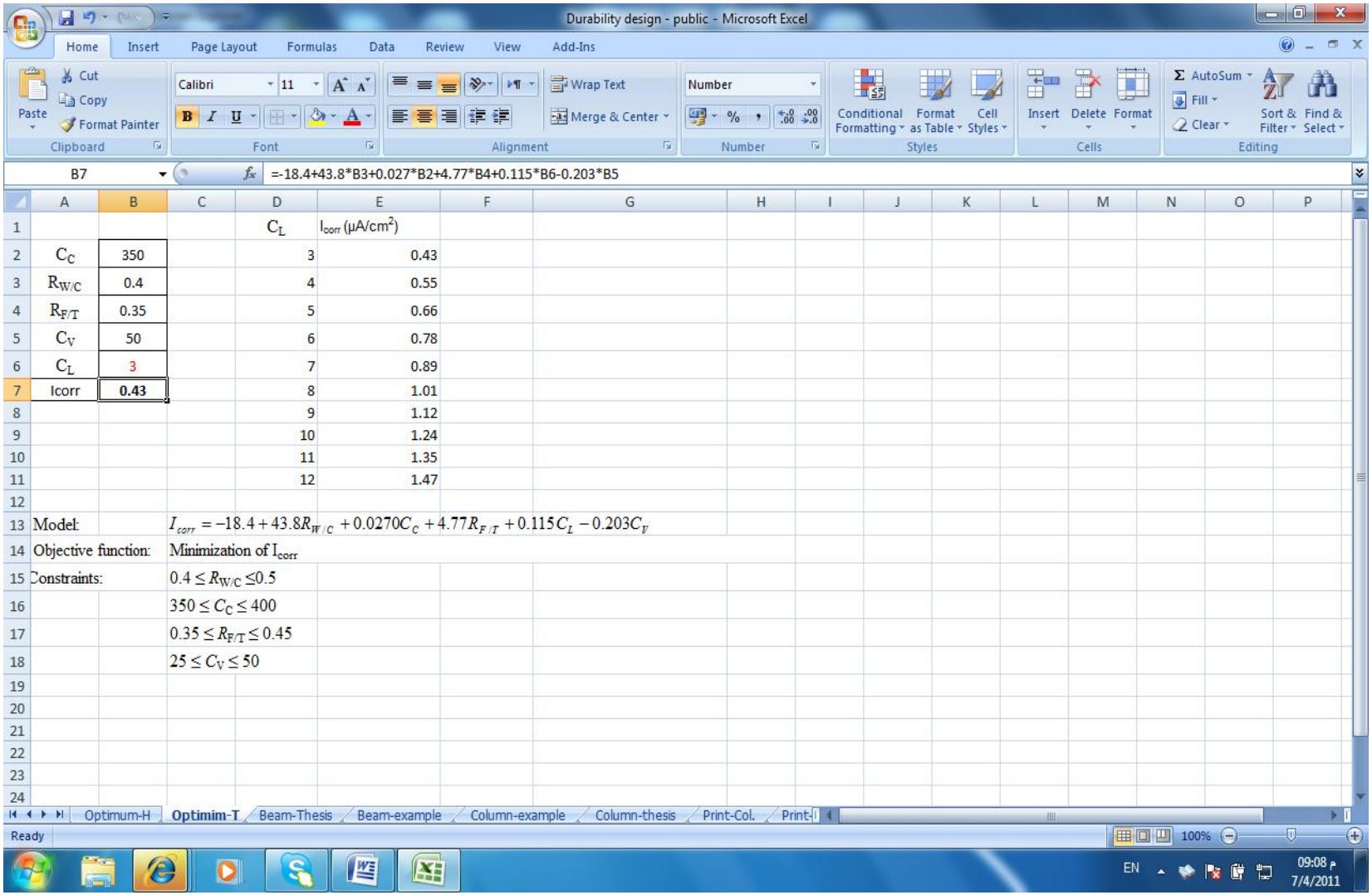

	A	B	C	D	E	F	G	H	I	J	K	L	M	N	O	P
1				C_L	I_{corr} ($\mu A/cm^2$)											
2	C_C	350		3	0.43											
3	$R_{W/C}$	0.4		4	0.55											
4	$R_{F/T}$	0.35		5	0.66											
5	C_V	50		6	0.78											
6	C_L	3		7	0.89											
7	Icorr	**0.43**		8	1.01											
8				9	1.12											
9				10	1.24											
10				11	1.35											
11				12	1.47											
12																
13	Model:		$I_{corr} = -18.4 + 43.8R_{W/C} + 0.0270C_C + 4.77R_{F/T} + 0.115C_L - 0.203C_V$													
14	Objective function:		Minimization of I_{corr}													
15	Constraints:		$0.4 \le R_{W/C} \le 0.5$													
16			$350 \le C_C \le 400$													
17			$0.35 \le R_{F/T} \le 0.45$													
18			$25 \le C_V \le 50$													
19																
20																
21																
22																
23																
24																

Table F3: Microsoft Excel Solver for H-type aggregates by using Yusuf's model [6]

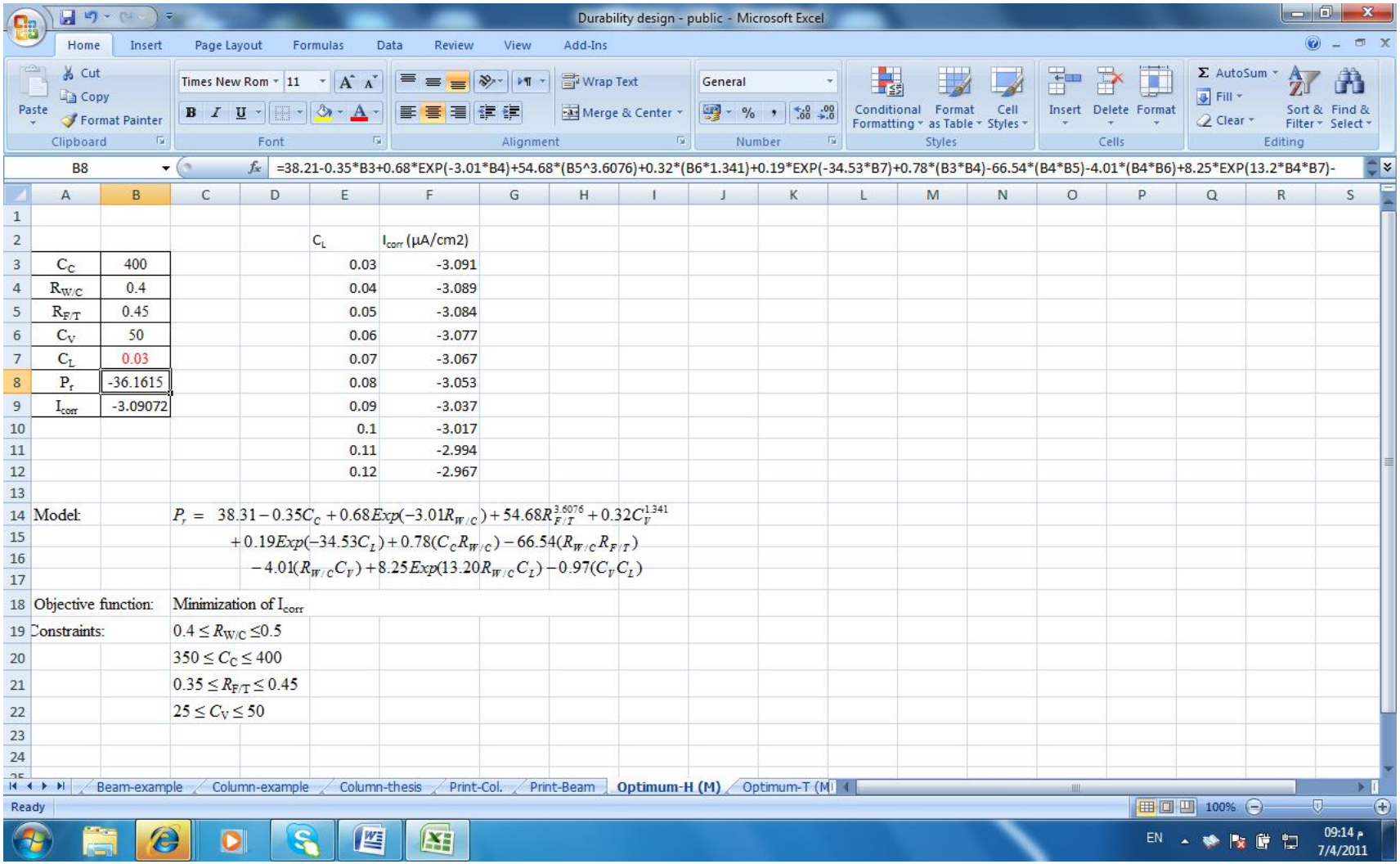

C_C	400
$R_{W/C}$	0.4
$R_{F/T}$	0.45
C_V	50
C_L	0.03
P_r	-36.1615
I_{corr}	-3.09072

C_L	I_{corr} (μA/cm2)
0.03	-3.091
0.04	-3.089
0.05	-3.084
0.06	-3.077
0.07	-3.067
0.08	-3.053
0.09	-3.037
0.1	-3.017
0.11	-2.994
0.12	-2.967

Model:

$$P_r = 38.31 - 0.35C_C + 0.68Exp(-3.01R_{W/C}) + 54.68R_{F/T}^{3.6076} + 0.32C_V^{1.341} + 0.19Exp(-34.53C_L) + 0.78(C_C R_{W/C}) - 66.54(R_{W/C} R_{F/T}) - 4.01(R_{W/C} C_V) + 8.25Exp(13.20R_{W/C} C_L) - 0.97(C_V C_L)$$

Objective function: Minimization of I_{corr}

Constraints:

$0.4 \le R_{W/C} \le 0.5$

$350 \le C_C \le 400$

$0.35 \le R_{F/T} \le 0.45$

$25 \le C_V \le 50$

Table F4: Microsoft Excel Solver for T-type aggregates by using Yusuf's model [6].

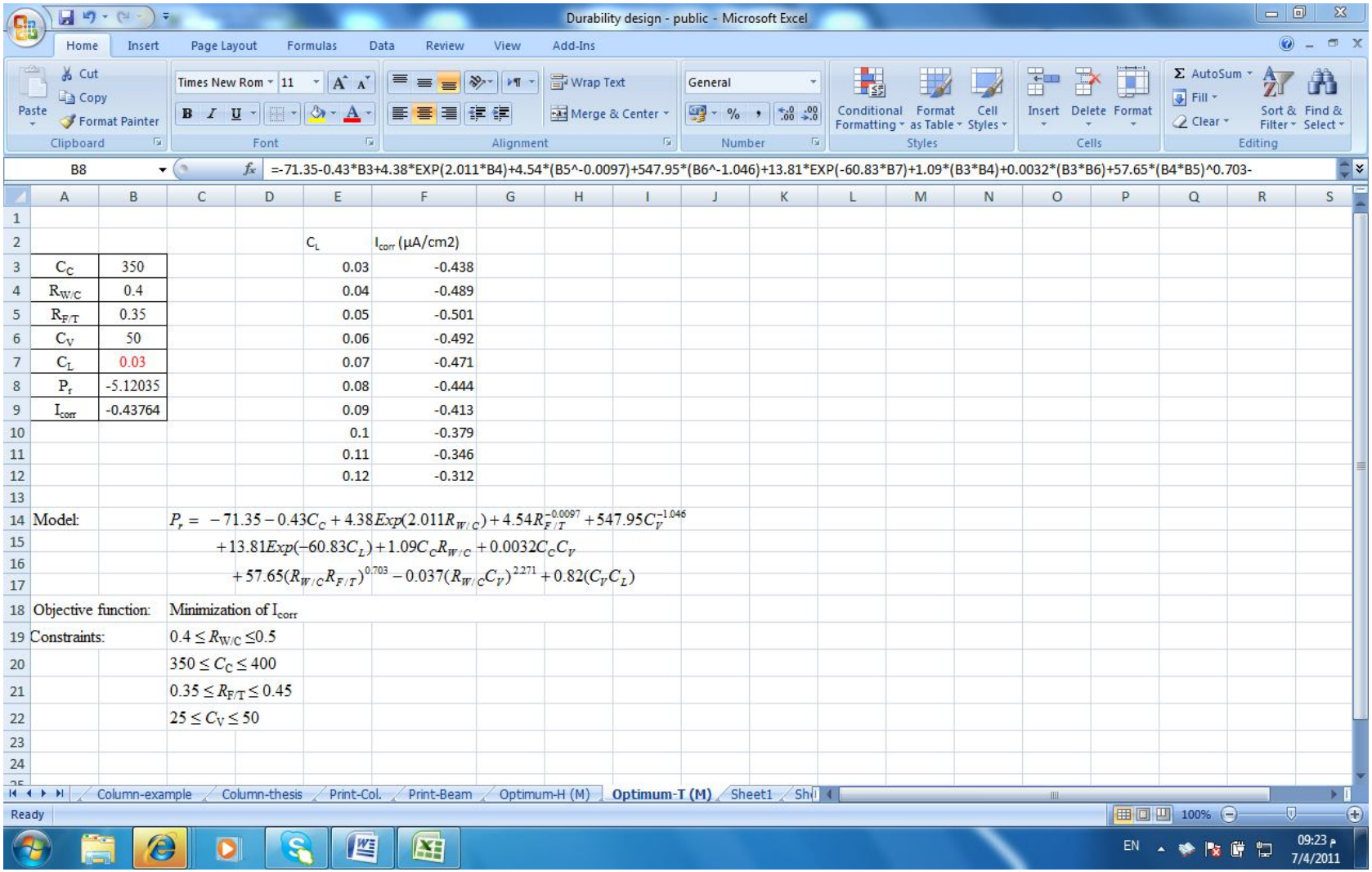

1																		
2					C_L	I_{corr} (μA/cm2)												
3	C_C	350			0.03	-0.438												
4	$R_{W/C}$	0.4			0.04	-0.489												
5	$R_{F/T}$	0.35			0.05	-0.501												
6	C_V	50			0.06	-0.492												
7	C_L	0.03			0.07	-0.471												
8	P_r	-5.12035			0.08	-0.444												
9	I_{corr}	-0.43764			0.09	-0.413												
10					0.1	-0.379												
11					0.11	-0.346												
12					0.12	-0.312												
13																		
14	Model:		$P_r = -71.35 - 0.43C_C + 4.38Exp(2.011R_{W/C}) + 4.54R_{F/T}^{-0.0097} + 547.95C_V^{-1.046}$															
15			$+13.81Exp(-60.83C_L) + 1.09C_CR_{W/C} + 0.0032C_CC_V$															
16			$+57.65(R_{W/C}R_{F/T})^{0.703} - 0.037(R_{W/C}C_V)^{2.271} + 0.82(C_VC_L)$															
17																		
18	Objective function:		Minimization of I_{corr}															
19	Constraints:		$0.4 \le R_{W/C} \le 0.5$															
20			$350 \le C_C \le 400$															
21			$0.35 \le R_{F/T} \le 0.45$															
22			$25 \le C_V \le 50$															
23																		
24																		

Appendix G

Microsoft Excel programs for durability-based design

Table G1: Durability-based design of a RC beam using Excel spreadsheet program RC_B_DDesign

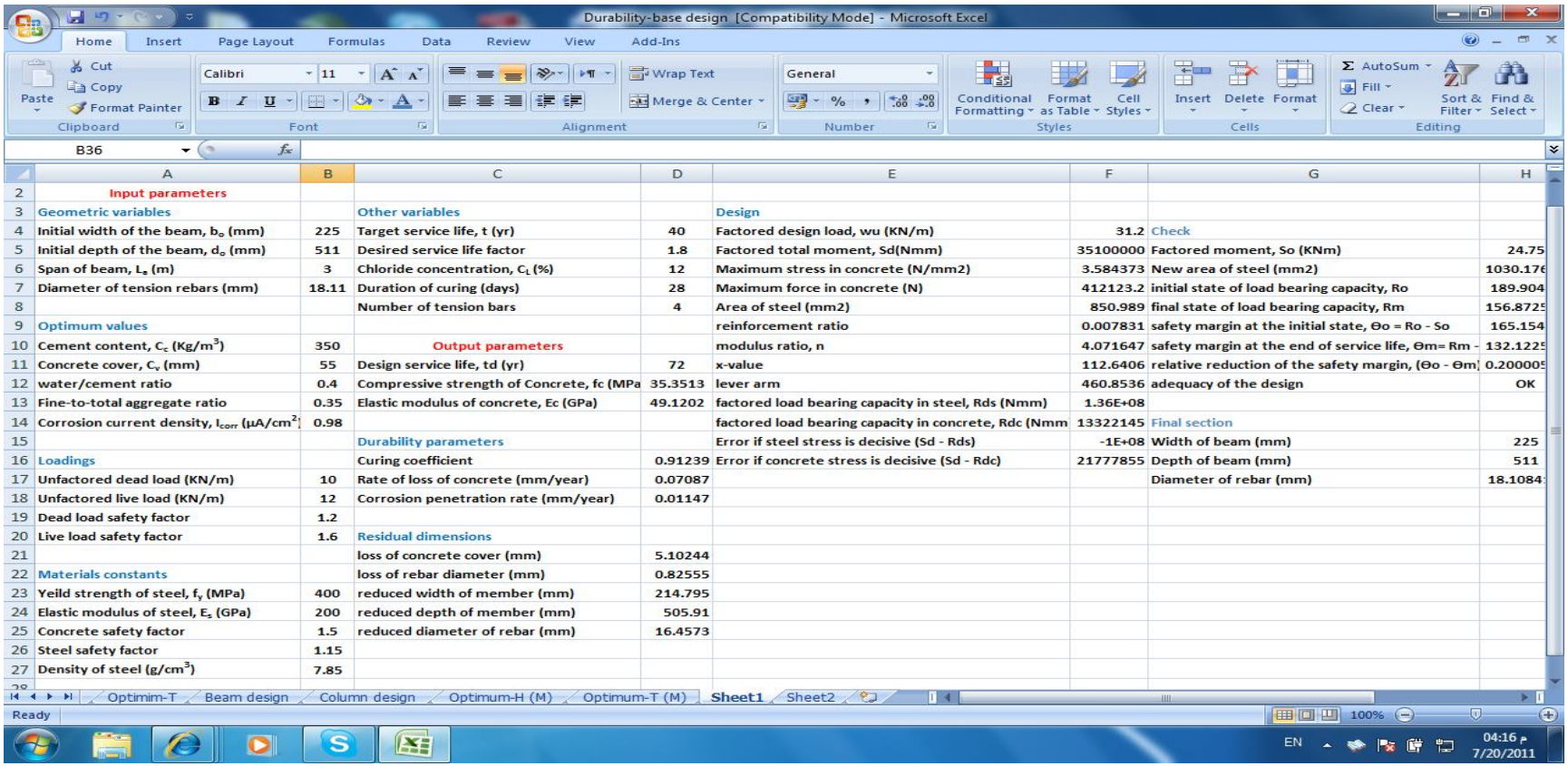

	A	B	C	D	E	F	G	H
2	Input parameters							
3	Geometric variables		Other variables		Design			
4	Initial width of the beam, b_o (mm)	225	Target service life, t (yr)	40	Factored design load, wu (KN/m)	31.2	Check	
5	Initial depth of the beam, d_o (mm)	511	Desired service life factor	1.8	Factored total moment, Sd(Nmm)	35100000	Factored moment, So (KNm)	24.75
6	Span of beam, L_s (m)	3	Chloride concentration, C_L (%)	12	Maximum stress in concrete (N/mm2)	3.584373	New area of steel (mm2)	1030.176
7	Diameter of tension rebars (mm)	18.11	Duration of curing (days)	28	Maximum force in concrete (N)	412123.2	initial state of load bearing capacity, Ro	189.904
8			Number of tension bars	4	Area of steel (mm2)	850.989	final state of load bearing capacity, Rm	156.8725
9	Optimum values				reinforcement ratio	0.007831	safety margin at the initial state, Θo = Ro - So	165.154
10	Cement content, C_c (Kg/m^3)	350	Output parameters		modulus ratio, n	4.071647	safety margin at the end of service life, Θm= Rm -	132.1225
11	Concrete cover, C_v (mm)	55	Design service life, td (yr)	72	x-value	112.6406	relative reduction of the safety margin, (Θo - Θm)	0.200005
12	water/cement ratio	0.4	Compressive strength of Concrete, fc (MPa	35.3513	lever arm	460.8536	adequacy of the design	OK
13	Fine-to-total aggregate ratio	0.35	Elastic modulus of concrete, Ec (GPa)	49.1202	factored load bearing capacity in steel, Rds (Nmm)	1.36E+08		
14	Corrosion current density, I_{corr} (μA/cm^2)	0.98			factored load bearing capacity in concrete, Rdc (Nmm	13322145	Final section	
15			Durability parameters		Error if steel stress is decisive (Sd - Rds)	-1E+08	Width of beam (mm)	225
16	Loadings		Curing coefficient	0.91239	Error if concrete stress is decisive (Sd - Rdc)	21777855	Depth of beam (mm)	511
17	Unfactored dead load (KN/m)	10	Rate of loss of concrete (mm/year)	0.07087			Diameter of rebar (mm)	18.1084
18	Unfactored live load (KN/m)	12	Corrosion penetration rate (mm/year)	0.01147				
19	Dead load safety factor	1.2						
20	Live load safety factor	1.6	Residual dimensions					
21			loss of concrete cover (mm)	5.10244				
22	Materials constants		loss of rebar diameter (mm)	0.82555				
23	Yeild strength of steel, f_y (MPa)	400	reduced width of member (mm)	214.795				
24	Elastic modulus of steel, E_s (GPa)	200	reduced depth of member (mm)	505.91				
25	Concrete safety factor	1.5	reduced diameter of rebar (mm)	16.4573				
26	Steel safety factor	1.15						
27	Density of steel (g/cm^3)	7.85						

Table G2: Durability-based design of a RC column using Excel spreadsheet program RC_C_DDesign

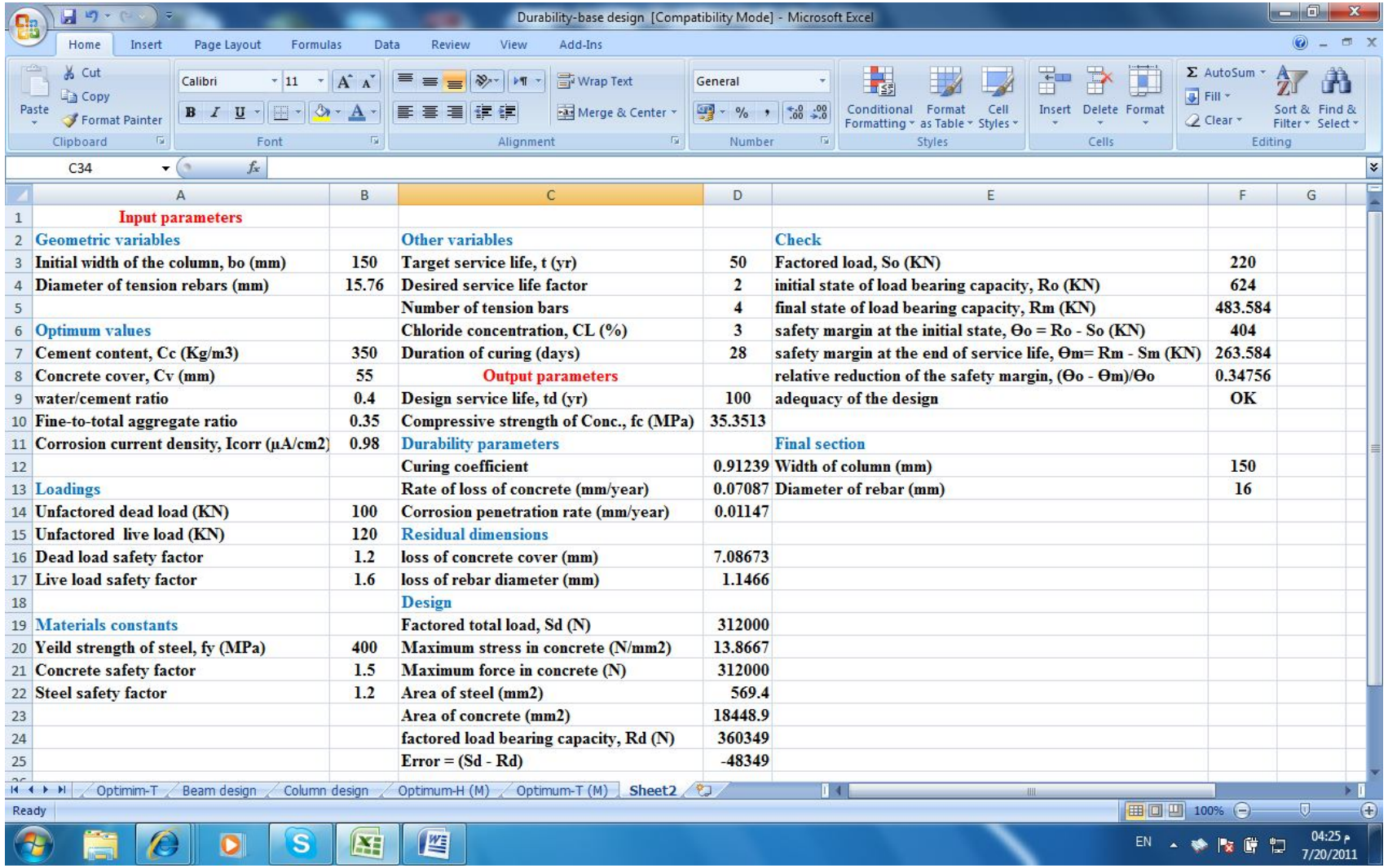

Durability-base design [Compatibility Mode] - Microsoft Excel

	A	B	C	D	E	F	G
1	**Input parameters**						
2	**Geometric variables**		**Other variables**		**Check**		
3	Initial width of the column, bo (mm)	150	Target service life, t (yr)	50	Factored load, So (KN)	220	
4	Diameter of tension rebars (mm)	15.76	Desired service life factor	2	initial state of load bearing capacity, Ro (KN)	624	
5			Number of tension bars	4	final state of load bearing capacity, Rm (KN)	483.584	
6	**Optimum values**		Chloride concentration, CL (%)	3	safety margin at the initial state, Θo = Ro - So (KN)	404	
7	Cement content, Cc (Kg/m3)	350	Duration of curing (days)	28	safety margin at the end of service life, Θm= Rm - Sm (KN)	263.584	
8	Concrete cover, Cv (mm)	55	**Output parameters**		relative reduction of the safety margin, (Θo - Θm)/Θo	0.34756	
9	water/cement ratio	0.4	Design service life, td (yr)	100	adequacy of the design	OK	
10	Fine-to-total aggregate ratio	0.35	Compressive strength of Conc., fc (MPa)	35.3513			
11	Corrosion current density, Icorr (μA/cm2)	0.98	**Durability parameters**		**Final section**		
12			Curing coefficient	0.91239	Width of column (mm)	150	
13	**Loadings**		Rate of loss of concrete (mm/year)	0.07087	Diameter of rebar (mm)	16	
14	Unfactored dead load (KN)	100	Corrosion penetration rate (mm/year)	0.01147			
15	Unfactored live load (KN)	120	**Residual dimensions**				
16	Dead load safety factor	1.2	loss of concrete cover (mm)	7.08673			
17	Live load safety factor	1.6	loss of rebar diameter (mm)	1.1466			
18			**Design**				
19	**Materials constants**		Factored total load, Sd (N)	312000			
20	Yeild strength of steel, fy (MPa)	400	Maximum stress in concrete (N/mm2)	13.8667			
21	Concrete safety factor	1.5	Maximum force in concrete (N)	312000			
22	Steel safety factor	1.2	Area of steel (mm2)	569.4			
23			Area of concrete (mm2)	18448.9			
24			factored load bearing capacity, Rd (N)	360349			
25			Error = (Sd - Rd)	-48349			

Optimim-T | Beam design | Column design | Optimum-H (M) | Optimum-T (M) | Sheet2

Ready

100%

EN 04:25 7/20/2011

VITAE

NAME: Adamu Lawan

NATIONALITY: Nigerian

HOME ADDRESS: 47, Aliyu Road, Tudun wada Zaria,
Kaduna State, Nigeria.

POSTAL ADDRESS: Department of Civil Engineering,
Ahmadu Bello University,
Zaria, Nigeria.

EMAIL: bnlawan@yahoo.co.uk

EDUCATIONAL QUALIFICATIONS

Master of Science in Civil Engineering (Structures)

Sept. 2009 – July 2011

King Fahd University of Petroleum and Minerals,

Dhahran, Saudi Arabia.

Bachelor of Engineering (Civil)

Jan. 2000 – Aug. 2005

Bayero University Kano, Nigeria.